



Electric Innovative Commuter Aircraft

D5.1 Enabling Technologies


	Name	Function	Date
Author:	Danilo Ciliberti Pierluigi Della Vecchia Fabrizio Nicolosi Vittorio Memmolo Vincenzo Cusati (Smartup) Salvatore Corcione (Smartup) Guido Wortmann (RR)		31.05.2020
Approved by:	Fabrizio Nicolosi	WP5 Lead	
	Qinyin Zhang	Project Lead	

Table of contents

1	Executive Summary	4
2	References	6
2.1	Definitions and Abbreviations	6
2.1.1	Terms & Definitions	6
2.1.2	Abbreviations & Symbols	6
2.2	Tables & Figures	6
2.2.1	List of Figures	6
2.2.2	List of Tables	8
3	Introduction	10
4	Propulsion	11
4.1.1	Conventional propulsion	13
4.1.2	Evolution of current gas turbines	13
4.1.3	Sustainable aviation fuels	15
4.1.4	Electric propulsion	17
4.1.5	Turbo-electric propulsion	18
4.1.5.1	Power electronics, distribution, and thermal management	20
4.1.6	Batteries	21
4.1.7	Fuel cells	23
4.1.8	Hydrogen-fuelled aircraft	27
5	Aerodynamics	30
5.1	Distributed Propulsion	30
5.1.1	Tip propeller	32
5.1.2	High-lift propeller	41
5.1.3	Directional control	46
5.1.4	Boundary layer control	46
5.1.5	Fuselage tail propeller	47
5.1.6	Noise	49
5.2	Laminar flow	50
5.2.1	Natural Laminar Flow	52
5.2.2	Laminar Flow Control	54
5.2.3	Riblets	59
5.3	High Aspect Ratio Wing	61
5.4	High lift Device	63
6	Airframe	64
6.1	Smart Intelligent Composite Structures	64
6.1.1	Composite Damage Mechanics	65
6.1.2	Composite Damage Tolerance Approach	67
6.1.3	Benefit of SHM System Within Aircraft Life Cycle	71
6.2	On Condition Maintenance of Aircraft	75
6.3	Integrated Landing Gear Health Management	82
6.3.1	Maintenance tasks for a landing gear system	84
6.3.2	Cost benefits integrating health management system	85
6.4	Aeroelastic Tailoring of Distributed Propeller Wing	86
6.5	Strut-braced Wing	90
6.6	Morphing Wing	93
6.7	Novel composite technologies, nanomaterial and multi-functional materials	94
6.7.1	Automatic Fibre Placement	94



6.7.2	Carbon Nanotubes	95
6.7.3	Structural Batteries.....	96
7	Design Tool Improvement.....	98
8	Certification Authority	99
9	Bibliography	103

1 Executive Summary

In this report, the enabling technologies for the ELICA project are presented. The objective is to achieve quasi-zero emissions on a 19-seat aircraft. According to the proposal progress indicators, ELICA project shall achieve reductions of CO₂, NO_x and noise by 50% with respect a 2014 reference aircraft. Enabling technologies will be related to propulsion, aerodynamics, airframe, and their integration. A resume of the powerplant and energy storage technology trends has been released with courtesy by Rolls Royce in the following Table 1 and Table 2.

	Parameter	Unit	Value 2025	Value 2035	Requires Cooling System	Comments
Low Speed Electric Machine (e.g. direct propeller drive)	Power density	kW/kg	6	7	yes	Independent from rotational speed and power level
	Efficiency	%	96.0	96.0		Constant
	Unit cost	\$/kW	1000	1000		
Inverter (Low Speed Machine)	Power density	kW/kg	25	30	yes	Independent from power and voltage level
	Efficiency	%	98.0	98.0		Constant
	Unit cost	\$/kW	1000	1000		
Power Management and Distribution (PMAD)	Power density	kW/kg	60	100	no	Considers electric network reconfiguration and protection devices
	Efficiency	%	100	100		
	Unit cost	\$/kW	TBD	TBD		
High Speed Electric Machine (e.g. turbine driven generator, geared propeller drive)	Power density	kW/kg	10	12	yes	Independent from rotational speed and power level
	Efficiency	%	96.0	96.0		Constant
	Unit cost	\$/kW	1000	1000		
Converter (High Speed Machine)	Power density	kW/kg	25	30	yes	Independent from power and voltage level
	Efficiency	%	98.0	98.0		Constant
	Unit cost	\$/kW	1000	1000		
Cooling System	Power density	kg/kW	1.2	1.0	n.a.	Applied on thermal losses! Not on installed component power!
	System cost	\$/kW	TBD	TBD		Considers cooling fluid, heat exchangers, pumps, controls, etc
Gearbox	Power density	kW/kg	6	7	yes	Applied on TO power, considers single stage planetary gearbox
	Efficiency	%	99.5	99.5		Constant
	Unit cost	\$/kW	TBD	TBD		
Thermal Engine	Power density	kW/kg	5.0	6.0	no	Applied on TO power
	Specific fuel consumption	kg/kW/h	290	280		Constant
	Unit cost	\$/kW	1250	1250		Applied on TO power

Table 1: Powerplant technology trend. Courtesy of Rolls Royce.

	Parameter	Unit	Value 2025	Value 2035	Requires Cooling System	Comments
Battery	Energy density	kWh/kg	0.35	0.50	yes	Includes BMS and housing
	Efficiency	%	90.0	90.0		Constant; assumed for high energy cell at 1C discharge rate
	Battery Cost	\$/kWh	190.0	100.0		Includes BMS and housing
PEM Fuel Cell System	Power density	kW/kg	0.65	0.65	yes	Includes all accessory components except cooling and hydrogen storage
	Efficiency	%	60.0	65.0		
	Stack System price	\$/kW	40	30		Projected to high-volume production of 500,000 systems per year
	Hydrogen Heating Value	kWh/kg	33.3	33.3		
Hydrogen Storage System	Tank mass	kg/kg(H2)	18.2	13.3	no	700bar CFRP tank
	Tank volume	dm ³ /kg(H2)	25.0	14.3		
	Storage System Cost	\$/kg(H2)	333	266		

Table 2: Energy storage technology trend. Courtesy of Rolls Royce.

For the same powerplant and energy storage technologies, an independent research has been pursued. Data from different sources have been collected and presented in charts and tables, highlighting a trend on specific power and energy where possible. Similarly, the improvements on aerodynamic efficiency and structural weight, together with their integration with the powerplant and energy storage system are discussed.

2 References

2.1 Definitions and Abbreviations

2.1.1 Terms & Definitions

Term	Definition
Sea Level Static	Operating point at sea level (0m) and zero velocity

Table 3: Terms & Definitions.

2.1.2 Abbreviations & Symbols

Abbreviations	Description
ASTM	American Society for Testing and Materials
BLI	Boundary Layer Ingestion
CMC	Ceramic Matrix Composite
DEP	Distributed Electric Propulsion
FRL	Fuel Readiness Level
LNG	Liquefied Natural Gas
MIL	Minimum Induced Losses
SAF	Sustainable Alternative Jet Fuel
SAT	Small Air Transport
TLAR	Top Level Aircraft Requirements
TRL	Technology Readiness Level
UHAR	Ultra High Aspect Ratio

Table 4: Abbreviations.

2.2 Tables & Figures

2.2.1 List of Figures

Figure 1: Power and energy required for vehicles ranging from small cars to large commercial aircraft [1,6].....	11
Figure 2: History of commercial aircraft fuel burn per seat-mile [1].....	11
Figure 3: Do-228NG design mission profile.	12
Figure 4: Simulation of Do-228NG power and energy required per flight segment.....	12
Figure 5: Thrust Specific Fuel Consumption over time for jet engines [10].....	15
Figure 6: Hybrid-electric propulsion scheme.	18
Figure 7: Turbo-electric propulsion scheme.	19
Figure 8: Trend of electric drives specific power. Reproduced from [1].	20
Figure 9: Specific energies of different battery technologies [18].....	23
Figure 10: Specific energy of fuel cells systems for aircraft applications.	26
Figure 11: Specific power of fuel cells systems for aircraft applications.	27
Figure 12: Forecasted climate impact (tank-to-thrust) of new aircraft fuel systems [40].	29
Figure 13: Economic and climate impact of a revolutionary commuter aircraft [40].	29
Figure 12: Disruptive configurations using DEP technologies.....	31
Figure 13: Induced angles due to wing and actuator disk.	33
Figure 14: Induced angles due to wing and rotating disk.	33
Figure 15: Four blade Tip-Propeller and Impeller models on a AR=8 wing [43].	34
Figure 16: Variation of effective aspect ratio caused by rotor speed, AR=8, Re=6.7E5 [43], Baseline AR _e =6.45.	34
Figure 17: Four blade Tip-Propeller effects on a AR=8 wing, Re=6.7E5, T _C =0.42 or 0.6 [43]. .	35
Figure 18: Effect of propeller speed and size on induced drag coefficient [43].	35
Figure 19: Wing-tip-mounted pusher turboprop model in Langley 7-by-10 foot Speed Tunnel, AR=6.10 [44].	36

Figure 20: Left: Vortex-propeller interaction on drag coefficient versus lift coefficient for 0° incidence; right: delta drag respect to isolated wing for counter-rotating and pro-rotating wing-tip pusher propeller; $M=0.7$, $Re=3.82E6$ [44].	36
Figure 21: NASA X57 Maxwell numerical analysis of tip-mounted propeller, $AR=15$.	37
Figure 22: Drag Polar Comparison of Power-On (WCP) and Power-Off (WC) Wings [45], $h=8000ft$, $V=150kn$, $AR=15$.	37
Figure 23: Drag reduction due to high-efficiency tip-propeller, $AR=8.47$, $M=0.23$, $Re=6.9E6$ [2].	38
Figure 24: TU Delft, Model II (modular cambered wing) installed in the wind tunnel, $AR=6.2$ (left) and 6.1 (right), conventional(left), tip-mounted(right).	39
Figure 25: Drag benefit of wingtip-mounted configuration compared to conventional configuration(left) and Effect of propeller thrust setting on the span-efficiency parameter (right).	39
Figure 26: Lift and drag polars of the conventional and wingtip-mounted configurations, including propeller forces.	40
Figure 27: Wing drag improvement due to the propeller tip-mounted on a $AR=11$ wing, $M=0.48$, $Re=15E6$, Thrust T in Newton.	40
Figure 28: NASA X57 Maxwell rendering.	41
Figure 29: Left: Predicted induced axial velocity distributions for the five propellers designed to produce the same average induced axial velocity; right: comparison of the chord lengths [50].	41
Figure 30: Left: X57 Wing configurations. Top right: The lift coefficient for the high-lift wing with high-lift and wingtip nacelles. Mid right: the sectional lift coefficient for the unblown (blue) and the blown (red) high-lift wing with high-lift and wingtip nacelles. The skin friction coefficient from FUN3D for the blown, high-lift wing with wingtip nacelles and HLN. 58 KTAS, $M=0.0878$, $Re=1.33$ million, $h=0$ ft, and $T=59^{\circ}F$. Blown, high-lift wing power conditions of 4548 RPM, 164.4 hp (13.7 hp/prop), and total thrust of 596.4 lbf. FUN3D SARC+QCR.	42
Figure 31: The effect of propeller spin direction approach on spanloading for the blown, high-lift wing (40° flap) at 73 mph, $M=0.096$, $Re=1$ million, $h=2300$ ft, $T=60^{\circ}F$, and 300.6 hp (16.7 hp/prop, 6147 RPM), and span loading $aoa=4deg$, [51].	43
Figure 32: Nasa high-lift propeller testbed, experiments and numerical. Mid: Unblown, prop removed, flaps=40deg. Down: Blown, flaps=40deg, 6860rpm.	43
Figure 33: Tecnam P2006T wing, Lift coefficient for Clean(left) and flapped(right) configurations, $M=0.08$, $Re=3.3E6$ [2].	44
Figure 34: Tecnam P2006T wing, Results of 5+1 propeller configuration for CL and CD, with high-lift propeller and nacelles, $M=0.08$, $Re=3.3E6$ [2].	44
Figure 35: High-lift propeller on a typical 40 passengers regional turboprop wing, $AR=11.07$, $M=0.15$, $Re=7.6E6$, DEP 8, DEP 12, DEP16 and DEP 20 configurations, T_0 per propeller.	45
Figure 36: Delta respect to an isolated wing, of high-lift propeller on a typical 40 passengers regional turboprop wing, $AR=11.07$, $M=0.15$, $Re=7.6E6$, DEP 8, DEP 12, DEP16 and DEP 20 configurations, top: DeltaCL (lift coefficient at $aoa=15deg$.), bottom left: DeltaCD0 (zero lift drag coefficient) and DeltaCM0 (pitching moment coefficient at $aoa=0deg$.)	45
Figure 37: Distributed propulsion as an alternative mean of directional control [52,55].	46
Figure 38: Distributed boundary layer ingestion concept [57].	47
Figure 39: Example of fuselage tail-mounted propeller.	47
Figure 40: TUDELFT Configurations Practiced for the Experiment [58].	48
Figure 41: TUDELFT Main results of tail propeller BLI [58].	48
Figure 42: (Top) GL-10 in (a) hover mode and (b) top view of the forward flight configuration; (Bottom) Example of directivity modification of the blade passage frequency on the ground plane via relative propeller phase control, for the GL-10 layout at 5,000 RPM, $J=0.6$, $\alpha=0^{\circ}$. The outlined regions are the observers given to the optimization for noise minimization, and the relative phase, ψ_r , of each propeller is given in degrees in the direction of rotation.	50

Figure 43: Schematic difference between NLF, LFC and HLFC [68].	51
Figure 44: Transition mechanisms on a swept wing [69].	51
Figure 45: Dominant laminar turbulent transition effect for forward swept and backward swept wings [70].	52
Figure 46: ELFIN project Fokker 100 natural laminar flow testbed [71].	53
Figure 47: BLADE demonstrator.	53
Figure 48: SHM-1 NLF airfoil shape and representative pressure coefficient distribution [73].	54
Figure 49: Pe [74] studies on HLFC suction system for a long-range aircraft.	55
Figure 50: B757 HLFC apparatus and major accomplishment [71].	56
Figure 51: Dassault Falcon 50 HLFC testing results [71].	56
Figure 52: Scheme of the ALTTA concept system [77] and wind tunnel tests.	57
Figure 53: Risse [78] simplified suction system.	57
Figure 54: HLFC integration and design evolution, impact on block fuel [78].	58
Figure 55: Relative changes with HLFC integration and comparison of key design parameters [78].	58
Figure 56: Riblets [80](left) and dimples [81](right).	59
Figure 57: Schematic of riblets cross sectional area [83].	59
Figure 58: Aircraft configuration examined in [80].	60
Figure 59: T-33 jet trainer riblet testbed (left) and velocity profile on wing for $M = 0.70$ (right).	61
Figure 60: A320 riblets testbed [85].	61
Figure 61: Example of potential weight increase and fuel burn variation due to aspect ratio variation.	62
Figure 62: Actuation systems implemented on the DLR F15 model[90]	63
Figure 63: Low velocity impact damage. Typical peanut shape in the plane of the plate (left) and conical distribution of delamination through the thickness (right).	66
Figure 64: Schematic representation of residual strain versus energy level and derived design constraints.	69
Figure 65: Schematic representation of scattering factors constraining the composite design.	69
Figure 66: Typical design allowables for carbon fibers reinforced plastics (CFRP).	70
Figure 67: Damage Assessment process based on NDE and SHM capabilities.	72
Figure 68: Cost breakdown for commercial aircraft.	72
Figure 69: Damage occurrence on a composite fuselage for wide and narrow-body aircraft (courtesy of Lufthansa Technik).	74
Figure 70: Technological level and SHM system category. Adopted scenario for categorization.	80
Figure 71: Hybrid SHM system approach for efficient replacing of maintenance tasks. In the schematization, the sun shows the pristine condition (calm and quite status) while the lightning represents and unforeseen and sudden impact.	80
Figure 72: Maintenance cost (a) and Labor cost (b) breakdown.	82
Figure 73: Typical Landing gear system of a 19 pax aircraft. Different views.	84
Figure 74: Flutter speed for engine placement along the span for two values of chordwise offset (a) and Normalized flutter speed in 4 engine configuration with one fixed (η_2) and one movable engine (η_1).	89
Figure 75: Cantilever beam model (a) versus strut-braced beam model.	92
Figure 76: Schematic concept of sandwich structural battery: (a) sandwich panel with a foam core and two face skins and (b) sandwich panel with battery core and two face skins [161].	96
Figure 77: Lift coefficient margin in approach as function of max lift coefficient.	100
Figure 78: Angle of attack margin in approach as function of max lift coefficient.	101

2.2.2 List of Tables

Table 1: Powerplant technology trend. Courtesy of Rolls Royce.	4
Table 2: Energy storage technology trend. Courtesy of Rolls Royce.	5
Table 3: Terms & Definitions	6
Table 4: Abbreviations	6



Table 5: Approved sustainable aviation fuels as per ASTM D5766.	16
Table 6: Greenhouse emissions savings (excluding carbon emissions from land use change) ⁵	17
Table 7: Trends in future batteries at cell level by year 2035 [21].	23
Table 8: Fuel cells performance in aircraft applications. Specific energies and powers refer to the fuel cell system (including tank, etc.). MTOM refers to the entire aircraft gross mass.	26
Table 9: Research and Industrial Projects applying hydrogen technologies.	27
Table 10: Comparison of energy carriers and storage solutions in terms of gravimetric and volumetric energy density.	28
Table 10: Scheduled maintenance levels for commercial aircraft.	73
Table 11: Approximate costs for C-check inspection for a variety of aircraft categories.	73
Table 12: Landing gear failure modes and detection mechanisms [128].	83

3 Introduction

Aviation contributes to the global carbon emissions only from 2.0% to 2.5%. Of this small contribution, more than 90% of the carbon emissions come from commercial operations of large passenger aircraft, which carry more than 100 passengers per trip. Nonetheless, a significant reduction of aviation emissions (including NO_x and noise) is the objective of developed countries for the following reasons: legislation policy may require further restrictions in the near future; it takes a long time for a technology to be consolidated and certified for aviation; because of the global impact of pollutant emissions.

Although the impact of the emissions of general aviation aircraft is tiny with respect to the global anthropic emissions, the small air transport (SAT) segment is seen as the bridge to overcome the gap from experimental aircraft to commercial aviation. It is believed that the success of many technologies can be better proved and demonstrated at the level of SAT rather than on large passenger transportation segment. This is the case of alternative propulsion system, which has been already introduced on light aircraft and has received a great deal of attention over the past years¹. Thus, the SAT segment can be a viable feasible platform to develop a systematic approach to fully design such aircraft system, define a best practice, and trace a technological roadmap for larger platform and aircraft demonstrators.

To achieve the near-zero emission target, several technologies and approaches are reviewed in this document. These enabling technologies define the design space of ELICA project and include advanced propulsion and energy systems such as all-electric and hybrid-electric propulsion systems, high-power batteries and fuel cells for propulsion, superconducting motors and generators, hybrid compound engines (which combine a gas turbine and another internal combustion engine such as a diesel), thermodynamic alternatives to the simple Brayton cycle, and alternative fuels such as sustainable jet fuels, hydrogen and liquefied natural gas (LNG).

Electrical propulsion can reduce carbon and nitrogen oxide emissions if new technologies enable higher specific powers and reliability. Batteries and fuel cells provide electrical power with no emissions, but only if the energy sources are sustainable.

Fuel cells convert the chemical energy of a fuel into electrical power without any combustion and their exhaust cells is totally carbon-free if hydrogen is used as the fuel. If a hydrocarbon fuel is used, the fuel cell exhaust still contains CO₂ in direct proportion to the amount of fuel consumed, but there are no NO_x or particulate emissions. However, safety in storage and utilisation is of paramount concern if hydrogen is used as fuel.

Cryogenic system and superconducting materials (operating at temperatures from 20 to 77 K) seem not feasible for commuter aircraft because of their size, weight, and safety constraints (due to the required robustness and redundancy), even with LNG stored at 112 K.

Sustainable aviation fuels (SAF) should produce approximately the same amount of CO₂ of a conventional jet fuel, but recycling the carbon already present in the biosphere and with reduced NO_x emissions. They may be an option in the immediate future since they do not require a radical change in the engine architecture.

Apart from the energy sources, airframe-propulsor integration shall increase the impact of advanced propulsion systems, as in the case of distributed propulsion, which use multiple propulsors to achieve beneficial aerodynamic-propulsion interaction [1–5]. Also, boundary layer ingestion and laminar flow technology may contribute to improve the aerodynamic efficiency by reducing the aircraft parasite drag.

Finally, airframe offers various key technologies to further improve performance versus weight ratio and even favour safety. That is the case of smart intelligent systems to monitor the whole airframe in IoT (Internet of Things) and Industry 4.0 perspectives. In addition, some challenging but promising advancements are forecast by introducing novel and multifunctional materials.

¹ https://en.wikipedia.org/wiki/List_of_electric_aircraft

4 Propulsion

The power needed to propel an aircraft increases at more than the airspeed squared. Thus, high powers and large energies are needed to fly at high speeds over long distances (Figure 1). The maximum power required for an aircraft is the power at take-off and it scales with aircraft weight. Requirements that determine the power levels include considerations of runway length, airport elevation and ambient temperatures, climb rate, and cruise efficiency.

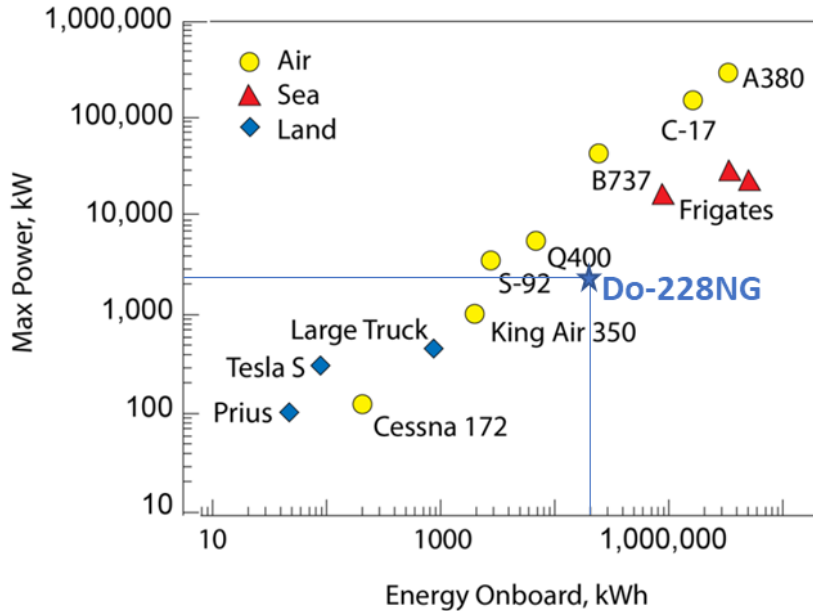


Figure 1: Power and energy required for vehicles ranging from small cars to large commercial aircraft [1,6].

Fuel efficiency has always been a primary design criterion for commercial aircraft since it is an important determinant of aircraft range, size, and economics. Overall, the fuel burn per seat mile of gas turbine-powered commercial aircraft has been reduced by 70 percent since service started in the 1950s, at an average rate of about 2% per year since 1970 (see Figure 2). About half the gain has been the result of improvements to the airplane, the rest to the engine.

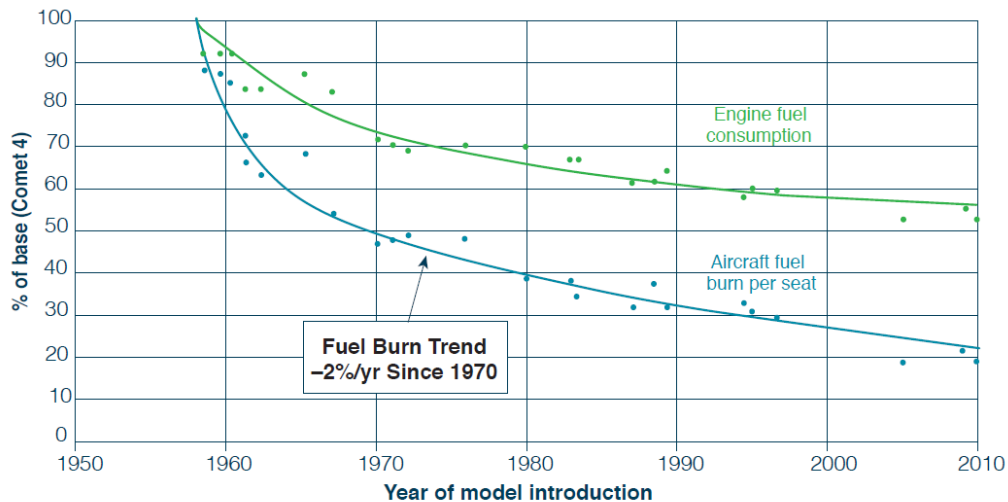


Figure 2: History of commercial aircraft fuel burn per seat-mile [1].

The typical mission profile for a 19 pax air transport is shown in Figure 3. It represents the design mission of the Do-228NG. Energy and power consumption during each flight phase have been simulated by UNINA with its preliminary design software and are shown in Figure 4.

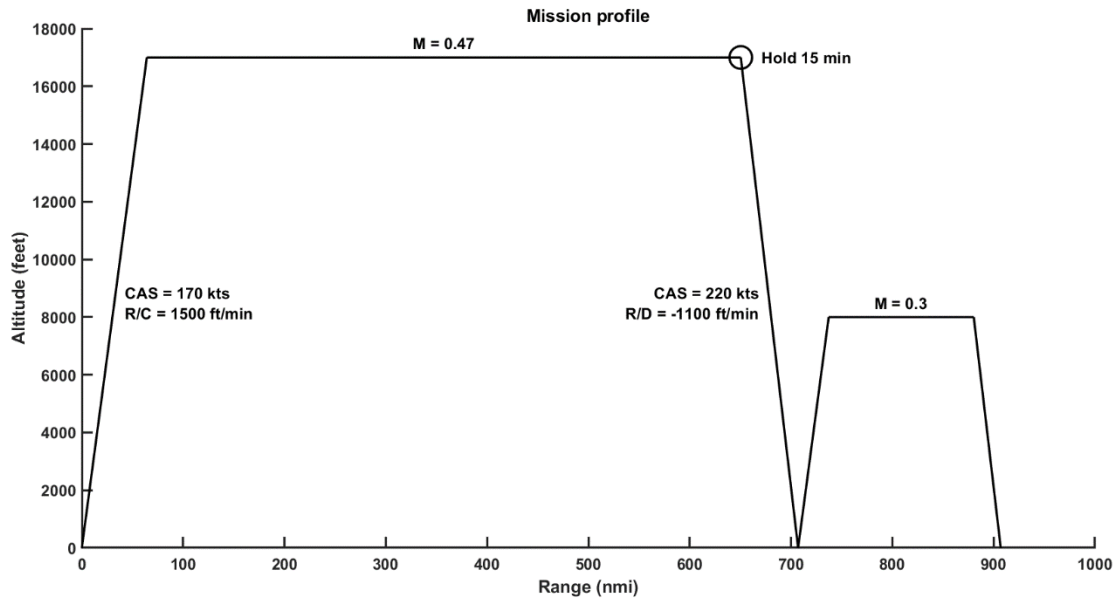


Figure 3: Do-228NG design mission profile.

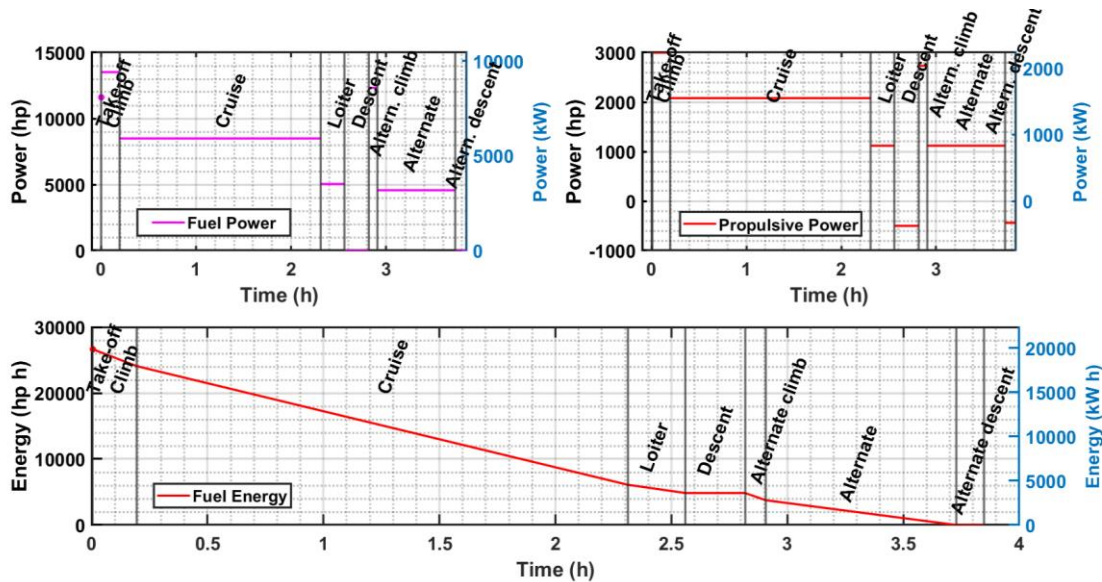


Figure 4: Simulation of Do-228NG power and energy required per flight segment.

Most fuel is stored in the wings. This arrangement has several advantages: the fuel is located at about the aircraft's centre of gravity to minimize its as fuel is burned; the wing's structural weight is reduced because the fuel weight partially offsets the bending moment produced by wing lift; no space useful for payload, which is carried in the fuselage, is lost.

In the search for alternative energy sources, aircraft weight and drag penalties must be considered if sources less dense than jet fuel (e.g. hydrogen and natural gas) will be employed. For example, given the low density of hydrogen, the drag and weight increase from the tanks needed for cryogenic liquid hydrogen will offset the gain in energy density for high-speed aircraft. Similarly, battery-powered concepts in which the batteries will be installed in the fuselage need to be compared with aircraft having similar net payload capabilities.

Aircraft burning fuel during their mission will lose weight. This is an advantage for long range aircraft (more than 3000 nmi), because the decreased weight leads to further increase in range. For range less than 1000 nmi the weight loss does not significantly affect the energy consumption. However, a battery-powered aircraft needs to be sized to account for landing at maximum take-off weight. For Li-Air batteries, the weight shall even increase during flight.

Apart from economic considerations on the development and operations of energy sources alternative to fuel (the case for electric energy has been discussed in D2.1), the following advance in propulsion are identified and discussed in the following sub-sections:

- conventional propulsion
 - evolution of current gas turbines
 - sustainable aviation fuels
- electric propulsion
 - turbo-electric propulsion
 - batteries
 - fuel cells

The best results will be obtained by integrating the enabling technologies. For instance, turbo-electric propulsion will be effective if coupled with distributed electric propulsion, which is discussed in Section 5.

4.1.1 Conventional propulsion

Gas turbines convert the fuel chemical energy into a rotating shaft mechanical energy. An aircraft engine converts the shaft power into propulsive power with a propeller (turboprop) or with a propulsive system made of a ducted fan and a nozzle (turbofan engine). If the propulsor consists in a two large contra-rotating (tandem) propellers it is sometimes called unducted fan or prop-fan. Propeller contra-rotation is a way to recover part of the energy loss due to the flow swirl in the propeller wake. The mechanical complexity, weight, and maintenance costs of such a feature often shadow the aerodynamic advantage, so that many propeller-driven airplanes employ a single propeller per engine.

Alternative (piston) engines are commonly used on very light and ultra-light aircraft, due to their compliance with the required power-to-weight and pressure ratio, simplicity, robustness, and the possibility to use automotive gasoline or diesel as fuel. Commuter aircraft category are propeller-driven by definition [7]. Power-to-weight ratio favours turboprop engines as conventional propulsive system for commuter aircraft.

4.1.2 Evolution of current gas turbines

Recent studies have considered the practical limits for simple cycle gas turbines given the potential for new materials, engine architectures, and component technologies. Their estimates provide a possible improvement of 30-35% in overall efficiency with respect to nowadays engines in service. It may be possible to achieve thermodynamic efficiencies of 65-70% and propulsive efficiencies of 90-95%. Improvements in turbomachinery performance and reduction in cooling losses could improve thermodynamic efficiency by 19% and 6%, respectively. This gain will not be achieved only by the adoption of such new technologies in existing engines, but it will require the optimization of the thermodynamic cycle from specific levels of component performance characteristics, temperature capability, and cooling. The practical limits to propulsive efficiency cannot be addressed at the engine level alone, but require integration within the airframe and airplane configuration [1].

As concern propeller efficiency, it is matter of aerodynamics studies. The adoption of high-fidelity numerical simulations into design and a swirl recovery system should provide the achievement of the abovementioned increase in propulsive efficiency. Also, it is known that the flow accelerated through a propulsor contains energy that is pushed away from the aircraft. Thus, a large propeller accelerating a large air mass is more efficient (i.e. lower specific fuel consumption) than a turbofan engine providing a significant acceleration to a small air mass, for a given thrust. For the same reason, several distributed small propellers instead of two big propellers may further increase the overall efficiency, provided that the weight and system complexity does not offset this advantage. Improvement of thermodynamic efficiency requires larger pressure at compressor exit and higher turbine inlet temperatures, while reducing structural weight and aerodynamic losses. Improvements in materials and manufacturing should continue the trend of the last 40 years, which provided forged titanium alloys, several nickel superalloys, single-crystal turbine airfoils, forged high-temperature powder metal alloys, coatings for environmental protection and for

thermal barriers, and, most recently, titanium aluminides. Advanced materials can reduce fuel burn by decreasing the engine structural weight and further improvements are expected with long lasting turbine blade resisting at 1700°C. This includes ceramic matrix composites (CMCs) and other monolithic ceramics, which should enter into service within few years. Challenges include low fracture toughness, low thermal conductivity, and manufacturing cost. If their thermal resistance could be brought to about 1500°C, they would dramatically reduce or eliminate cooling in many parts of an engine, significantly increasing efficiency and lowering its weight.

Advances in high-temperature metallic alloys, such as nickel-based alloys as well as new materials classes such as niobium and molybdenum, have temperature capability comparable to that of CMCs and much higher fracture toughness and thermal conductivity, but a higher density. They seem suitable for static cooled parts such as combustors or turbine vanes. Further studies on manufacturing and coatings are needed.

Coatings can add value to many engine parts. They are required at high temperature for environmental protection. For cooled parts, thermal barrier coating can significantly increase the temperature capability and reduce cooling requirements. Erosion coating can extend part life and retain performance. Ice-phobic coating can reduce the threats posed by ice formation. Further progress in coatings of all types can be expected given sufficient investment [1].

Different manufacturing techniques such as additive manufacturing offer the possibility to produce structures or properties that would otherwise be unrealizable or prohibitively expensive. Some manufacturers claim to achieve improved performance with fewer parts and saving millions of dollars per plane by using additive manufacturing on jet engines².

At time of writing, it is difficult to further quantify the impact of the evolution of the gas turbine. If the overall engine efficiency 30% increase is directly linked to fuel burn, then it may be argued that carbon and presumably also NO_x emissions will reduce by the same amount in the 2035-2050 time frame. This improvement is consistent with the 2% fuel burn reduction achieved from the 70's (see again Figure 2). Historical data, presented in Figure 5, show a 25% reduction in jet engines cruise thrust specific fuel consumption over 40 years, with turboprop gaining from 10% to 30% more efficiency over regional jets and large turbofans. However, fuel consumption and emissions from cruise data are not sufficient to describe the impact of the advancing technology. As concern turbofan engines, it has been shown [8] that during the last 40 years, thrust specific emissions during a landing-take-off cycle have been almost constant. Also, despite significant investments in aero engine technology, emissions savings are decreasing over time. This is due to several factors: emissions of carbon monoxide and hydro-carbons significantly increase at low thrust settings (landing), while NO_x high emissions at high thrust settings (take-off) and high thermal efficiency are counterbalanced by high bypass ratios engines. The emissions of CO₂ follow the same trend of thrust specific fuel consumption with engine ratings. Similar conclusions may be drawn for turboprop engines. Also, the impact of emissions at low altitudes, especially in take-off and landing phases, may be critical because of the highly urbanized areas near the airports and photochemical reactions in the low troposphere [9].

This explain why even if all the above mentioned technological improvements are successfully integrated in a turboprop engine, they will not be sufficient for the target 50% emissions reduction of the ELICA project. Therefore, the only evolution of the gas turbine engine does not satisfy the project progress indicators.

² <https://www.ge.com/additive/additive-manufacturing/industries/aviation-aerospace>

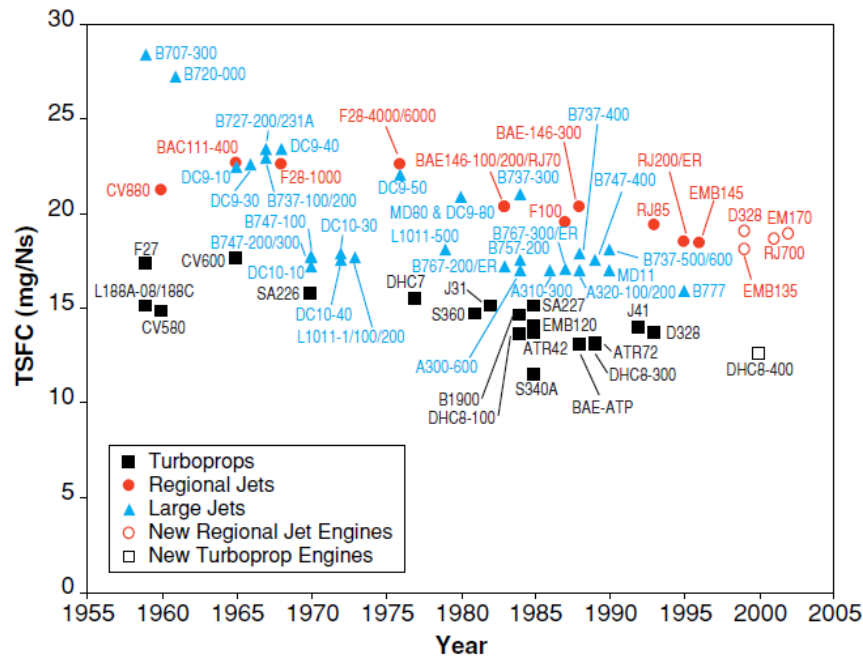


Figure 5: Thrust Specific Fuel Consumption over time for jet engines [10].

4.1.3 Sustainable aviation fuels

Sustainable aviation fuels (SAF) are alternative to petroleum-based jet fuels, fully compatible with the existing aircraft and fuel infrastructure, miscible with conventional jet fuels, and sustainable in the sense that they have a smaller carbon footprint in their entire life cycle and are acceptable also from socio-economic point of view. While burning SAF will produce nearly the same amount of CO₂ per unit of fuel as conventional jet fuel, the use of SAF reduces net life-cycle carbon emissions because SAF enable reusing or recycling carbon that is already in the biosphere to create the fuel. If their commercialization takes place on a large scale, aviation can significantly lower its net carbon emissions more quickly and effectively than improving operations, infrastructure, and aircraft. This reduction can also be achieved without impacting the time frame or suitability of other potential carbon-lowering approaches.

Jet fuel is a generic term that encompasses many specific variants, such as Jet A, Jet A-1, JP-5, and JP-8. In most cases, the other names imply specific variants of the fuel, as often detailed in the specifications themselves. Jet A is the most common form of jet fuel used by commercial aviation in the United States, while Jet A-1 predominates in the rest of the world [1].

To be fully compatible with conventional jet fuels, SAF must have high energy per unit mass, high energy per unit volume, low freezing point, low vapor pressure, materials compatibility, low toxicity, must be stable and non-volatile. These properties ensure safety and meet the required performance. Any synthetic fuel that have such characteristics is also called a “drop-in” fuel, in the sense that it can substitute conventional jet fuel without changing the existing aircraft fuel system or airport infrastructure.

Sources other than petroleum include woody biomass, hydrogenated fats and oils, recycled waste and other renewable sources. The American Society for Testing and Materials (ASTM) International has developed standards ASTM D4054 and D5766 to approve new bio-based aviation fuels, and currently six production pathways have been certified for blending with conventional aviation fuel. These are reported in Table 5. Additional pathways are currently in the ASTM certification process.

Name	Abbrev.	Description	Feedstocks ³	Max blend	FRL ⁴
Fischer-Tropsch Synthetic Paraffinic Kerosene	FT-SPK	Biomass is converted to synthetic gas and then into bio-based aviation fuel.	Wastes (MSW, etc.), coal, gas, sawdust	50%	7
Fischer-Tropsch Synthetic Paraffinic Kerosene and Aromatics	FT-SPK/A	A variation of FT-SPK, where alkylation of light aromatics creates a hydrocarbon blend that includes aromatic compounds		50%	7
Hydroprocessed Fatty Acid Esters and Free Fatty Acid	HEFA	Lipid feedstocks, such as vegetable oils, used cooking oils, tallow, etc. are converted using hydrogen into green diesel, and this can be further separated to obtain bio-based aviation fuel	Vegetable oils: palm, camelina, jatropha, used cooking oil	50%	9
Hydroprocessing of Fermented Sugars - Synthetic Iso-Paraffinic kerosene	HFS-SIP	Using modified yeasts, sugars are converted to hydrocarbons	Sugarcane, sugar beet	10%	5-7
Alcohol-to-Jet Synthetic Paraffinic Kerosene	ATJ-SPK	Dehydration, oligomerization and hydroprocessing are used to convert alcohols, such as iso-butanol, into hydrocarbon	Sugarcane, sugar beet, sawdust, lignocellulosic residues (straw)	50%	7
Co-processing		Biocrude of lipidic feedstock in petroleum refinery processes		5%	6-7

 Table 5: Approved sustainable aviation fuels as per ASTM D5766⁵.

Actual potential for local bio-fuels production are 0.3% of US [1] and 4% of Europe jet fuel demand⁵. The price of SAF obtained from exhausted cooking oil range from 950 to 1015 €/tonne, versus the 600 €/tonne of the conventional jet fuel. Some sources of SAF are used to produce the biodiesel powering road vehicles, thus enabling a competition that is expected to grow in the following years. Current consumption in Europe is very low when compared to the potential production capacity⁵.

The European Union define a SAF as bio-fuels which life cycle greenhouse emissions are reduced with respect to fossil fuels by at least 50% for production plants older than 5 October 2015, 60% for production plants built later, 65% for installations from year 2021. Also, raw materials cannot be sourced from land with high bio-diversity or high carbon footprint. The consideration of the life cycle is important because, even if a biomass grows by absorbing the same amount of CO₂ produced during its combustion, yielding to a zero net carbon footprint, the cultivation, harvesting, transportation, and conversion of biomass into fuel produce further carbon emissions⁵.

Depending on the biomass source and difference in production chains, a HEFA bio-fuel should reduce the direct greenhouse gas emissions by about 50%, from the 89 gCO₂eq/MJ to the 40-50 gCO₂eq/MJ. Further details are reported in Table 6. It is here remarked that these estimates do not include indirect effects as land use change (e.g. a cropland previously used for agriculture)⁵. Having the same basic molecular structure (i.e. hydro-carbons), the burning of SAF produces the same amount of CO₂ of conventional jet fuel. The so-called pump-to-wake contribution to greenhouse emissions is practically the same. The overall emissions, the so-called well-to-wake, can be reduced up to 90% since most of the emitted carbon is absorbed by new biomass [1].

³ IATA webpage: <https://www.iata.org/contentassets/d13875e9ed784f75bac90f000760e998/saf-technical-certifications.pdf>

⁴ Fuel Readiness Level: http://caafi.org/information/pdf/FRL_CAAFI_Jan_2010_V16.pdf

⁵ EASA SAF webpage: <https://www.easa.europa.eu/eaer/climate-change/sustainable-aviation-fuels>
 D5.1 Enabling Technologies

SAF	Feedstock	Direct emission savings*	Average
FT-SPK-A	Agricultural residues	89-94%	81%
	Forestry residues	88%	
	Municipal Solid Waste (MSW)	68%	
	Short-rotation woody crops	81%	
	Herbaceous energy crops	87%	
HEFA	Tallow	78%	61%
	Used cooking oil	85%	
	Palm fatty acid distillate	76%	
	Soybean	53%	
	Rapeseed/Canola	48%	
	Camelina	54%	
	Palm oil - closed pond	61%	
Palm oil - open pond	29%		
SIP	Sugarcane	62%	65%
	Sugarbeet	68%	
iso-butanol for ATJ	Agricultural residues	71%	67%
	Forestry residues	74%	
	Sugarcane	69%	
	Corn grain	54%	
	Herbaceous energy crops (switchgrass)	66%	
	Molasses	69%	
ethanol for ATJ	Sugarcane	69%	48%
	Corn grain	26%	

*with respect to 89 gCO₂eq/MJ jet fuel baseline

 Table 6: Greenhouse emissions savings (excluding carbon emissions from land use change)⁵.

4.1.4 Electric propulsion

Electric propulsion systems convert the electric energy into mechanical energy, which is converted into thrust by a propeller or a fan. They are an effective way to reduce pollutant emissions as long as the energy sources are renewable. Electric propulsion can be all-electric, hybrid-electric, and turbo-electric. There are several variants of the logic schemes of an electric propulsion system [11–14]. A possible representation of the hybrid series/parallel electric powertrain is given in Figure 6. All of the possible main elements of a hybrid-electric powertrain are present and are connected. The arrows indicate direction of the power flow. The power can flow through electric drives and propellers in both directions. Fuel and gas turbine can only provide power to other devices but cannot absorb or store power. An electric storage like a battery can be recharged in flight. The primary propulsive unit is powered by the gas turbine and may be boosted by an electric drive. The secondary propulsive unit is powered by an electric drive, whatever the source of the electric power, may be a battery, a fuel cell, a gas turbine generator. Gearbox on the secondary propulsive unit can be avoided if the secondary electric drives' rpm match those of the propellers. The following architectures of electric propulsion can be derived from the scheme of Figure 6:

- all electric
- hybrid-electric
 - parallel hybrid
 - series hybrid
 - series/parallel partial hybrid
- turbo-electric

- full turbo-electric
- partial turbo-electric

More details on the architecture can be found in D3.1. From the technological point of view, it is worth to notice that the main difference in the architecture is the “disappearing” of some of the components and the way the remaining are linked. Therefore, the following sections will treat turbo-electric propulsion, where the electric energy is completely generated by a gas turbine, and electric energy sources like battery and fuel cells, which are used in hybrid-electric and all-electric powertrains.

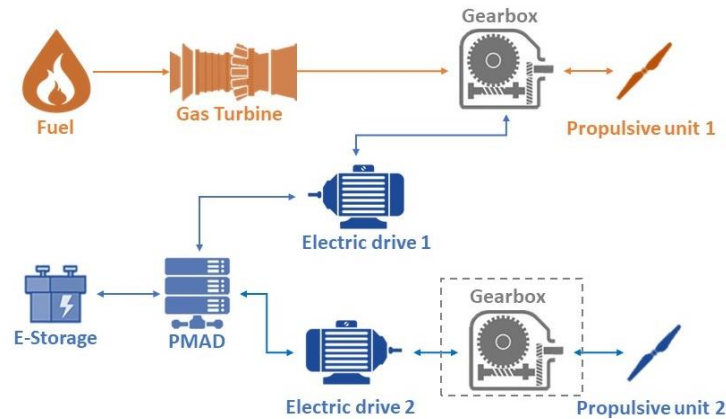


Figure 6: Hybrid-electric propulsion scheme.

4.1.5 Turbo-electric propulsion

The scheme of a turbo-electric powertrain is shown in Figure 7. The propulsion power in a pure turbo-electric powertrain is entirely achieved with electric power, while in a partial turbo-electric powertrain only a fraction of the electric power is converted in propulsive power. The power electronics – power management and distribution (PMAD) system – between the gas turbine and the electric generator allows the former and the electric motors to rotate at different speeds. In this way, the gas turbine may operate at max efficiency most of the time, while propulsive units could be directly installed on the electric motor shaft, if the rotations speeds are compatible (otherwise a gearbox is necessary). In both the full and partial turbo-electric configurations, the power can only flow from the fuel to the propulsive units. In principle, it may be possible to extract power from one propulsive unit and move it to the other, but even with the absence of mechanical losses, there would be an aerodynamic drag increase, hence the system must be sized such that the propulsive units always consume power.

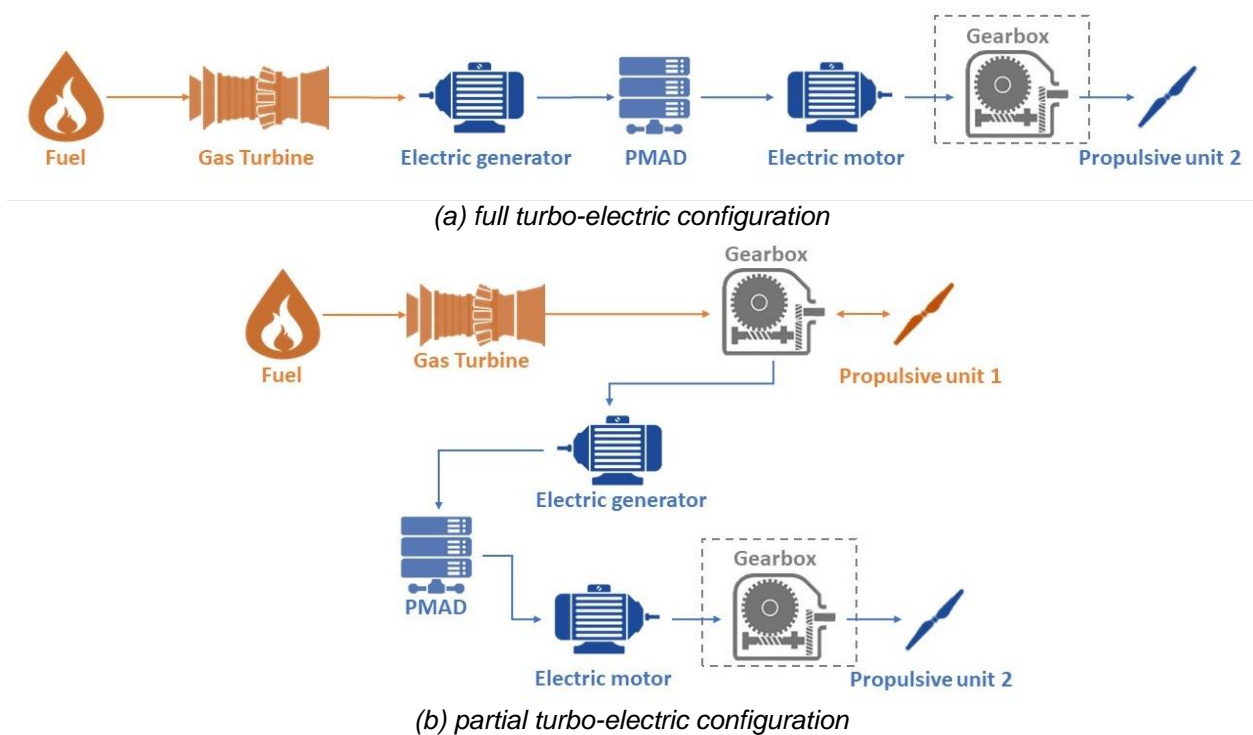


Figure 7: Turbo-electric propulsion scheme.

A turbo-electric concept does not rely on electric energy storage, by definition. The overall efficiency of such powertrain is lower than the conventional gas turbine configuration, because of additional energy conversion and transmission losses. This is apparent from Figure 7. Therefore, the effectiveness of turbo-electric architecture relies on its integration in the airframe, leading to beneficial aero-propulsive interactions that are unfeasible to obtain with a conventional powertrain. In fact, electric propulsion enables the possibility to distribute the propulsors on the wing (distributed electric propulsion, DEP) and to cancel most of the fuselage wake with boundary layer ingestion (BLI), which are discussed in Section 5.

A key benefit of DEP is the reduction of motor size and power required as there are many more motors. Also, electric motors can be easily scaled down, in contrast with gas turbines. The potential applications and time frame for turboelectric concepts will be based largely on projected advances in the specific power of components. Current electric generators installed on in-service aircraft have a specific power around 2.2 kW/kg. Future trends are shown in Figure 8, where most of data is derived from research studies on possible future large passenger airplanes [1]. An average grow of 0.33 kW/kg is forecasted, so that a specific power of 10 kW/kg is expected in the next 25 years.

For commuter and general aviation aircraft it is claimed that the electric motor power, including power electronics will be below 1 MW and the required specific power should be around 7 kW/kg [1]. In April 2015, Siemens announced the development of a direct-drive (2500 rpm), 260 kW aircraft electric motor weighing a little over 50 Kg. The motor specific power is on the order of 5 kW/kg, and it is capable of powering aircraft with a maximum take-off gross mass of 2000 Kg. The potential availability of such an engine suggests that twin-engine commuter aircraft could be powered by electric motors using current technology. It will be the energy source that will determine the potential range of such aircraft and hence their economic viability. This is argument of the following sections.

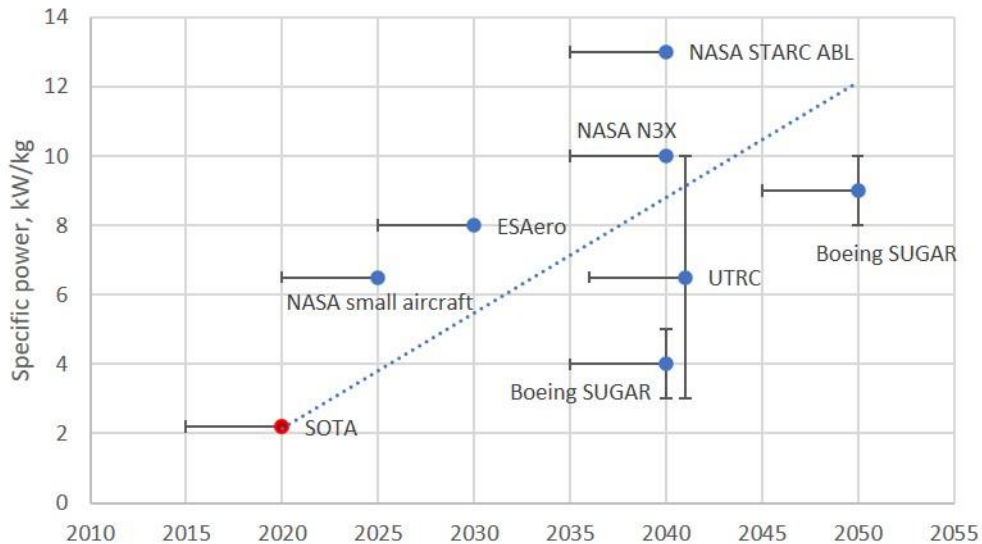


Figure 8: Trend of electric drives specific power. Reproduced from [1].

4.1.5.1 Power electronics, distribution, and thermal management

Power electronics already play a key role for aircraft electrical power systems and that role becomes more critical with turbo-electric propulsion systems. Power electronics are used for power conversion (including motor drives) and power distribution (circuit protection).

Silicon carbide (SiC) power electronics enable MW-class aircraft power due to their improved efficiency and high voltage performance characteristics compared to today's silicon-based power electronics. SiC is also a more reliable technology than silicon in commercial aircraft environments. Specific power for silicon-based power electronics systems today is approximately 2.2 kW/kg for aircraft applications, and their use for circuit protection is limited to 25 A at 270 V DC (7kW). Higher powered circuit protection is provided by mechanical breakers and relays up to about 500 A at 270 V DC (135 kW) using state-of-the-art equipment. It is envisioned that in 20 years SiC-based power electronics systems for aircraft applications will have a specific power of 30 kW/kg⁶ for power conversion and circuit protection using electronic components up to 200 A at ± 270 V (essentially 540 V, for a power capacity of 108 kW) or using mechanical breakers up to 1,000 A at ± 270 V (540 kW). High specific powers will be facilitated by advances in components that make power electronics heavy: switching components, materials, switching topologies, passive filter components such as transformers, packaging, and thermal management components [1]. Especially the passive components (e.g. filters and the DC capacitor) and connection interfaces and housing make the power electronics large and heavy. The power density of power electronic devices can be increased significantly by increasing the switching frequency and by integrating the inverter into the electric machine. Increasing the switching frequency is enabled by SiC technology, which has very low switching losses. High switching frequencies reduce the amount of energy for which the passive filters and capacitors must be sized for.

As concern power distribution, the standard system works at 115 VAC 400 Hz. Smaller and older aircraft use a 28 VDC system and smaller airports may only have a 28 VDC power source. A third option is the 270 VDC standard. The 270 VDC system for aviation was first defined in MIL-STD-704B 17 Nov. 1975⁷. As matter of fact, a higher DC voltage has several advantages: lower cables weight, as cables and converters are lighter. Thus, ± 270 V (or 540 V) standard seems to be the limit for the foreseeable future due to physics-based limits referred to as Paschen curve limits. At this voltage, there will be no electric sparks (due to the breakdown of the dielectric, which is air) whatever the altitude and the gap between electrodes. This voltage is used on the Boeing 787 today, and the U.S. Air Force is investigating the use of ± 270 V for future high power aircraft.

⁶ Rolls-Royce forecast.

⁷ <https://fcxinc.com/benefits-of-270-vdc-in-the-aviation-industry/>

As future turboelectric system concepts include kilovolt-class power distribution systems, new types of insulation systems and electrical conductor spacing rules and practices are required. In fact, as micro voids in the insulation coat of the cables will reduce the breakdown field, partial discharges that may generate will degrade the coat and the time-to-failure due to following a disruptive discharge is a crucial safety issue. The health of the electric insulation is monitored by "insulation monitoring devices" IMD. These measure the total insulation resistance between the conductors (plus and minus) and the aircraft structure. The insulation resistances will degrade over time until a lower threshold is reached at which components need to be maintained. The IMD can measure the insulation resistance of the entire system, even those of the electric machines behind a power electronic device. The measurement can be performed once per minute and while the system is operating. Like this, the failure of the insulation due to partial discharge and ageing can be predicted quite well.

Also, a higher temperature of the air medium between electrodes will reduce the thermodynamic pressure, thus lowering the pressure-distance product and trigger an electric discharge [15]. This is the reason for the 270 VDC standard is below the 327 V minimum of the air Paschen curve.

The ability of aircraft to manage heat will be a limiting factor for the high-power electrical power systems needed for turboelectric propulsion. The thermal management system itself will require electrical power to operate, and that power demand will need to be accounted for along with the demands of other non-propulsive power systems.

4.1.6 Batteries

Batteries are electrochemical cells that store chemical compounds holding a voltage difference between the electrodes. The battery (which usually is made up of several individual cells in series) provides electric energy with a chemical reaction when the electric circuit at its poles is closed. Electrochemical cells convert the energy stored in the chemical bonds directly into electricity, without producing heat or thermal energy as an intermediate stage of the energy conversion process. Because of this, electrochemical cells are not subjected to the Carnot limitations, hence their efficiency as energy in releasing energy can be very high. The total chemical energy that may be converted to electric energy is equal to the exergy of the electrode materials [16].

No combustion takes place; hence batteries are theoretically an alternative to the fossil fuels since no emissions are generated during flight. However, when compared to the jet fuel as energy storage, the current battery technology loses its attraction. The most important parameter is the equivalent specific energy, which determines how much energy can be stored per mass unit. Jet fuel stores about 13000 Wh/Kg, while actual batteries are below 250 Wh/Kg. For regional hybrid-electric turboprop specific energies higher than 500 Wh/kg, ideally 800 Wh/kg, are needed. For an all-electric system, the required specific energy may be around 2000 Wh/kg, if the actual design range are to be kept [1,12,13,17].

A trend on specific energy derived from NASA/Boeing Sugar study (Figure 9) indicates that an increment of 7.6% per year is needed to achieve 750 Wh/kg by year 2030 [18]. Although additional improvements are foresighted, it is unlikely that an electrochemical cell or a super capacitor may achieve more than 1500 Wh/Kg, while even 500 Wh/Kg within year 2035 seems optimistic. Current trends in battery technology concern Lithium-Ion, Lithium-Sulphur, and Lithium-Oxygen cells. Expected achievements by year 2035 *at cell level* are reported in Table 7. While theoretical specific energy are much higher than those reported, in practice the attained value will be significantly lower, because of the added weight of current collectors, electrolytes, separators, battery cases, and terminals. Even if specific energies of 1500 Wh/kg may be achievable, such high specific energies will require major breakthroughs. Furthermore, the requirement to simultaneously achieve long cycle life, low cost, and acceptable safety greatly increases the complexity of the overall challenge [1]. *At pack level* the specific energy will further decrease, due to the additional weight of casing and connectors. Packaging of electrochemical cells is necessary to achieve the desired voltage. A single Li-ion cell has a nominal voltage from 3.3 V to 4.0 V, with a typical value of 3.7 V, depending on the component bound to the lithium [16].

Lithium-ion batteries currently dominate the market in both consumer electronics and electric vehicles. Batteries can be scaled to meet power and energy requirements for aviation, as lithium-ion battery systems with power capability greater than 10 MW and energy storage capacity greater than 10 MWh have already been demonstrated in stationary energy storage for electric

utility applications [1]. The maximum theoretical specific energy that can be obtained by chemical reaction is about 550 Wh/Kg. In practice, a single cell is around 210 Wh/kg and a cell pack, necessary to achieve the desired voltage, is about 150 Wh/Kg [19,20]. As regards safety, Li-ion batteries have proven to be susceptible to thermal runaway, a process where in which the heat from a failing cell causes itself and surrounding cells to fail, thereby generating more heat. This happened to the Boeing 787 Dreamliner of Japan Airlines and, together with an emergency landing to another 787 of All Nippon Airways, prompted the U.S. Federal Aviation Administration to ground the entire 787 fleet in 2013⁸. In conditions like overcharging, the high local temperatures can release oxygen from the cathode. If the oxygen reacts with the flammable organic electrolyte there is a serious risk of combustion and even explosion. Improvements of Li-ion batteries regard lighter casing and safer electrodes and electrolytes. This should lead to specific energies between 250 and 350 Wh/kg at cell level by year 2035 [21].

The lithium-sulphur combination is being investigated to increase the specific energy of lithium batteries. The chemical reaction provides a maximum of 2500 Wh/Kg, while specific energies of 300-350 Wh/kg at cell level and 200-250 Wh/kg at pack level are available [20]. Lower TRL Li-S batteries with specific energy of 600 Wh/kg have been tested in controlled environment, hence it is expected that such values could be achieved by year 2035 for electric aircraft propulsion. The practical application of Li-S batteries is hindered by very low life cycle and low efficiency that does not permit the full extraction of the chemical energy. Both of these drawbacks could be overcome by the application of nano-structures and graphene at the electrodes [21].

The lithium-oxygen (also known as lithium-air) technology is the most promising concept for Li-ion batteries. The maximum theoretical specific energy is about 3450 Wh/Kg, with actual battery packs for ground vehicles ranging from 300 to 700 Wh/kg and 400 Wh/kg at system level (including the gas delivery system) [22]. It is forecasted a value of 1500 Wh/kg at cell level by 2035 [21], although some authors claim a theoretical value of 11000 Wh/kg [23], quite close to the jet fuel value⁹. Similarly to the Li-S battery, Li-Air cells have problems with safety, low charge and discharge rates, poor energy efficiency and limited life cycles. This is due to the nature of the battery, which needs gaseous oxygen to work. The oxygen may be extracted from the air (open-cycle) and this will theoretically reduce the mass of the battery, since one of the compounds is already present in the air. In practice, impurities as CO₂ and moisture, require a separator and perhaps a purifier to get the oxygen for the chemical reaction. At high altitudes, the oxygen must be compressed to counteract its lower density at ambient conditions. In such open-cycle process, the mass of the battery increases while discharging, due to the additional oxygen bounded to the electrodes, a curious effect for the aviationist used to airplane weight decrease with fuel burn. Such increase is about 0.2 g/Wh [21].

Alternatively, a closed-cycle process eliminates the need for the oxygen separator, compressor, and purifier, but a pressure vessel is needed to keep the oxygen at the desired pressure value. The vessel would naturally pressurize during the charge cycle with only small losses due to heat of the compression. However, the entire battery reactants will be located within the pressure vessel, with the presence of flammable electrodes with pure oxygen, yielding to a non-trivial safety issue. This is complicated by the difficulty of cooling or heating the battery within the vessel. Actually, the forecast provide better achievements for the open-cycle battery [21].

Major technological innovation in "beyond lithium-ion" battery systems will be required to achieve the range of acceptable specific energies needed for commercial introduction of battery-powered electric and hybrid aircraft propulsion systems before these systems can make a significant contribution to reducing carbon emissions in aviation [1].

⁸ <https://www.scientificamerican.com/article/how-lithium-ion-batteries-grounded-the-dreamliner/>

⁹ Ref. [23] also states theoretical specific energy values of aluminum, magnesium, iron, and zinc cells to about 8000, 6800, 1800, and 1300 Wh/kg respectively. However, the same report, dating back to the 1979, projects a 290 Wh/kg value for the Li-Air battery and no attractive commercial applications.

	Unit	Li-Ion	Li-S	Li-O _{2,open}	Li-O _{2,closed}
Specific Energy	Wh/kg	250-350	600-700	800-1500	600-1200
Specific Power	W/kg	500-600	350-500	300-400	300-400
Energy Density	Wh/l	600-800	300-350	1000-1700	1000-1600
Charge/Discharge efficiency	%	90-95	70-90	60-85	60-85
Cycle life #	cycles	1000-3000	1000-2500	500-1000	500-1000
Degree of Discharge	%	70-90	90-100	70-90	70-90
Lifetime	yrs.	7-15	7-14	5-10	5-10
Cost (\$ 2010)	\$/kWh	250-350	250-500	400-800	300-700
Uncertainty	-	low	medium	high	high

Table 7: Trends in future batteries at cell level by year 2035 [21].

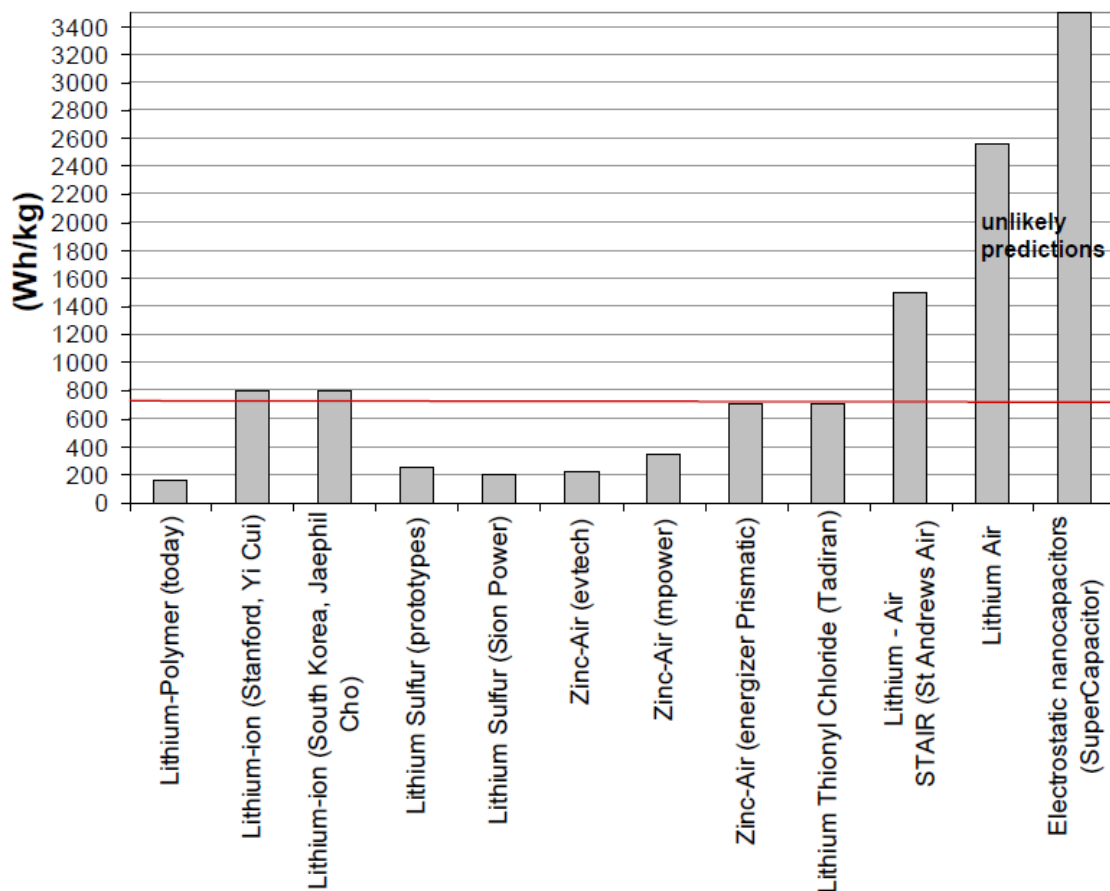


Figure 9: Specific energies of different battery technologies [18].

4.1.7 Fuel cells

Fuel cells convert the chemical energy in a fuel into electrical power without any combustion. The exhaust from fuel cells is totally carbon-free if hydrogen is used as the fuel. However, if a hydrocarbon fuel is used, the exhaust still contains CO₂ in direct proportion to the amount of fuel consumed, but there are no NO_x or particulate emissions [1]. Fuel cells are similar to batteries, but are open thermodynamic systems, which may operate without stop. They are continuously supplied with fluid fuels and oxidants, their electrodes are not part of the reaction process and, hence, do not need to be regenerated or recharged. In general, the oxidant is air at sea level pressure, while the fuel is hydrogen or a hydrocarbon. Fuel cells produce a maximum voltage of the order of 1 V, therefore higher values of the output voltage are achieved by having several fuel

cells in series, or "stacks". Typically, fuel cells are in stacks of 20-30 units, which provide operational voltages close to 30 V [16].

Two types of fuel cells that have been developed for automobile transportation and stationary power generation applications can be considered for aviation. The proton exchange membrane (PEM) fuel cells operate at 80°C to 120°C and require pure hydrogen as the fuel; if a hydrocarbon fuel is used for them, it will have to be first reformed to produce pure hydrogen without any CO, which easily poisons PEM fuel cells. This type of fuel cell works perfectly when replacing the APU as it provides multiple advantages when small sized (e.g.: water generation, etc). However, when sized for primary propulsion, these advantages turn into problems. Especially the low efficiency of 55 to 60% in combination with the low operating temperature from 80 to 120°C make the cooling particularly challenging. Instead, solid oxide fuel cells (SOFCs) operate at 750°C to 1000°C and can use a variety of hydrocarbon fuels, including jet fuels. Fuel cells have been investigated for a variety of aviation applications [1]:

- Auxiliary Power Units (APUs) [24,25]
- Low-altitude aircraft propulsive power [26]
- High-altitude long-endurance aircraft
- Airport applications
- Ground support equipment
- Mobile lighting
- Mobile generators
- Unmanned Air Vehicles [27–31]

Hydrogen is an attractive fuel because of its enormous amount of specific energy (about 40000 Wh/kg against the 13000 Wh/kg of kerosene), it is stable, uniformly available on Earth, the outputs of the chemical reaction with oxygen are pure water and heat, it can be produced by electrolysis of water, and it can be directly fuelled into a PEM fuel cell. As drawbacks it is a flammable and explosive gas, so that it must be carefully stored and transported in special containers, it is the lightest element in the universe, it has a very low density at ambient conditions (0.08 Kg/m³ against the 1.225 Kg/m³ of air), and it must be compressed or liquified to store a significant mass. The hydrogen molecule is so tiny that it may diffuse through metal containers like steel and cause embrittlement and decarburization, in practice it can weaken and break the metal structure of its container [16].

As concern hydrogen storage or production on aircraft, there are at least four solutions available. Pure hydrogen may be stored as a compressed gas in a pressurized tank or as a liquid in a cryogenic tank. It may be also safely stored as a metal hydride, a heavier compound that is stable at ambient conditions that can be safely heated to separate the hydrogen. Finally, the hydrogen can be extracted from a hydro-carbon like jet fuel, a process known as reformation. It has been shown that the reformation process is the lightest solution to generate hydrogen on-board for long range applications [32]. The high specific energy of kerosene as hydrogen source is advantageous in terms of system mass saving, while the hydride tank is the heavier solution, due to the significant mass of the metal compound (more than 90% [25]) which does not participate in the chemical reaction, but it only serves to store the hydrogen at ambient conditions. However, from the system efficiency point of view, the reformer is the worst option because of the lower heating value of the kerosene with respect to pure hydrogen. The metal hydride solution is also penalized from the heat needed to extract the hydrogen from the compound, where the heat produced by the fuel cell itself is not sufficient to enable this process, hence lowering the system efficiency. The pressurized hydrogen seems to be the most efficient solution, followed by the cryogenic tank [32].

Since the objective of the ELICA project is a significant abatement of the aircraft emissions, the use of hydro-carbon, both as hydrogen storage for a PEM or fuel for a SOFC, should be avoided, unless such hydrocarbon is obtained through biomass, thus significantly lowering the CO₂ emission during its life cycle (see Sec. 4.1.3), and its utilization is advantageous in terms of aircraft performance and safety. Otherwise, the storage of pure hydrogen is advised, since it enables higher efficiency and the system mass (fuel cell, tank, air compressor, etc.) is competitive with the mass of the reformer for short flight times (≈100 minutes) [32].

Since a fuel cell can be continuously fuelled to produce electric power, it can be represented as a power conversion unit (hence its contribution to aircraft powerplant performance can be evaluated in W/kg) [1], while the entire system made up of chemical (including storage tank and accessories) plus fuel cell can be valued with the specific energy [27]. Current SOFC power systems have a specific power of less than 100 W/kg compared to about 1000 W/kg for internal combustion engines. SOFCs are being developed for both large-scale stationary power applications (more than 100 kW) and small-scale (1 to 10 kW) APUs and residential applications. SOFCs work better under consistent, steady power conditions; for aviation applications, transient response times, and on/off thermal cycles need to be improved. PEM fuel cells are presently being designed and built for automotive and APU applications, generally in 1 to 100 kW sizes. The hydrogen storage and operation at altitude remains a challenge [1]. Dealing with PEM challenges related to the maturity of the technology, the cell aging is faster if compared to the alternatives (e.g.: piston engines) and the management of toxic waste produced during the membrane production has high environmental and manufacturing costs. The environmental impact of fuel cell production needs to be inspected in detail. Moreover, the acquisition costs of PEM are still two orders of magnitudes above the alternatives employed in automotive industry. Current PEM specific power also are around 100 W/Kg, depending on flight time and assuming a constant electric power [32]. Because of their low specific power, fuel cells are often installed in a hybrid system with a battery or other power sources to boost the power when required, while the fuel cell supplies a nearly constant load [24–26,28,33,34]. Specific power of hybrid SOFC systems range from 150 to 500 W/kg [25].

The efficiency and voltage of a fuel cell stack significantly reduce when high currents are required. An entire PEM fuel cell system (hydrogen storage, air compressor, electrolyze recharger, fuel cell, etc.) with a charge efficiency of 80% and a discharge efficiency of 50% may achieve more than 320 Wh/kg, a specific energy higher than today advanced batteries or small internal combustion engines (about 200 Wh/kg) [27]. A less recent work [30] calculates a 125 Wh/kg specific energy for a long endurance, small UAV, a value comparable to the internal combustion engine conventionally installed, which generates more noise and a bigger thermal signature. Others claim to have designed a UAV with a 360 Wh/kg fuel cell system [31]. Long range (>2000 km) UAV would need fuel cell system with 600 Wh/kg [29]. The by-product of a fuel cell may be also exploited to provide water and inerting gas for filling the emptying kerosene fuel tank, although these solutions are more attractive for commercial flights [32].

Thus, it seems that fuel cells alone are competitive only for small aircraft and yet even in low altitude, short range applications they would better be coupled with batteries, ultracapacitors, internal combustion engine or gas turbine to cope with the high power required during transient manoeuvres. Table 8, Figure 10 and Figure 11 resume the presented data and attempt to establish a trend in fuel cell performance, although not all authors explicitly declare specific power and energy, some results are only design, and others are laboratory applications or installations on small UAVs. A trend may be extracted from specific energy data (an increase of 65 Wh/kg per year), but not on specific power, due to the data scatter. In conclusion, it may be stated that fuel cells will be attractive if the entire electrical energy generation system provides a comparable or superior performance with future batteries specific energy (say 600 Wh/kg by 2035) and specific power, with equal safety.

Authors	Year	Technology	Spec. Energy (Wh/kg)	Spec. Power (W/Kg)	MTOM (Kg)	Notes
Kim et al. [36]	2012	PEM	165	n.a.	2.1	Sodium borohydride (NaBH ₄) as hydrogen source. Battery supports fuel cell, but has not considered in the specific energy calculation
Rhoads et al. [31]	2010	PEM	360	n.a.	13.4	24 hours endurance
Bradley et al. [30]	2009	PEM	125	n.a.	12.5	24 hours endurance
Bradley et al. [27]	2007	PEM	7.1	52	16.4	320 Wh/kg may be achieved if fuel cell powerplant scaled linearly (from 800 Wh/kg of compressed hydrogen, 80% charge efficiency, 50% discharge efficiency)
Renouard-Vallet et al. [32]	2012	PEM	330	n.a.	n.a.	Simulation with 50 kW of electric power and system mass (H ₂ tank) scaled for 200 min of operation
Nicolay et al. [35]	2020	PEM	n.a.	1160	1261	Installing the Toyota MIRAI fuel cell stack with a specific power of 2.0 kW/kg
Dudek et al. [37]	2013	PEM	530	117	5.5	Installing the AEROPACK by Horizon Fuel Cell Technologies
Herwerth et al. [38]	2007	PEM-hybrid	n.a.	70	5	The fuel cell system without battery gives 51 W/kg, the fuel cell stack alone gives 600 W/kg
Yang et al. [39]	2016	PEM-hybrid	n.a.	76	21.2	Battery is used for take-off and climb, while fuel cell for cruise
Freeh et al.	2005	SOFC-hybrid	n.a.	230	n.a.	Weight and power data resumed by Santin et al. [25]
Bundschuh et al.	2006	SOFC-hybrid	n.a.	155	n.a.	
Nether et al.	2005	SOFC-hybrid	n.a.	326	n.a.	
Rajashekara et al.	2006	SOFC-hybrid	n.a.	500	n.a.	
Mak and Meier	2007	SOFC-hybrid	n.a.	360	n.a.	

Table 8: Fuel cells performance in aircraft applications. Specific energies and powers refer to the fuel cell system (including tank, etc.). MTOM refers to the entire aircraft gross mass.

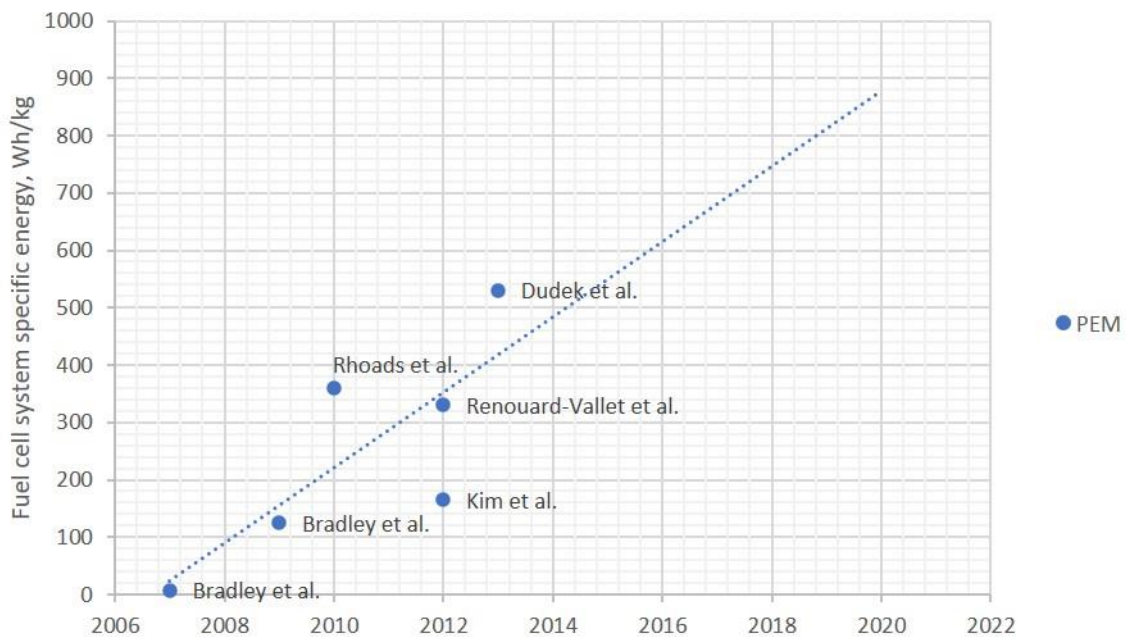


Figure 10: Specific energy of fuel cells systems for aircraft applications.

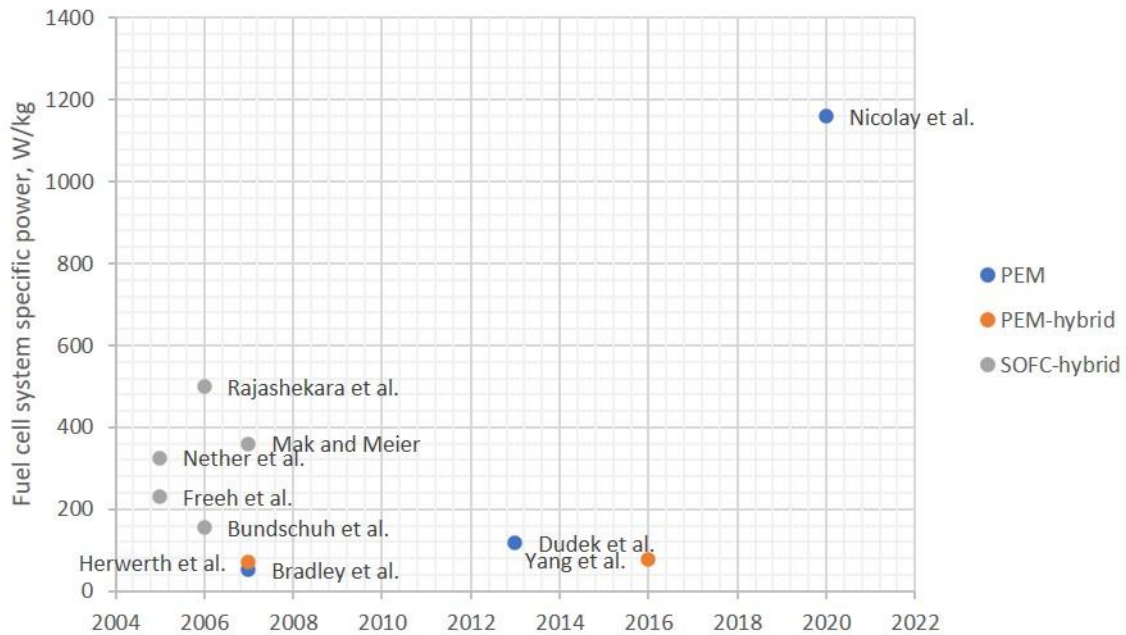


Figure 11: Specific power of fuel cells systems for aircraft applications.

4.1.8 Hydrogen-fuelled aircraft

Hydrogen-fuelled aircraft are dealt in a different section of the present work to cover both the use of hydrogen as alternative power source for conventional and hybrid-electric propulsive systems and for fuel-cell. In the first type of hydrogen combustion system, thrust is generated through the combustion of hydrogen in a modified jet engine, which eliminates most but not all green-house gases emissions. Overall, the transition would require less aircraft and engine redesign than hydrogen fuel cell propulsion, making it somewhat less disruptive to the current setup of the aerospace industry. On the other hand, hydrogen fuel cell (HFC) are a near-zero emission solution as the only output of fuel cells is water vapor, the impact of which can be minimized through careful aircraft operation. Moreover, considering the high efficiency of hydrogen fuel cell, the efficiency would be increased from 20% to 40% with respect to hydrogen combustion designs¹⁰. Considering these benefits, hydrogen application in aviation industry are approaching to fuel cell solutions. Table 9 shows ongoing projects on applications of hydrogen applied to aircraft propulsion.

Project	Range (km)	Seats	Power System	Status
HY4	1000	4	Hydrogen Fuel Cell and Batteries	Flown
HES Element One	500-5000		Hydrogen Fuel Cell	Under Development
Alaka'i Skai	640		Hydrogen Fuel Cell	
Apus i-2	1000		Hydrogen Fuel Cell	
NASA CHEETA	-		Hydrogen Fuel Cell	
Pipistrel E-STOL	-		Hydrogen Fuel Cell	
ZeroAvia	800		Hydrogen Fuel Cell	
Airbus Cryoplane	-		Hydrogen Combustion	Feasibility study
NASA Concept B	6500		Hydrogen Fuel Cell	

Table 9: Research and Industrial Projects applying hydrogen technologies.

¹⁰ <https://www.rolandberger.com/en/Publications/Hydrogen-A-future-fuel-of-aviation.html>

Hydrogen technology is not currently ready for a mature application in aviation industry. Some challenges should be faced before that moment. First, the propulsive system is a minor issue if compared to the fuel storage challenge due to the required light-weighting storage tanks for aviation application, which should, at the same time, have a safe and complex cryogenic cooling systems. To take advantage of hydrogen's high energy density, the cooling system of the tank is a critical element. A comparison between gravimetric (specific) and volumetric energy density among different technologies is reported in Table 10. Second, the cost of production methods for "green" hydrogen in order to compete with kerosene on a cost basis. Third, the so called "green" hydrogen, which is the result of an emission-free hydrogen production, is still not possible on large scale.

Technology	Gravimetric Energy Density (kWh/kg)	Volumetric Energy Density (kWh/l)
Fuel	12.0	10.4
Jet Fuel + Storage System	8.9	9.5
Current Batteries	0.3	0.8
Hydrogen (liquid)	33.0	2.4
Hydrogen (liquid) + Storage System	10.0 – 21.0	1.6 – 2.1

Table 10: Comparison of energy carriers and storage solutions in terms of gravimetric and volumetric energy density.

A recent Clean Sky 2 study states that hydrogen propulsion has the potential to reduce CO₂ equivalent emissions¹¹ up to 90% [40]. Hydrogen may be used to produce synfuel (synthetic fuel), a SAF (see Sec. 4.1.3) like a biofuel, but with the potential of obtaining zero net carbon emissions (tank-to-thrust) if CO₂ is captured from air. The production of a synfuel from hydrogen requires electricity, which should be generated in a sustainable way. A synfuel has the potential to reduce the climate impact up to 60% with respect conventional (kerosene) aviation.

Hydrogen may be also directly used as a fuel with minor gas turbine evolution if the installation of a cryogenic tank (20 K) on aircraft to provide liquid hydrogen (LH₂) is feasible. The jet engine would require additional heat exchangers to heat the hydrogen from tank temperature to injection conditions [41]. Such feasibility may be achieved on short/medium range aircraft with lighter LH₂ tanks, bringing the system energy density to 12 kWh/kg and climate impact reduction to 75% [40]. It is expected that a hydrogen-powered commuter aircraft should be a revolutionary design, with a fuel cell system with a specific power of 2 kW/kg and distributed electric propulsion (see Sec. 5.1) to enhance the aerodynamic efficiency. It is also expected that such aircraft could be commercially available in the next 15 years. Such revolutionary design may have a 90% climate impact reduction, weight 15% more and cost 5% more (cost per available seat kilometre) [40], see Figure 12 and Figure 13.

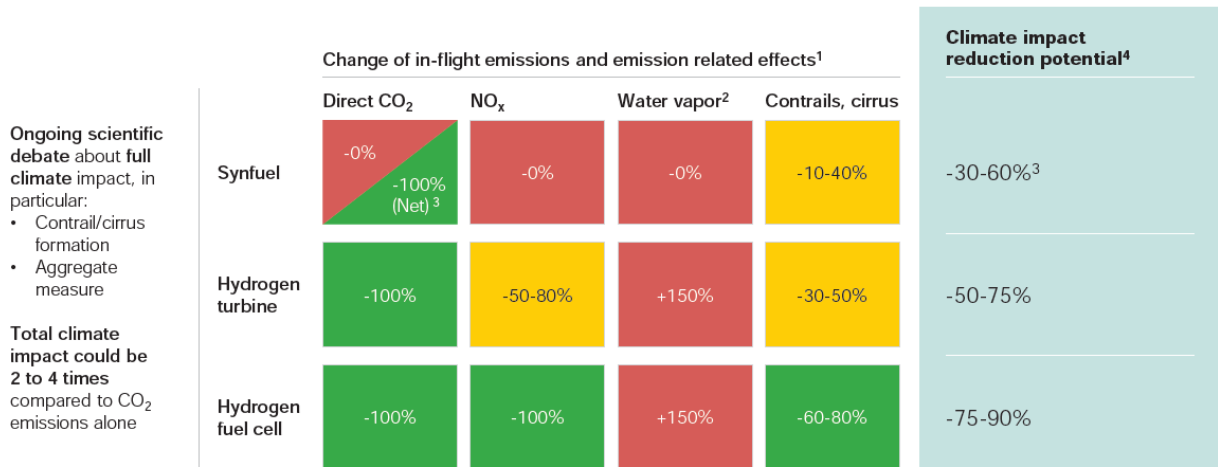
Of course, airports will require minor changes in a short time frame (2035) if the transition to the hydrogen fuel technology is coordinated with regulators and airlines and starts with few operators, then major changes are expected as hydrogen consumption increase and bigger aircraft shall be served [40].

¹¹ By equivalent CO₂ emissions it is meant a climate impact of non-CO₂ emissions comparable to CO₂ emissions. These include NO_x, water vapor, soot, contrails/cirrus formation.

Exhibit 4

Comparison of climate impact from H₂ propulsion and synfuel

Compared to kerosene-powered aircraft, timeframe until 2100



1. Assuming decarbonized production and transportation of fuels in 2050
2. 10 times lower climate impact than from CO₂ emissions
3. Net CO₂ neutral if produced with CO₂ captured from the air
4. Measured in CO₂ equivalent compared to full climate impact of kerosene-powered aviation

Figure 12: Forecasted climate impact (tank-to-thrust) of new aircraft fuel systems [40].

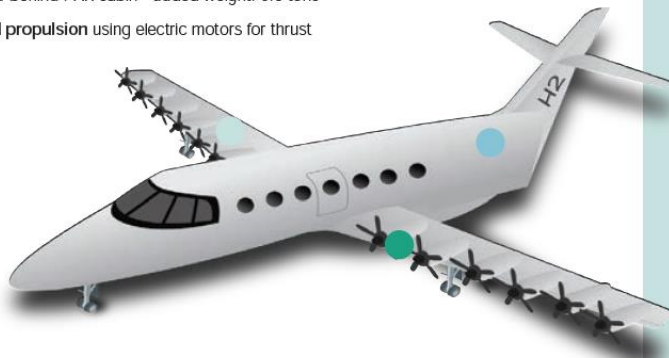
Exhibit 6

Commuter aircraft powered by fuel cells

Revolutionary aircraft

Design mission: 19 PAX, 500 km range, cruise speed 500 km/h

- Highly efficient wing
- 2 LH₂ tanks behind PAX cabin - added weight: 0.5 tons
- Distributed propulsion using electric motors for thrust



1. Major assumptions: 25% gravimetric index of LH₂ tank, 90% useable LH₂ fuel, FCS mass 1.5 kW/kg (incl. cooling) and 58% peak efficiency (LHV), e-motors and PMAD with 97% efficiency, battery with 0.6 kWh/kg
2. Cost per available seat kilometer
3. Maximum take off weight

Figure 13: Economic and climate impact of a revolutionary commuter aircraft [40].

5 Aerodynamics

Improvements in aerodynamics have direct impact on the whole aircraft performance. From the beginning of aeronautics up-to-date, researches in the aerodynamic field are pushing the aircraft technology to ever improved performance.

An improvement in terms of aerodynamic can be achieved by both upgrading *current designs* and adopting innovative technologies, by keeping in mind that such an introduction should not only guarantee a positive impact on A/C main performance but should also contribute strongly to product cost and operability.

ICAO identifies several aerodynamic assets potentially leading to drag reduction¹²:

A. basket improving viscous drag

- Riblets
- Active turbulence control
- Natural laminar flow
- Hybrid laminar flow control

B. basket improving non viscous drag

- Increased wingspan (increased aspect ratio)
- Improved aero tools
- Excrescence reduction
- Variable camber with control surfaces
- Morphing wing

Each one of the previous technologies properly actuated could potentially allow a drag reduction, improving the aircraft performance (suitable for such aircraft category rather than other).

Another potential asset, emerging in the last decade (one of the most investigated technology) has been the **Distributed Propulsion** (DP). DP can be described as a propulsion system where the vehicle thrust is produced from an array of propulsors located across the air vehicle. While a formal definition of a DP system has not yet been established, in general the distributed thrust capabilities of a DP system should serve an enabling role in improving the system-level efficiency, capabilities, or performance of the air vehicle. Otherwise, any aircraft with more than one propulsor could be classified as such. DP could improve aircraft aerodynamic not only for what concerns the drag coefficient, but also improving the lift characteristics.

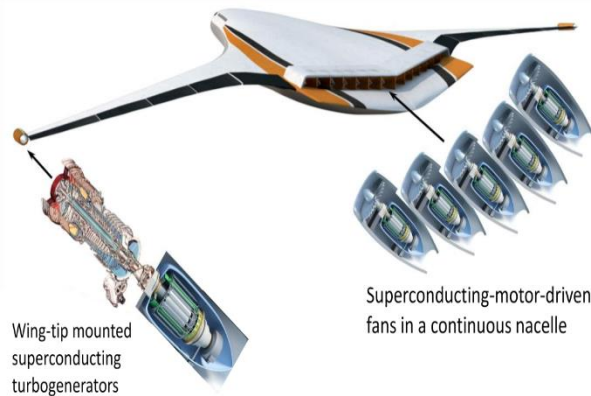
In the following paragraphs, a selection of the most promising technologies to be applied on hybrid commuter aircraft is done.

5.1 Distributed Propulsion

Distributed electric propulsion (DEP) concepts for aircraft systems has enabled new possibilities in the overall efficiency, capabilities, and robustness of future air vehicles. Distributed electric propulsion systems feature the novel approach of utilizing electrically driven propulsors which are only connected electrically to energy sources or power-generating devices. As a result, propulsors can be placed, sized, and operated with greater flexibility to leverage the synergistic benefits of aero-propulsive coupling and provide improved performance over more traditional designs[42]. Several conventional aircraft concepts that utilize distributed electric propulsion have been developed, along with various short and vertical take-off and landing platforms. Careful integration of electrically driven propulsors for boundary-layer ingestion can allow for improved propulsive efficiency and wake-filling benefits. The placement and configuration of propulsors can also be used to mitigate the trailing vortex system of a lifting surface, by using a "tip-propeller" or leverage increases in dynamic pressure across blown surfaces for increased lift performance, so called "high-lift propellers" or blowing. Additionally, the thrust stream of distributed electric propulsors can be utilized to enable new capabilities in vehicle control, including reducing requirements for traditional control surfaces and increasing tolerance of the vehicle control system to engine-out or propulsor-out scenarios. Furthermore, the small propulsors of a DEP system can be installed to leverage an acoustic shielding effect by the airframe, which can further reduce noise signatures.

¹² Appendix A of ICAO Doc. 9988

The rapid growth in flight-weight electrical systems and power architectures has provided new enabling technologies for future DEP concepts, which provide flexible operational capabilities far beyond those of current systems. While several integration challenges exist, DEP is a disruptive concept that can lead to unprecedented improvements in future aircraft designs. Several examples of disruptive configurations using DEP technologies can be seen in Figure 14.



NASA N-X3. Nasa image



NASA X-57. Nasa image



STARC-ABL. Nasa image



Aurora Flight Sciences XV-24 LightningStrike aircraft. Image Aurora Flight Sciences



Esaero-ECO 150. Esaero image



Joby S2 aircraft, JobyAviation



Volotea-DANTE aircraft. Image newsroom.aviator.aero



Eviation's Alice aircraft. Image ainonline.com

Figure 14: Disruptive configurations using DEP technologies.

In recent years, the increased popularity of the DEP concept and the rapid developments in electrical machinery for aircraft applications have enabled a variety of new technologies and aircraft concepts to be developed. DEP aircraft concepts generally involve the use of multiple electric propulsors around an airframe with one or more independent electric generators or energy storage devices. Based on currently-available and near-term electrical components and subsystems, there are now a number of electric aircraft concepts that are configured and even manufactured at various organizations throughout the world. However, due to the limited specific power or specific energy density of currently-available hardware, the majority of early adopters of this technology have been found in small aircraft applications. With the enduring interest of increasing efficiency, decreasing operating costs, and encouraging environmental responsibility of larger commercial aircraft applications, there are now a number of organizations investing in and researching DEP aircraft systems for larger passenger and cargo-carrying capabilities[42]. One of the inherent features of a DEP-enabled aircraft is the tight integration of the propulsion system into the wing-body surfaces of the aircraft [33]. With the increased number of propulsion units near the aircraft's aerodynamic surfaces, a level of aero-propulsive coupling will be present. The manifestation of this coupling depends largely on the type of propulsion unit in use (For example, propeller versus ducted fan) and the proximity of those propulsion units to the wings, tail surfaces, or fuselage. The upside to this facet of a distributed propulsion system is that with careful design, the propulsion-airframe integration (PAI) can be used advantageously. The benefits of aero-propulsive coupling can be broken into several categories. First, a wide range of vehicle configurations which have been developed claim propulsive efficiency benefits due to boundary-layer ingestion. Second, the strategic placement of propulsors can reduce vehicle drag through a variety of mechanisms, including wake filling and vortex suppression. Finally, various applications have been developed which make use of the propeller or fan slipstream interacting with an aerodynamic surface to produce some form of enhanced lift or control authority [42]. Each of these categories of aero-propulsive coupling, which occur on a variety of distributed propulsion aircraft configurations, are discussed in the following paragraphs.

5.1.1 Tip propeller

Wing-tip vortex can be mitigated installing a propeller at the wing tip. The main impact of propeller slipstream on wing performance is to increase the speed downstream of the propeller. A first simple assumption that can be done is that only the speed component normal to the propeller plane is increased. However, this assumption neglects the swirl in the propeller slipstream, whose interaction with the *tip vortex* of the wing causes a variation of induced drag, even more than the increase in axial speed.

In general, the induced drag can be approximated accordingly to Eq. 1, and this is due to the wing finiteness. Reducing the induced angle, induced drag is reduced. As shown in Figure 15, the presence of the wing cause a decrease of the angle angle of attack related to the downwash speed induced. The induced angle of attack due to the wing, also called downwash angle, α_{i_w} can be approximated as in Eq. 2. The effect of the increase in axial speed (red arrow in Figure 15) due to the presence of the propeller is shown. The variation of the axial speed causes an upwash effect counteracting the downwash due to the wing. The actuator disk theory drives the estimation of the axial induction factor at the propeller disk as a function of thrust to weight ratio and the diameter of the propeller, Eq. 3 and finally the axial speed due to the propeller V_p (Eq. 4)

$$C_{Di} = C_L \alpha_i \quad (1)$$

$$\alpha_{i_w} = \frac{w}{V_\infty} = \frac{C_L}{\pi A R e} \quad (2)$$

$$a_p = \frac{1}{2} \sqrt{1 + \frac{8}{\rho \pi V_\infty^2} \frac{T_p/W}{D_p^2/W}} - 1 \quad (3)$$

$$V_p = a_p V_\infty \quad (4)$$

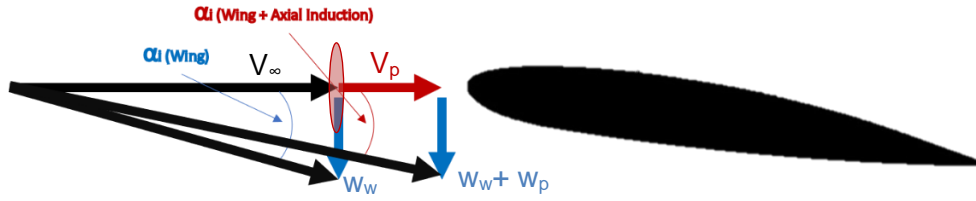


Figure 15: Induced angles due to wing and actuator disk.

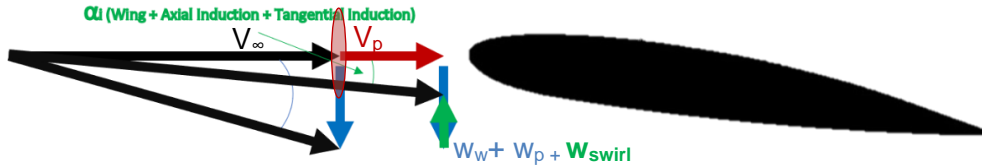


Figure 16: Induced angles due to wing and rotating disk.

Beyond the axial induction, the flow rotation due to the propeller slipstream must be also accounted, as shown in Figure 16. Assuming a certain rotation direction of the propeller, the tangential induction is a measure of the ratio between the propeller angular speed, Ω , and the angular speed induced on the flow downstream of the propeller, ω , and it can be used to estimate the vertical speed, due to the slipstream. The tangential induction due to a propeller can be computed through Eq. 5. The tangential speed, w_{swirl} , perceived in the propeller slipstream is a function of the tangential induction, the tangential speed of the tip of the propeller and the propeller radius, and it can be computed through Eq. 6. Finally, the induced angle can be computed accordingly to Eq. 7

$$a_{pt} = \frac{\omega}{2\Omega} = \frac{1}{2} - \sqrt{\frac{1}{4} - \frac{V^2}{\Omega^2 R_p^2} (1 + a_p)} \quad (5)$$

$$w_{swirl} = a_{pt} \Omega R_p \quad (6)$$

$$\alpha_i = \tan^{-1} \left(\frac{w_w + w_p + w_{swirl}}{V_\infty + V_p} \right) \quad (7)$$

It is clearly understandable that, properly rotating the tip propeller in the opposite direction respect to the tip-vortex (inner-up direction), it is possible to reduce the induced angle of attack and so the induced drag. Numerical and experimental analysis clearly confirm the induced drag reduction due to the tip-propeller properly rotated.

In the 1969 Snyder and Zumwalt [43] proposed that aircraft can be designed using propellers at the wingtips in such a way that the L/D ratio can be varied by changing the effective aspect ratio in flight. An experimental program testing a wing with propellers mounted at the wingtips, showing that the use of a propeller at the wingtip, turning in the direction opposite to that of the wing vortex, shifts the trailing vortex core outboard, decreases the wing drag coefficient, increases the maximum lift coefficient and increases the effective aspect ratio. Rotating the propeller in the opposite direction has the reverse effect. The test model was a reflect-plate $AR = 8$ simply tapered wing, with a tip-nacelle, and 1) a typical 4-blades propeller and a 2) an impeller (shaped something like an orange juice extractor). As they stated, a limitation to the use of a propeller in affecting the wing trailing-vortex was the efficiency of the propeller; about 80% of the energy provides axial acceleration of the air and only about 20% is available to produce rotation with which to supplement or to counteract the trailing vortex and the attendant downwash pattern. Earlier tests of an impeller (shaped something like an orange juice extractor) had shown that the device does produce thrust, but the propulsive efficiency peaks at less than 50% (according to Lippisch, then, 50% of the energy to this propeller is used to produce rotation). This type of propeller was chosen

to serve as the inefficient propeller for these tests. The "orange juicer" is referred to as the **impeller** and the four-bladed propeller is called the **propeller**.

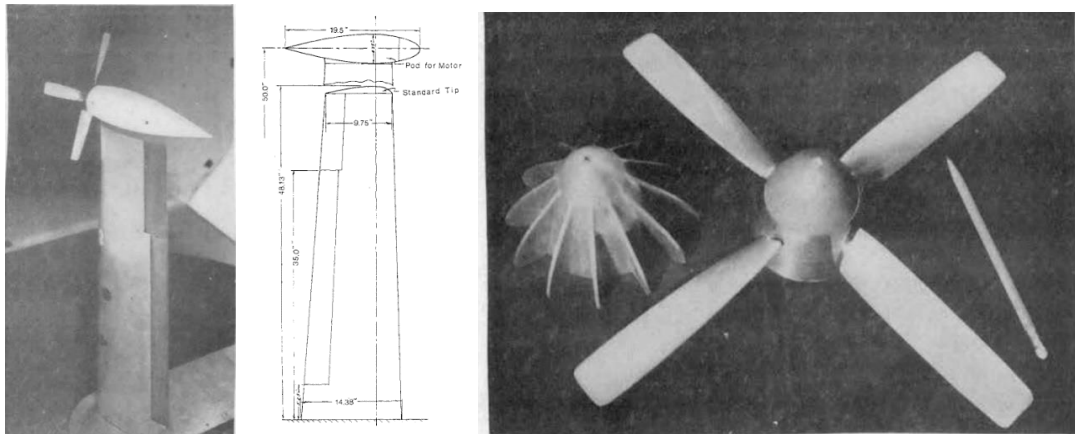


Figure 17: Four blade Tip-Propeller and Impeller models on a AR=8 wing [43].

The main results were summarized in terms of lift coefficient, drag coefficient and effective aspect ratio, i.e AR times e_w , as function of Vortex rotating direction and Counter vortex rotating direction, number of revolution per second, as shown in Figure 18.

Starting from a baseline reference geometry, prop-off, pod with dummy spinner(which can be considered a reference baseline to compare the wing-tip effects), with and $AR_e=6.45$, the propeller allows an increment of AR_e of about 35% (at a certain rotational speed), even better for the impeller, with a increment almost three times the baseline.

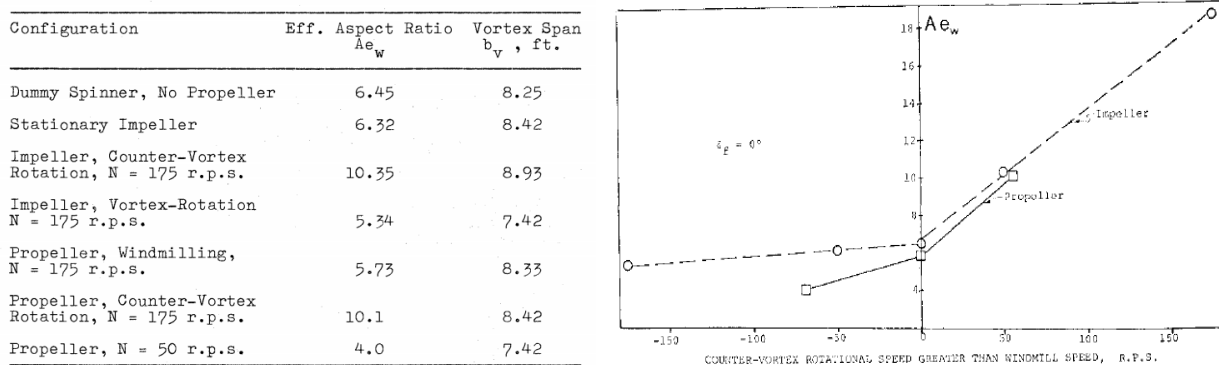


Figure 18: Variation of effective aspect ratio caused by rotor speed, AR=8, $Re=6.7E5$ [43], Baseline $AR_e=6.45$.

By combining results coming from previous experiences, they also summarized the effects as function of engine position in spanwise direction. The results are shown in Figure 19, showing the benefit of counter-vortex rotating propeller on efficiency, AR_e and lift curve slope. Figure 19 illustrates the effects of spanwise position of the propeller on the wing performance. In each case listed there is only one propeller operating at the spanwise position listed. All points plotted correspond to $N=175$ rev/s or 188 rev/s and $T_c = 0.42$ or 0.6. To generalize the results and make them useful, a general curve on the induced drag effect has been drawn. Here, the parameter $\Delta C_D / C_L^2$ has been evaluated for various values of $N d/b$, where N is the difference between rotor speed and windmilling speed, d is the propeller diameter and b the wing span. It was found that $\Delta C_D / C_L^2$ varies with the cube root of $N d/b$. This relation is shown graphically in Figure 19.

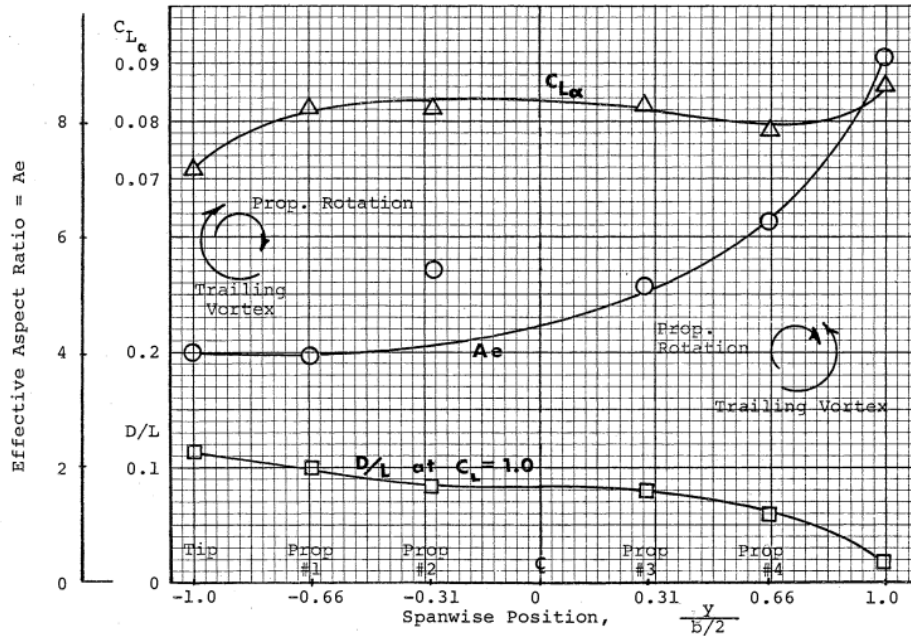


Figure 19: Four blade Tip-Propeller effects on a AR=8 wing, $Re=6.7E5$, $T_C=0.42$ or 0.6 [43].

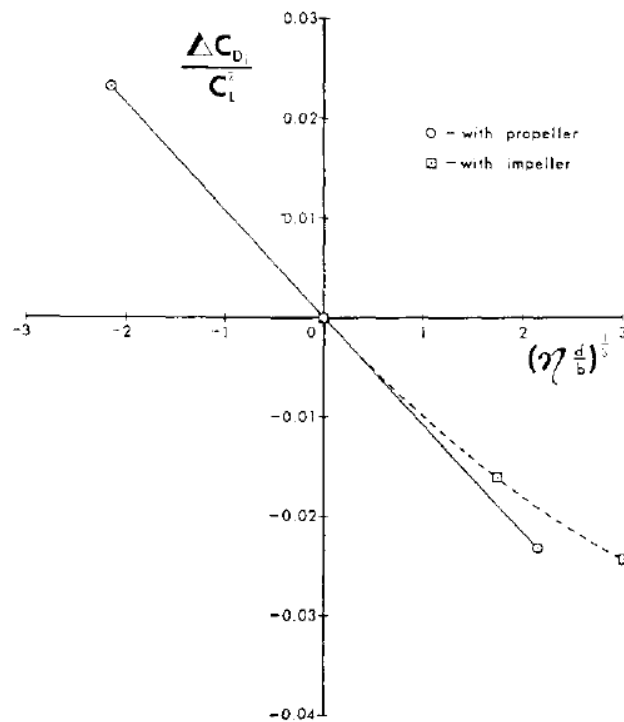


Figure 20: Effect of propeller speed and size on induced drag coefficient [43].

Moreover they already highlight the main disadvantages of this solution including: 1) difficulty (or impossibility) of trimming the aircraft for one engine-out operation; 2) production of aeroelastic problems created by the changing of the torsional moment of inertia of the wing and the interaction of bending and torsional modes of flutter or vibration. Nowadays these drawbacks could be partially overcome with new technologies, design, materials, and powertrain strategies.

In 1989 at NASA the wing-tip pusher propeller on a wing-body configuration with an AR=6.10, analysed in NASA Langley wind-tunnel facility [44], as shown in Figure 21. All tests were conducted at $M=0.70$ and $Re=3.82E6$, within -2 to 4 degrees of angle of attack.

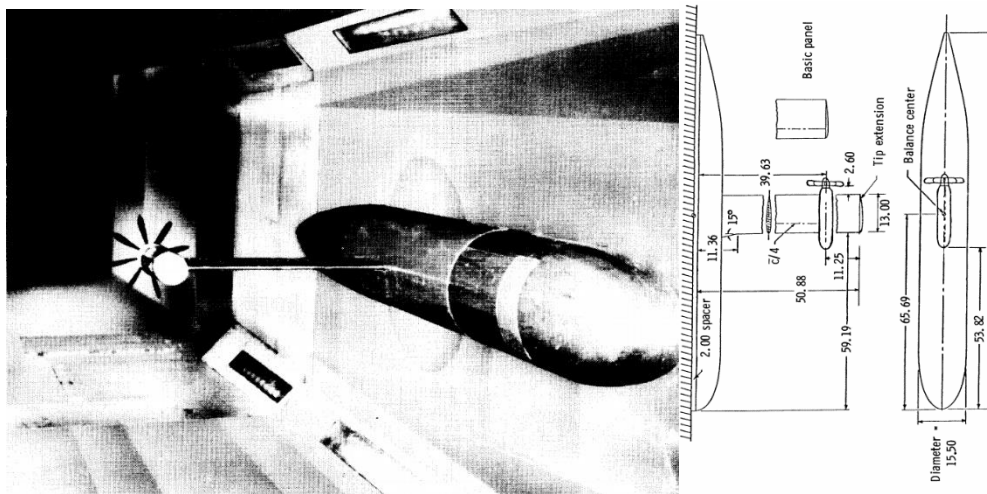


Figure 21: Wing-tip-mounted pusher turboprop model in Langley 7-by-10 foot Speed Tunnel, AR=6.10 [44].

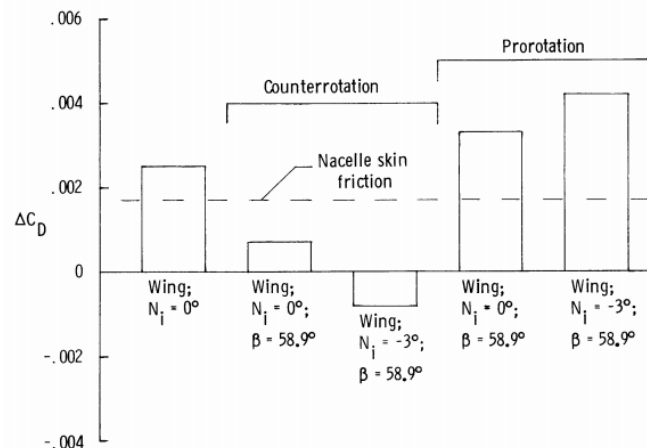
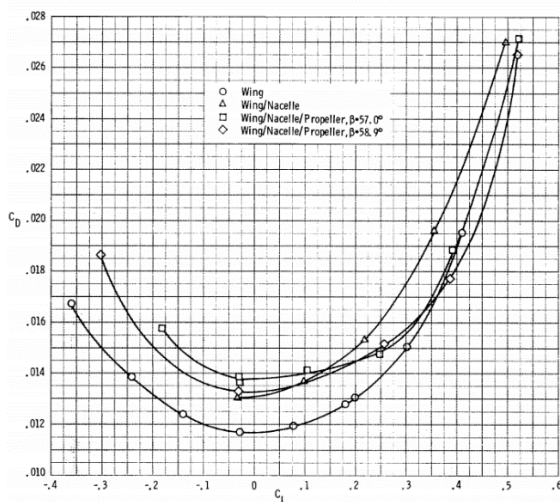


Figure 22: Left: Vortex-propeller interaction on drag coefficient versus lift coefficient for 0° incidence; right: delta drag respect to isolated wing for counter-rotating and pro-rotating wing-tip pusher propeller; $M=0.7$, $Re=3.82E6$ [44].

Main results are shown in Figure 22, where a drag reduction of about 20 drag counts for the counter-rotating wing-tip pusher propeller is achieved, in the range of low value of lift coefficient. In the last decade the NASA program X57 program has investigated also the effect of tip-propeller on the X57 Maxwell aircraft (see Figure 23). A lot of numerical studies were performed, highlighting potential benefits of a tip mounted engine, useful in whole flight phases, reducing the induced drag. Some NASA CFD numerical analyses are shown in Figure 24, for a region of lift coefficients and power settings that are in the vicinity of the steady-state cruise condition. The efficiency difference can be inferred by the relative difference between the unpowered (solid) and powered (dashed) cases in these figures. Results shown an average drag reduction in the range of 20-40 drag counts, slightly dependent from the solvers and transitional model [45], in line with what shown at NASA for pusher wing-tip propeller [44].

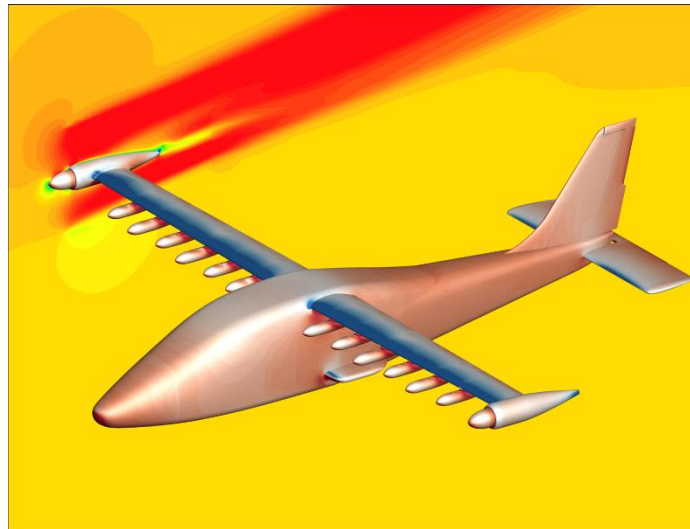
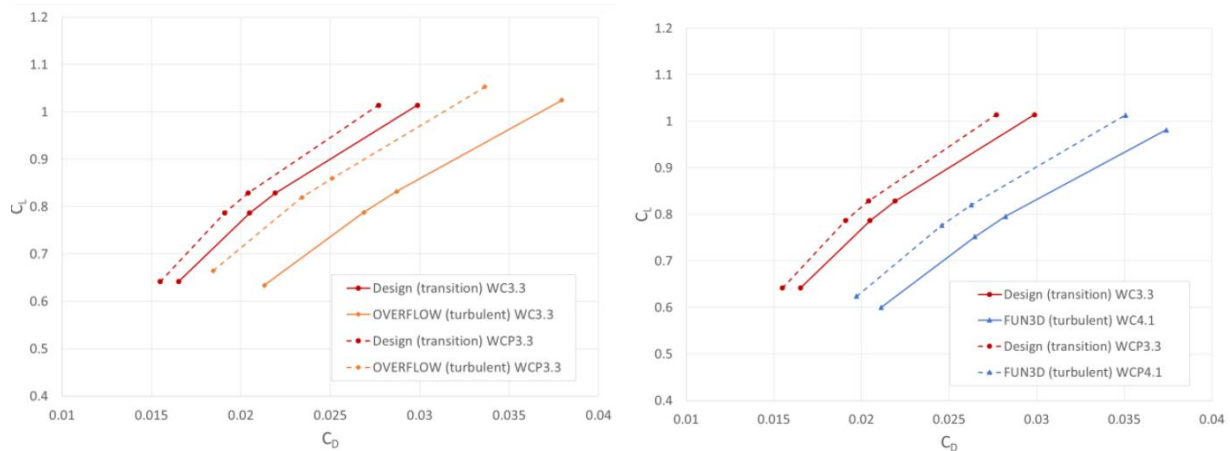


Figure 23: NASA X57 Maxwell numerical analysis of tip-mounted propeller, AR=15.


 Figure 24: Drag Polar Comparison of Power-On (WCP) and Power-Off (WC) Wings [45], $h=8000\text{ft}$, $V=150\text{kn}$, AR=15.

Della Vecchia et alii [2] studied the effects of high-efficiency tip-propeller on the Tecnam P2006T wing, varying the diameter and the thrust level in the range of typical cruise settings. They confirmed the previous results that a high-efficiency propeller (i.e. $\eta_p > 0.8$), allows smaller drag reduction than low efficiency propeller, improving the axial component than the available thrust. Moreover the numerical analyses show that, for a given propeller characteristics, decreasing the diameter, the drag reduction decreases, in the whole range of lift coefficient, while increasing the thrust level, the drag reduction increases (see Figure 25). This behaviour is due to the variation of RPM, which must increase, decreasing the diameter, to provide the same level of thrust. Results globally show that, in the typical cruise attitude of the Tecnam P2006T, a drag reduction of about 10-15 drag counts can be attained for a propeller diameter equal to 1.78m (the same propeller diameter installed on the aircraft).

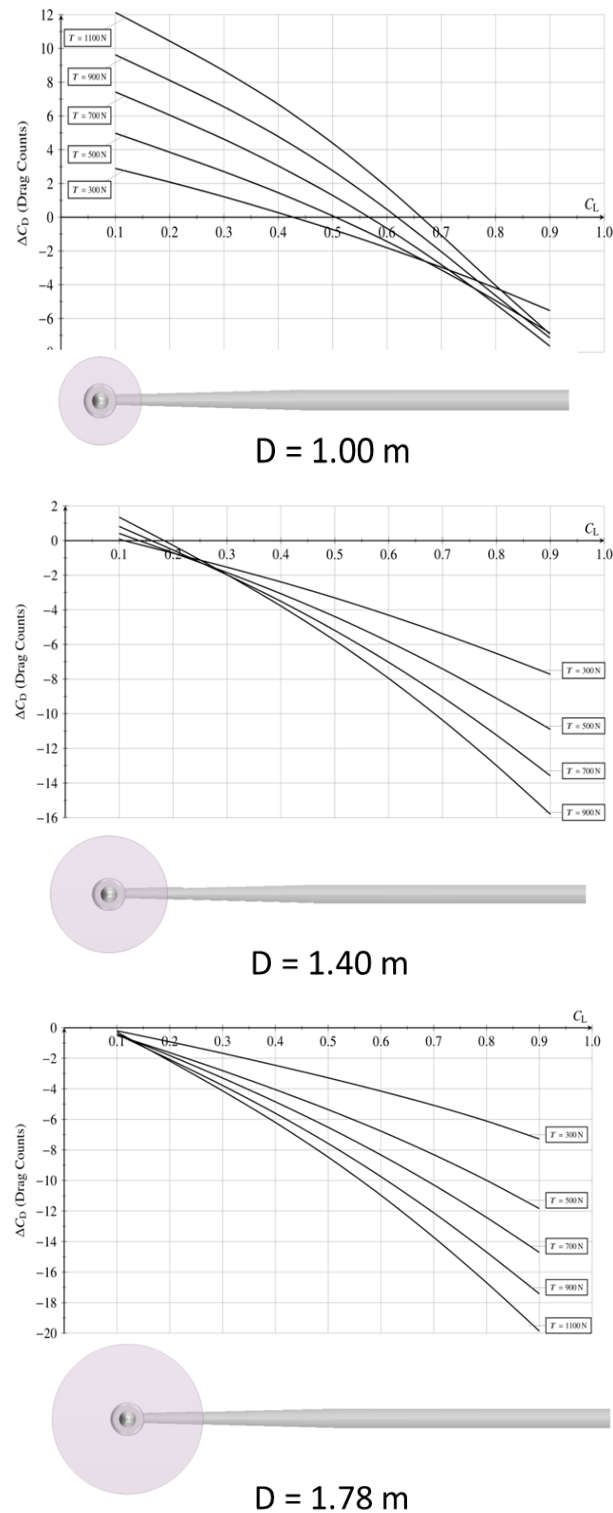


Figure 25: Drag reduction due to high-efficiency tip-propeller, $AR=8.47$, $M=0.23$, $Re=6.9E6$ [2].

At Technical University of Delft, several numerical and experimental studies have been conducted in the last two decades on the wing-tip-propeller, especially on low-and-medium aspect ratio wing from 3 up to 6.2 [46–48]. In one of the last research, they experimented conventional wing mounted configuration, versus wing-tip-mounted propeller configuration, as shown in Figure 26 from Ref. [48].

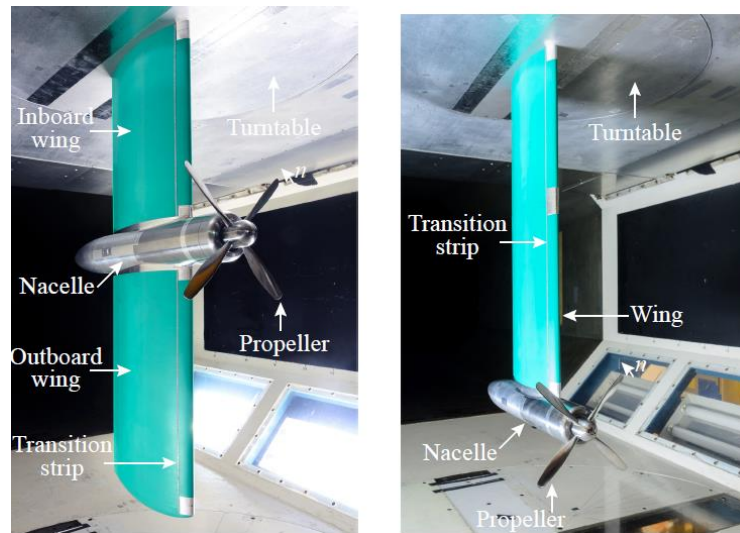


Figure 26: TU Delft, Model II (modular cambered wing) installed in the wind tunnel, AR=6.2(left) and 6.1 (right), conventional (left), tip-mounted (right).

The majority of the measurements discussed in this paper were taken at a freestream velocity of $V_1 = 40$ m/s. This velocity provided the best compromise between achievable Reynolds number and the operating range of the propeller, which was constrained by the output power of the electric motor. The resulting Reynolds number based on the wing chord was about $Re_c = 650,000$, while the Reynolds number based on the propeller diameter was $Re_D = 640,000$. The propeller was operated at four thrust settings, corresponding to advance ratios J of 0.7, 0.8, 0.9, and 1.0. The associated thrust coefficients C_T were equal to 0.123, 0.095, 0.053, and 0.014, respectively, while the Reynolds number at $r/R = 0.7$ was in the range of 130,000-180,000 (for $J = 1.0$ to 0.7). For Model II, additional measurements were taken at $V_1 = 28$ m/s to achieve higher thrust coefficients. At this velocity, the propeller was also operated at advance ratios J of 0.5 and 0.6, resulting in thrust coefficients C_T of 0.168 and 0.144, respectively. The corresponding Reynolds numbers were 455,000 based on the wing chord, 450,000 based on the propeller diameter, and 90,000 to 170,000 based on the effective velocity and chord at $r/R = 0.7$ (for $J = 1.0$ to 0.5), see Ref. [48]. As expected the results shown a drag reduction increasing the thrust setting level and the lift coefficient, leading to a drag reduction of about 30 up to 60 drag counts in a typical C_T range of 0.1-0.2 of cruise lift coefficient 0.5 condition of general aviation small regional aircraft (see Figure 27 and Figure 28).

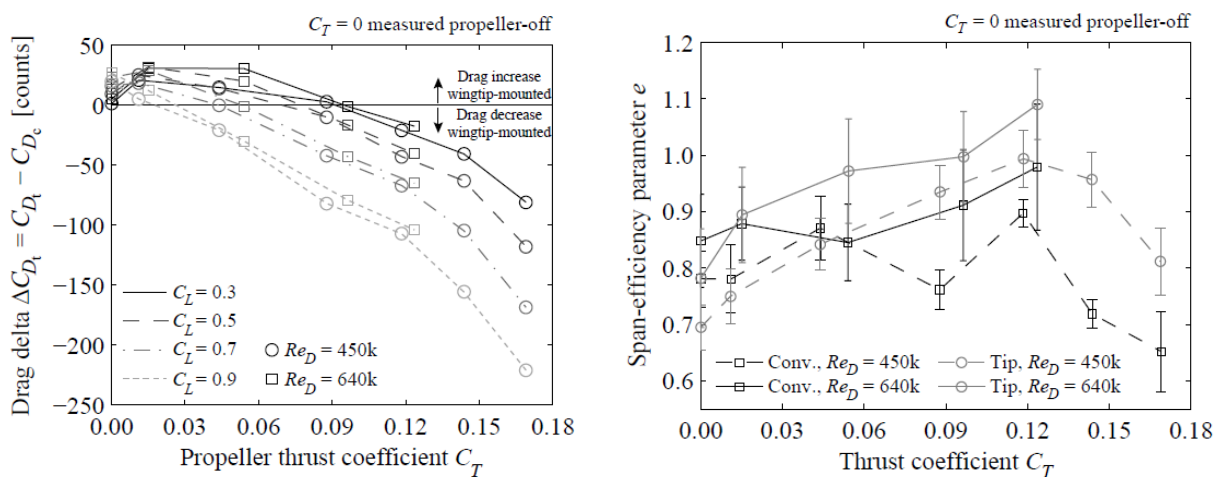
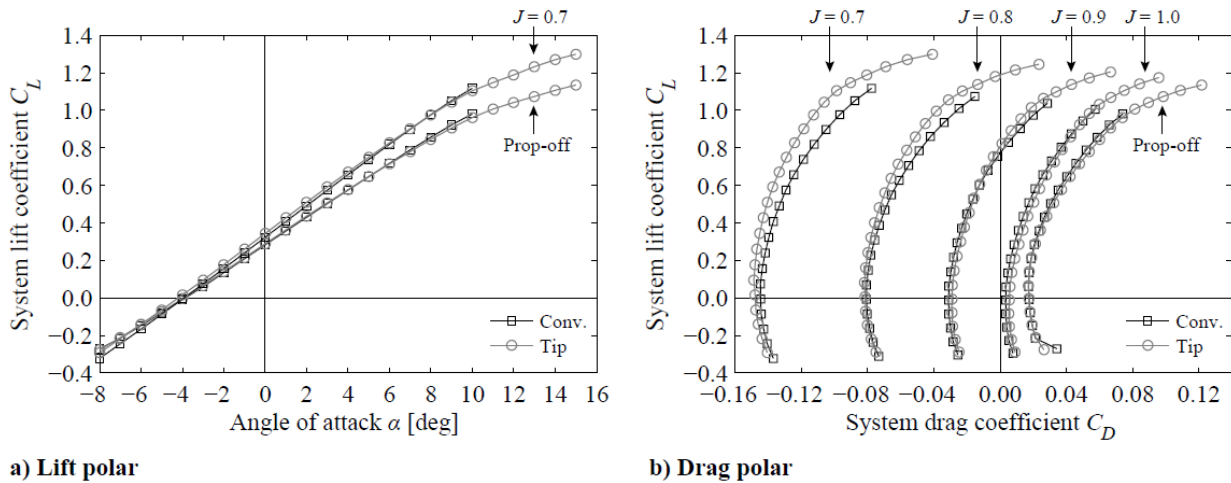


Figure 27: Drag benefit of wingtip-mounted configuration compared to conventional configuration (left) and Effect of propeller thrust setting on the span-efficiency parameter (right).



a) Lift polar

b) Drag polar

Figure 28: Lift and drag polars of the conventional and wingtip-mounted configurations, including propeller forces.

At University of Naples Federico II, high-fidelity Navier-Stokes analyses have been performed on a typical 40 passengers regional turboprop wing, to evaluate the tip-mounted propeller impact, by varying the thrust level and the propeller diameter. High-efficiency propellers, suitable for cruise and climb performance, designed accordingly minimum-induced-loss procedure, have been used to obtain required thrust, changing the number of revolution opportunely.

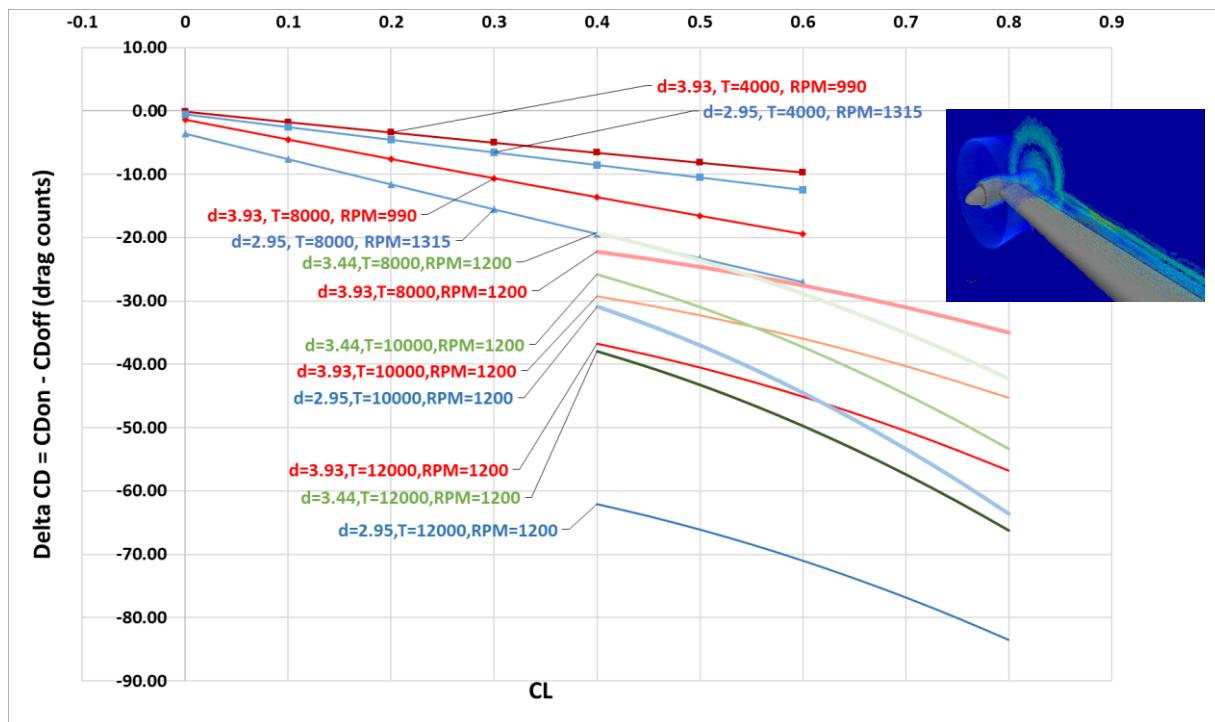


Figure 29: Wing drag improvement due to the propeller tip-mounted on an AR=11 wing, $M=0.48$, $Re=15E6$, Thrust T in Newton.

Results are shown in Figure 29 in terms of wing drag reduction versus lift coefficient, for several thrust settings, propeller diameter and RPM (which means C_T). For a given thrust value, what usually happens is that decreasing the propeller diameter (i.e. increasing the C_T) the drag reduction increases. Increasing the thrust level from 4000 N up to 12000 N (three times more), the drag reduction increases of about 4-5 times.

As conclusion, it is clear that a properly counter-rotating tip-mounted propeller can reduce the induced drag, improving the aerodynamic efficiency, accounting directional control and structural drawbacks.

5.1.2 High-lift propeller

DEP system can be incorporated into the airframe to augment high-lift capabilities at low speed. One popular example is the NASA X-57 Maxwell aircraft (see Figure 30), which is based on a Tecnam P2006T aircraft fuselage and reconfigured with a much smaller wing than the baseline aircraft. The smaller wing is achievable for this design due to the high lift provided by 12 small electric propellers along the leading edge of the wing during the take-off and landing phases of flight. The purpose of having these distributed propellers is to increase the dynamic pressure, hence the lift, over the wing at low speed [49].



Figure 30: NASA X57 Maxwell rendering.

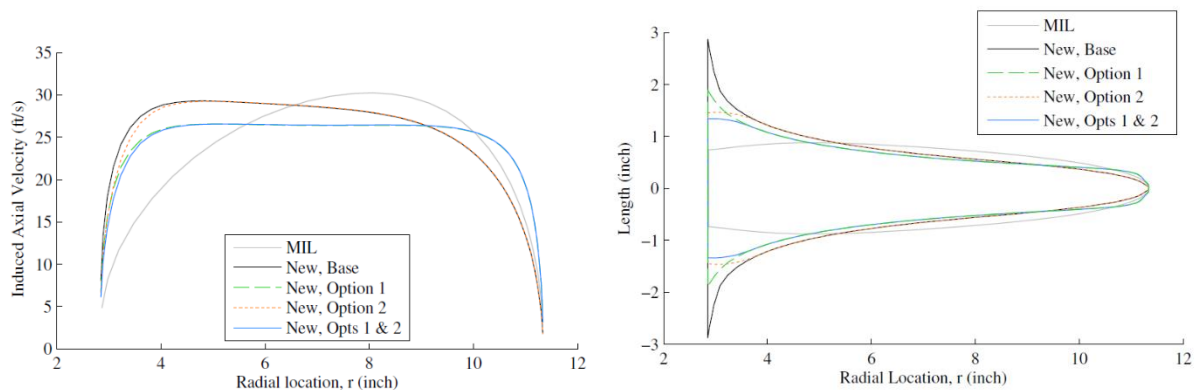
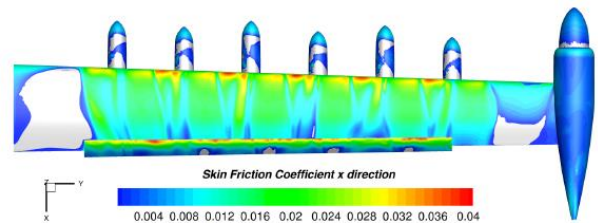
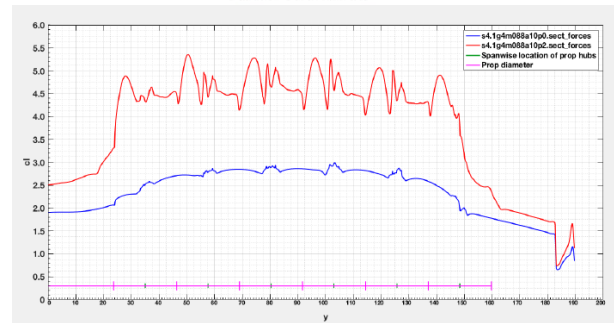
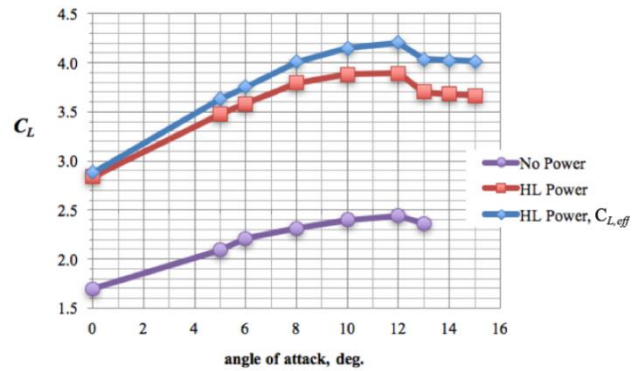
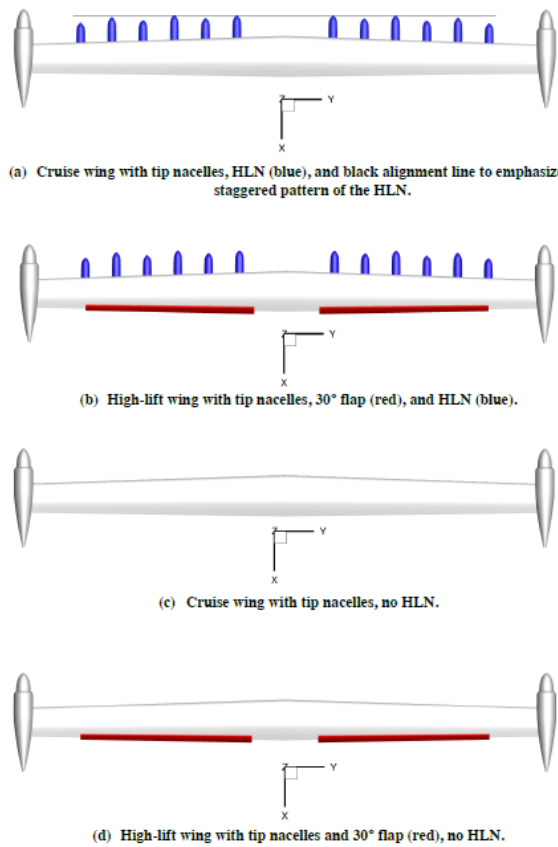


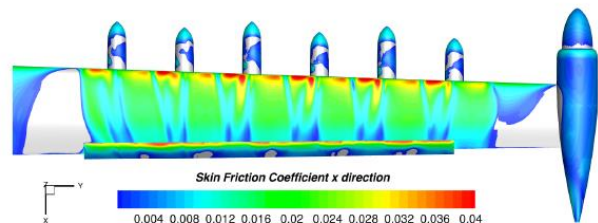
Figure 31: Left: Predicted induced axial velocity distributions for the five propellers designed to produce the same average induced axial velocity; right: comparison of the chord lengths [50].

The high-lift propellers must be properly designed, aiming to improve the wing-blowing. According to Patterson [50], to improve the axial velocity and so the high-lift capability, a near-uniform axial velocity must be produced aft of the propeller.

At NASA the high-lift propellers for the X57 Maxwell were designed and installed on the aircraft configuration (see Figure 30). The X-57 Maxwell airplane has 12 high-lift propellers mounted on nacelles upstream of the wing leading edge that are positioned in an alternating fore-and aft staggered pattern. The high-lift propellers are designed to fold smoothly onto the nacelle for the cruise configuration, which is referred to as the cruise wing. The high-lift propellers are positioned on the nacelles in an alternating fore- and aft-staggered pattern for the high-lift blown wing (30° flap shown in red in Figure 32). Preliminary results shown a maximum achievable lift coefficient of about 4.3, almost double respect to the unblown wing.



(a) SARC+QCR turbulence model, $\alpha = 13^\circ$



(b) BSL turbulence model, $\alpha = 16^\circ$

Figure 32: Left: X57 Wing configurations. Top right: The lift coefficient for the high-lift wing with high-lift and wingtip nacelles. Mid right: the sectional lift coefficient for the unblown (blue) and the blown (red) high-lift wing with high-lift and wingtip nacelles. The skin friction coefficient from FUN3D for the blown, high-lift wing with wingtip nacelles and HLN. 58 KTAS, $M=0.0878$, $Re=1.33$ million, $h=0$ ft, and $T=59^\circ\text{F}$. Blown, high-lift wing power conditions of 4548 RPM, 164.4 hp (13.7 hp/prop), and total thrust of 596.4 lbf. FUN3D SARC+QCR.

Analyses were performed also to evaluate the rotation direction of each propellers, highlighting how co-rotating propellers were better than counterrotate propellers, as shown in Figure 33 [51]. Moreover, in 2016 NASA prepared and tested a DEP high-lift propeller testbed, highlighting a good agreement between numerical and experimental data (scattered results). The lift augmentation was about double respect to the unblown solution, increasing from about $C_L=2.8$ up to $C_L=6$.

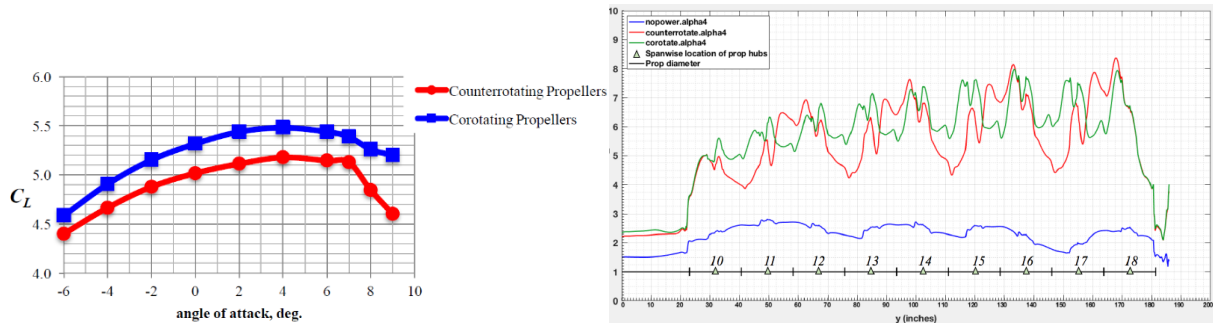


Figure 33: The effect of propeller spin direction approach on spanloading for the blown, high-lift wing (40° flap) at 73 mph, $M = 0.096$, $Re = 1$ million, $h = 2300$ ft, $T=60^\circ\text{F}$, and 300.6 hp (16.7 hp/prop, 6147 RPM), and span loading $\text{aoa}=4\text{deg}$, [51].

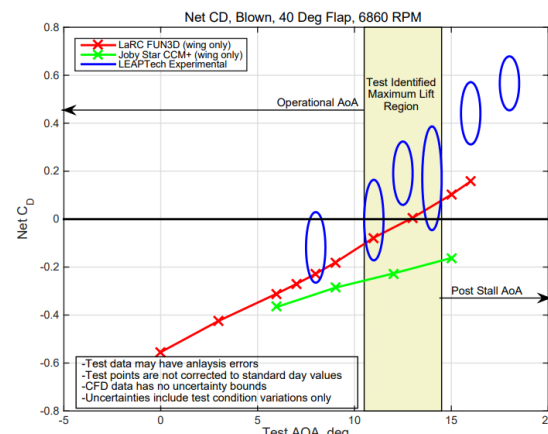
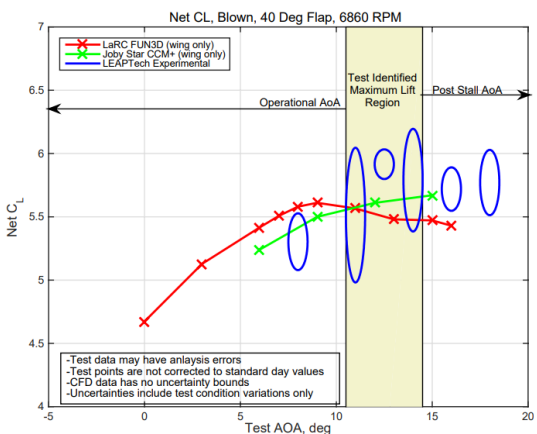
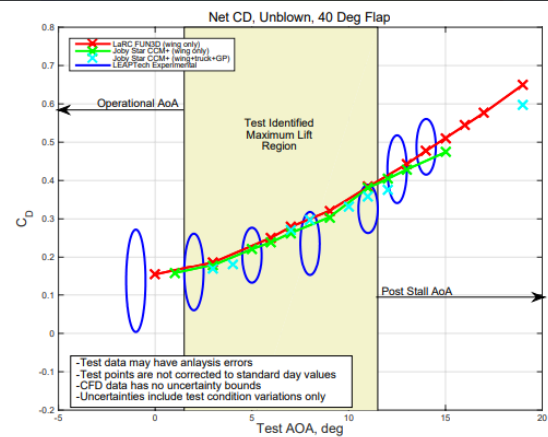
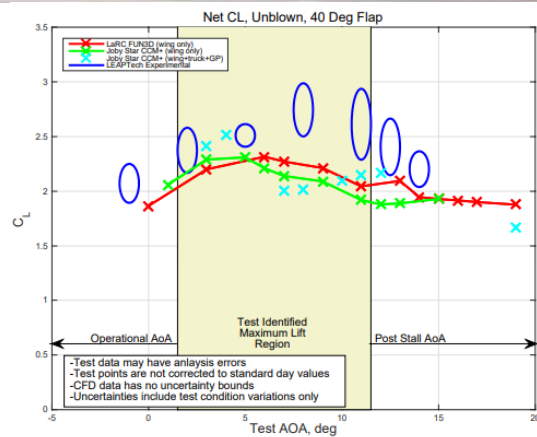
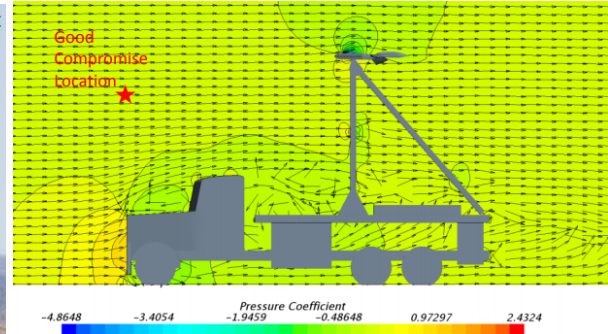


Figure 34: Nasa high-lift propeller testbed, experiments and numerical¹³. Mid: Unblown, prop removed, flaps=40deg. Down: Blown, flaps=40deg, 6860rpm.

¹³ The LEAPTech Experiment, Approach, Results, Recommendations, <https://ntrs.nasa.gov/archive/nasa/casi.ntrs.nasa.gov/20160012394.pdf>, retrieved 25052020

Della Vecchia et alii evaluated the wing high-lift propellers effect on the Tecnam P2006T baseline wing, splitting the same available power of 200hp through several distributed propellers, considering 120 hp needed for cruise tip-mounted propellers [2], see Figure 35. Results shown a reduced lift increment at about 1.0-1.5 due to small engine power, reduced blowing area and conventional propellers used for high-lift. Moreover, a key aspect is the propeller/chord ratio, $d_p/c = 0.42$, which was half respect to the NASA X57 Maxwell ($d_p/c = 0.9$), see Figure 35 and Figure 36.

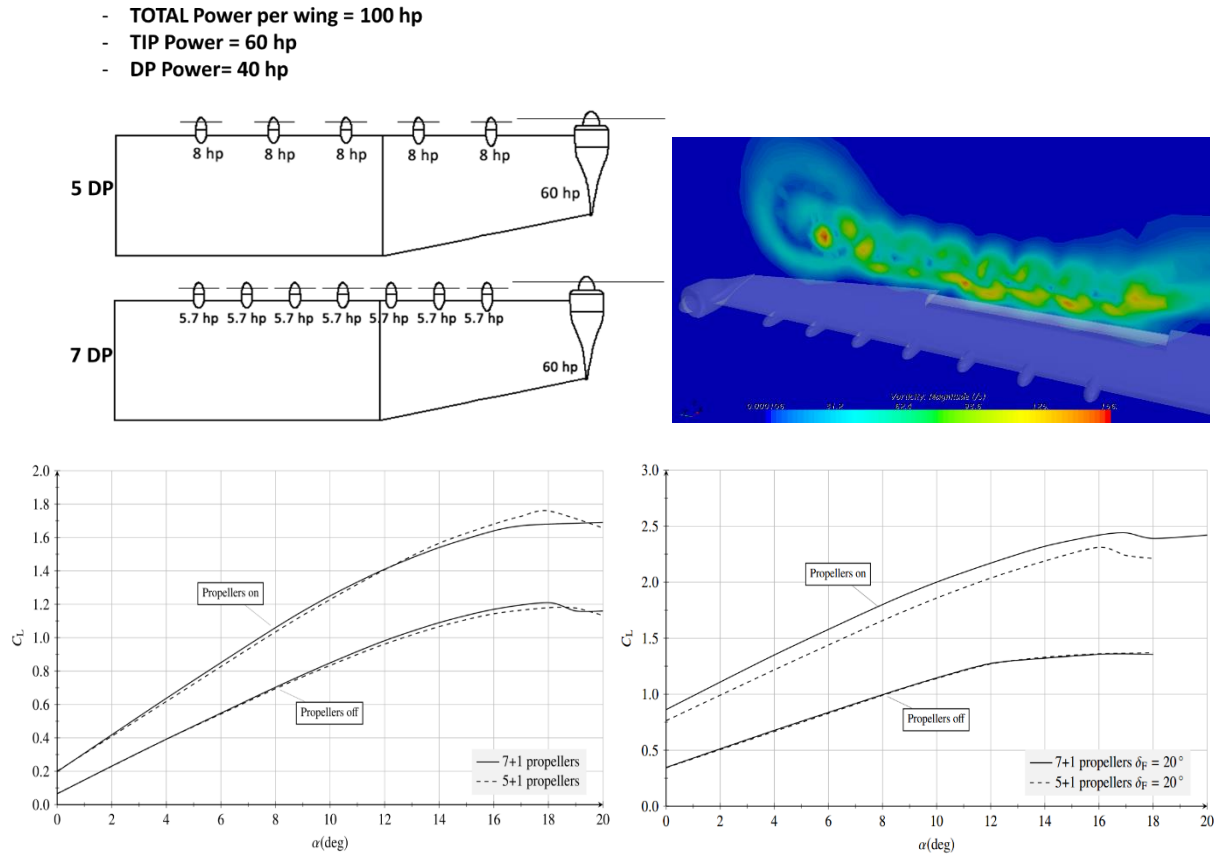


Figure 35: Tecnam P2006T wing, Lift coefficient for Clean(left) and flapped(right) configurations, $M=0.08$, $Re=3.3E6$ [2].

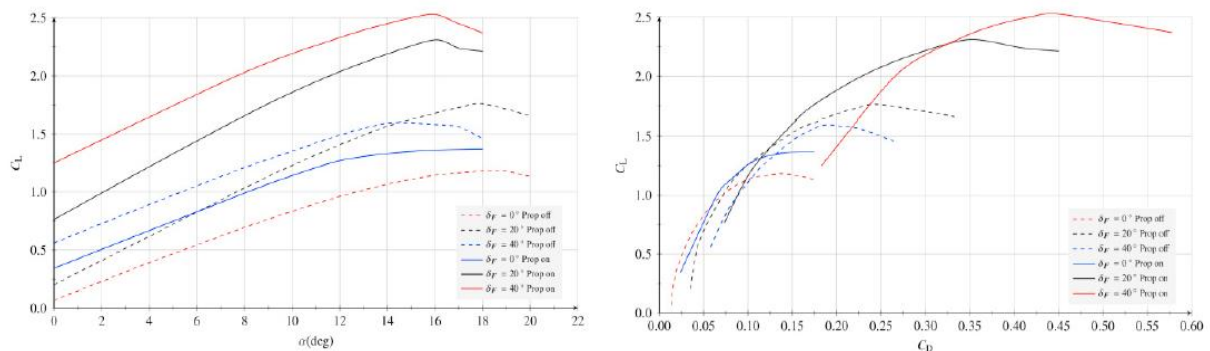


Figure 36: Tecnam P2006T wing, Results of 5+1 propeller configuration for C_L and C_D , with high-lift propeller and nacelles, $M=0.08$, $Re=3.3E6$ [2].

At University of Naples Federico II, the aerodynamic effects of high-lift propellers on a typical 40 passengers regional aircraft have been numerically analysed, varying the number of blown propellers, the thrust per propeller, the flap settings, blowing on the same wing area (see Figure 37). High-lift propellers were designed for each configuration accordingly MIL theory. Figure 38 shows the main achieved results: for a given reference wing, increasing the number of high-lift

propellers generally speaking leads to a increment of maximum lift coefficient, an increment in drag coefficient and a increment in the pitching moment. This behaviour slightly change by deflecting a conventional flap: as it can be seen in Figure 38 (top), the flap deflection promotes the trailing edge wing separation, reaching maximum lift coefficient increment ever before with a lower number of high-lift propellers. Conversely, drag coefficient increment exhibits a minimum in a certain range of $T/(D^2 V^2)$, meaning a certain number of high-lift propellers. Not negligible, as shown in Figure 38 bottom right, the pitching moment increment due to high-lift propellers.

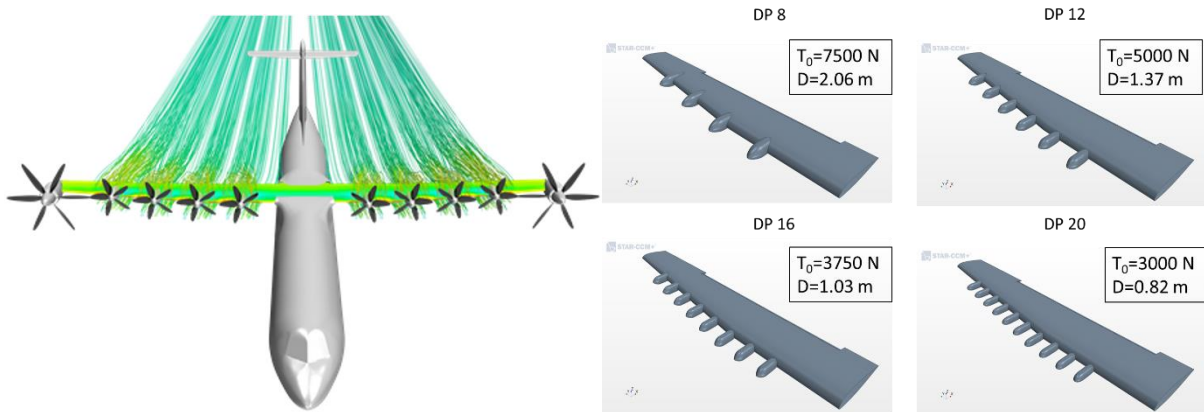


Figure 37: High-lift propeller on a typical 40 passengers regional turboprop wing, AR=11.07, $M=0.15$, $Re=7.6E6$, DEP 8, DEP 12, DEP16 and DEP 20 configurations, T_0 per propeller.

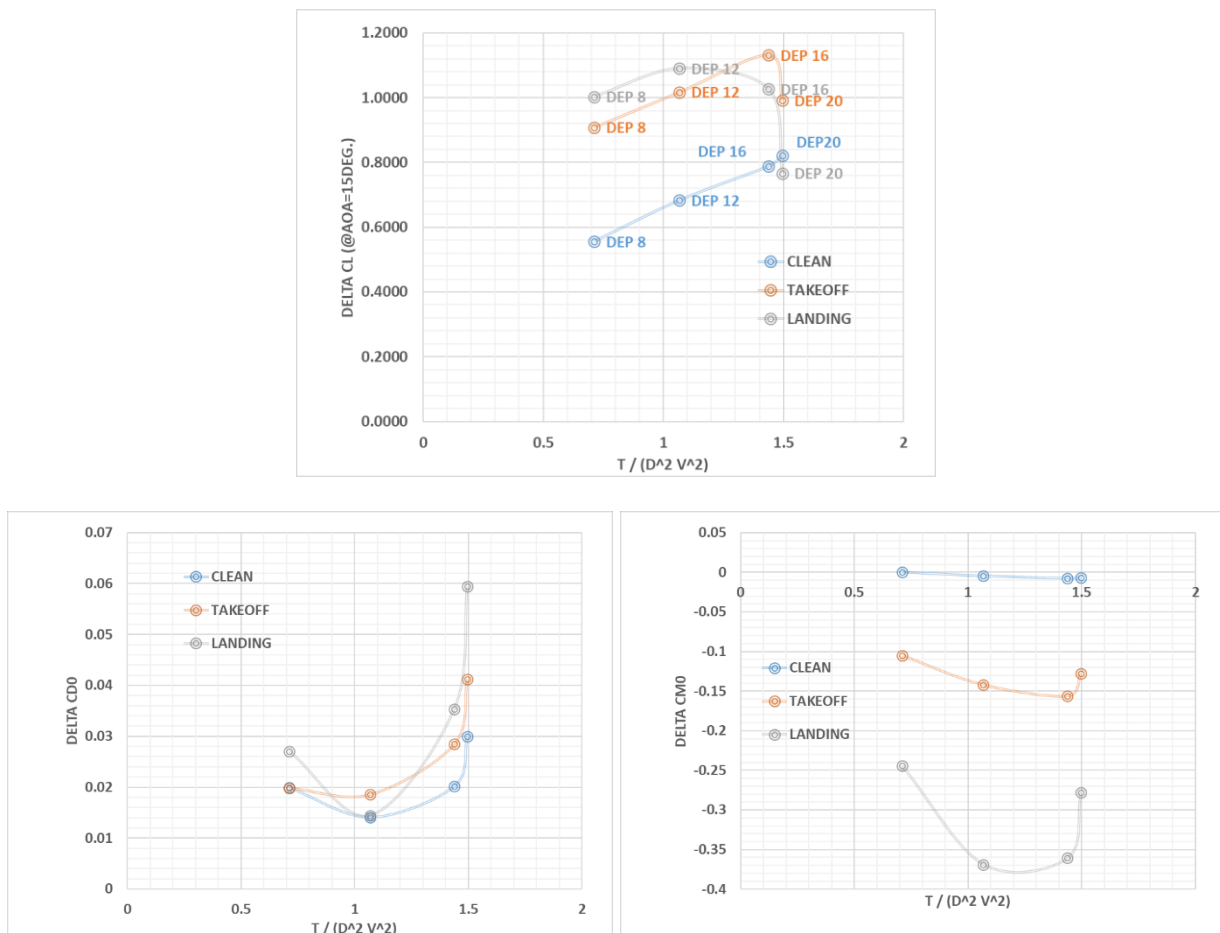


Figure 38: Delta respect to an isolated wing, of high-lift propeller on a typical 40 passengers regional turboprop wing, AR=11.07, $M=0.15$, $Re=7.6E6$, DEP 8, DEP 12, DEP16 and DEP 20 configurations, top: DeltaCL (lift coefficient at $aoa=15deg.$), bottom left: DeltaCD0 (zero lift drag coefficient) and DeltaCM0 (pitching moment coefficient at $a0a=0deg.$)

All the results on high-lift propellers highlights how promising could be this technology. The main key factors to take into account in the design stage are:

- 1) The operative speed: must be as lower as possible to obtain the main benefit
- 2) The thrust levels: must be as much as possible
- 3) The propeller diameter over the chord ratio d_p/c , must be as much as possible
- 4) The propeller design, must have an axial induction as much constant as possible
- 5) The propeller-high-lift device interaction, must carefully accounted with high-fidelity methods

5.1.3 Directional control

Aircraft with distributed propulsion may employ differential thrust as a mean to reduce or eliminate the vertical tail and be still compliant with regulations, although aero-propulsive interactions and system robustness must be carefully investigated, while different safety criteria could be applied [52–55]. Examples on regional and light aircraft model are shown in Figure 46. Certification issues on DEP configurations are discussed in Section 8.

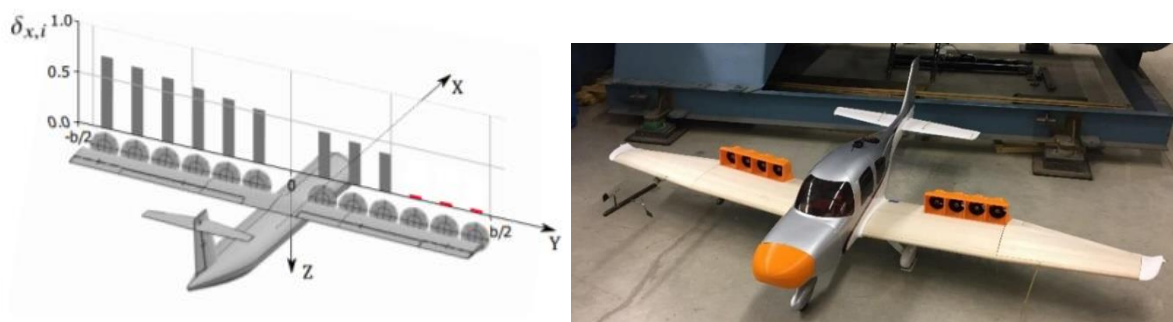


Figure 39: Distributed propulsion as an alternative mean of directional control [52,55].

5.1.4 Boundary layer control

The primary benefit associated with boundary layer ingestion (BLI) is the potential for reduction in energy usage due to ingestion of the thin, low-momentum air region at the aircraft surface, known as the boundary layer. The ingestion of this low-momentum air leads to an increased propulsive efficiency and can also lead to wake-filling benefits when the air is re-energized and used to reduce the velocity deficit and turbulent mixing losses in the wake. For these reasons, BLI propulsors are located at the end of the fuselage (in the case of an annular BLI concept) or on the top of the trailing edge lifting surface (which is the case of DEP concepts, which deal with distorted inflow, as shown in Figure 40). BLI can reduce the required propulsive power by 4% to 8% [56,57].

Several conceptual DEP aircraft aim to take advantage of BLI. First among these is the N3-X aircraft, where the large fuselage boundary-layer provides an excellent opportunity to take advantage of BLI. Studies were performed to incorporate the effects of BLI in the propulsion system design for the BWB aircraft, and additional work has been done to investigate the potential for incorporating a boundary-layer ingesting crossflow fan into the N3-X propulsion system. Experimental and numerical work has also been performed to assess the effects of BLI on propulsion system performance and inlet distortion problems. Finally, the E-Thrust and Lilium aircraft propulsion systems also utilize BLI as a performance improving mechanism [42].

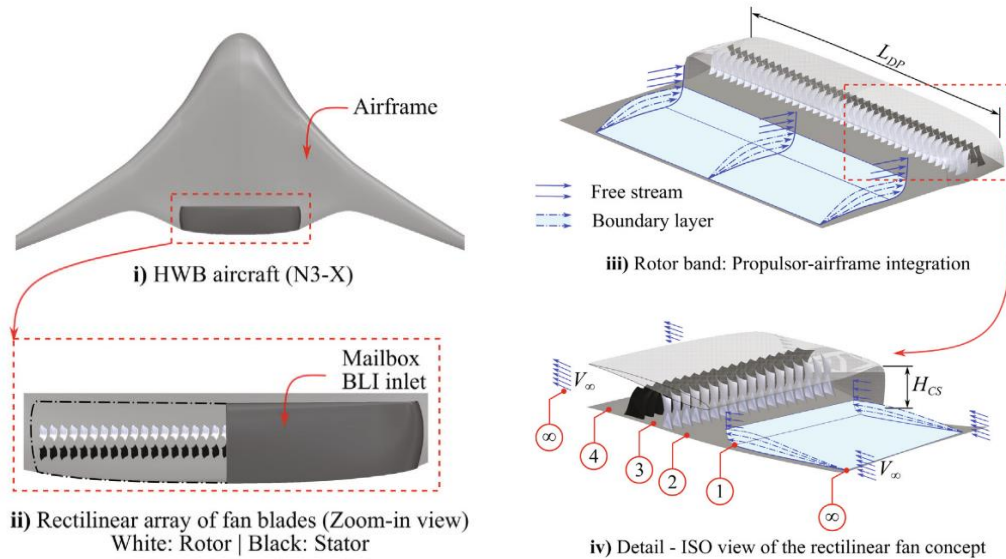


Figure 40: Distributed boundary layer ingestion concept [57].

5.1.5 Fuselage tail propeller

Numerical and experimental analyses show a potential propeller efficiency improvement, hence propulsive thrust, due to a fuselage tail mounted propeller (Figure 41) used as BLI device. It is demonstrated that the required power for BLI is lower respect to the required power without BLI. Experimental results at TU Delft [58] performed on different architectures (see Figure 42) show:

- 1) A net-force benefit $(T-D)/(qS)$ of about 9% benefit for WI and 18% for BLI w.r.t. free-stream case;
- 2) A propeller efficiency improvement, taking an advance ratio equal to 1, 11% efficiency increase for WI and 21% increase for BLI configurations w.r.t. free-stream propulsor configuration, see Figure 43.

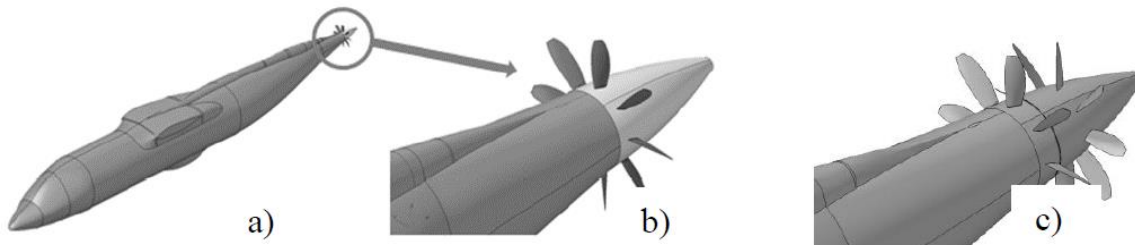


Figure 41: Example of fuselage tail-mounted propeller.

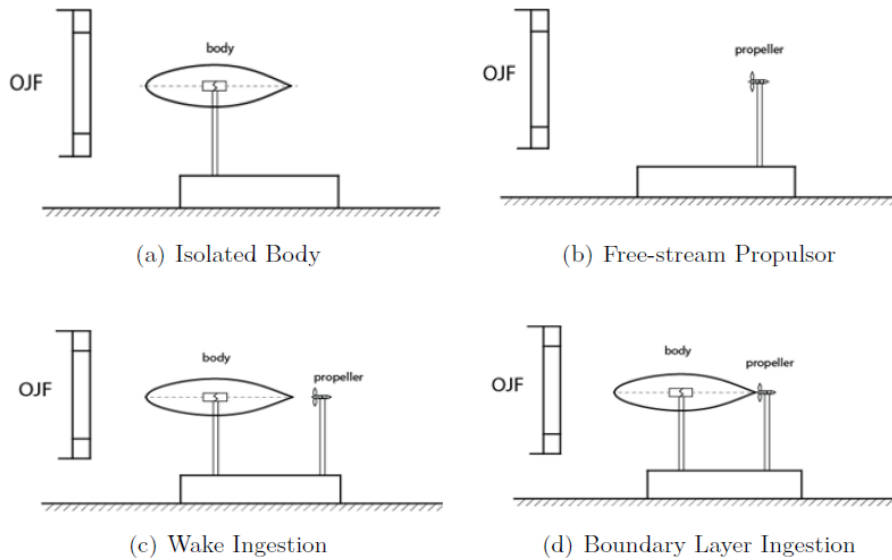
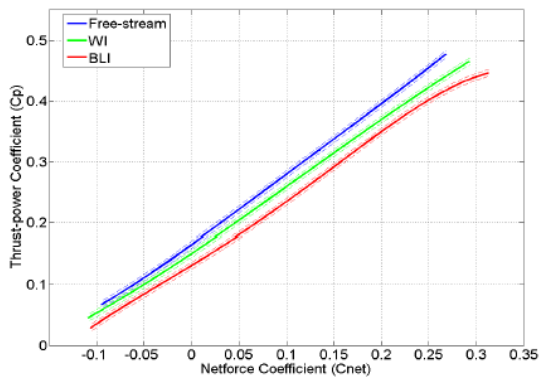


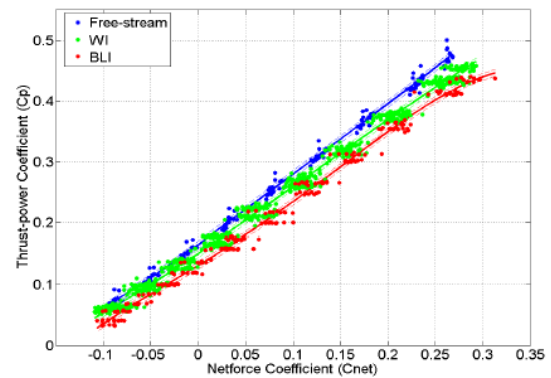
Figure 42: TUDELFT Configurations Practiced for the Experiment [58].

$$C_{(net-force)} = \frac{T - D_{body}}{q \times s}$$

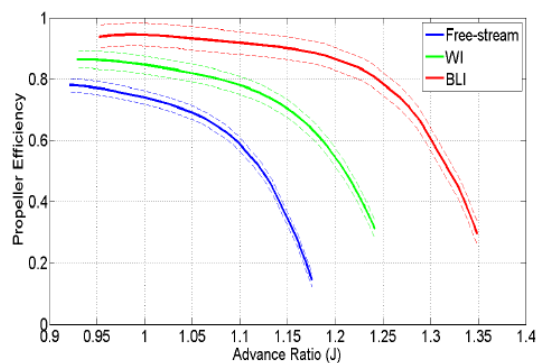
$$\eta_{propeller} = \frac{TV_{\infty}}{P_{shaft}} = \frac{TV_{\infty}}{2\pi \times Tor \times RPS}$$



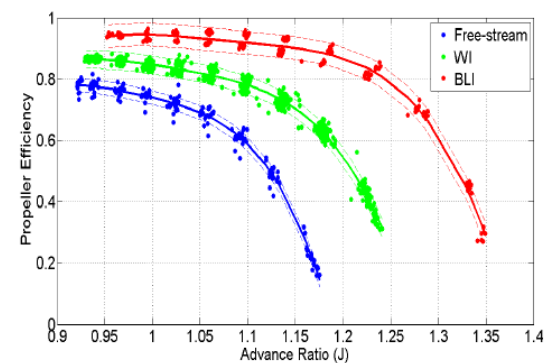
(a) $C_{(net-force)}$ vs. C_p for Various Configurations



(b) $C_{(net-force)}$ vs. C_p for Various Configurations with Observations



(a) Propeller Efficiency for Various Configurations



(b) Propeller Efficiency for Various Configurations with Observations

Figure 43: TUDELFT Main results of tail propeller BLI [58].

5.1.6 Noise

Several studies ([42,59–61]) indicate that DEP architectures offer promising perspectives for noise reduction and appear as a viable solution for delivering the strict mid-to-long term environmental goals set in the ACARE addendum [62].

This may a priori seem counter-intuitive if one considers the multiplicity of aerodynamic interactions taking place in a DEP system, which are generally synonymous of load fluctuations and noise production. Several factors are actually in favour of noise reduction [42].

Positive aerodynamic interactions such as wing blowing opens indirect perspectives for quieter transport. Besides, the efficiency of electric motors does not depend much on their size, so that the overall conversion efficiency of a large number of electric motors driving many small propellers can be as good as that of a single motor driving a single large propeller. This means that either a smaller wing sized for cruise can be used, or that lower take-off and landing speeds are possible. The latter option is very promising in terms of noise emissions, since the aerodynamic noise radiated by the fixed parts of the airframe (landing gear and high-lift devices in particular) would typically radiate noise in proportion of the 5-6th power of the flight speed [63]. Moreover, the high lift-to-drag ratio allows steeper take-off and landing trajectories, which further reduces the noise footprint affecting communities.

The noise emitted by electric machines is much less than that associated to the compressor, combustor, and turbine components. Huff et alii [64] reported that the noise generated by the electric motor system alone was 8-20 dB below the fan noise for a regional jet-sized aircraft, and 17-29 dB lower than that of a single-aisle commercial transport class aircraft.

While the proximity of the propulsive system with the airframe is normally a source of important tonal noise, the multiplicity of propulsors opens interesting perspectives for noise control via an adequate clocking of the propellers [61,65], as shown in Figure 44.

The flexibility offered by DEP systems permits placing the propulsors over the airframe in such a way to enhance noise shielding effects. Posey et alii [66] achieved low-frequency noise reductions of the order of 20 dB across a significant community area.

For turbo-electric distributed propulsion systems, i.e. when the electric power is provided by a common turbine, an effective by-pass ratio can be defined as the ratio of mass flow rate of all combined airflows by the one that enters the turbine. A high effective by-pass ratio is generally beneficial to noise reduction.

The main conclusion to be drawn from the above discussion, is that in order to properly address the noise reduction potential of DEP systems, all the relevant aspects must be tackled simultaneously: aero-propulsive benefits, noise shielding, tonal interference effects as well as non-aerodynamic noise sources. Naturally, the noise resulting from the unsteady aerodynamic interactions between the multiple propulsors and the airframe must not over-compensate the gains obtained from increased aero-propulsive efficiency. In that respect, quite innovative flow and noise control technologies have been proposed over the last decade, which may prove very efficient to reduce aerodynamic interaction noise and provide broadband acoustic absorption.

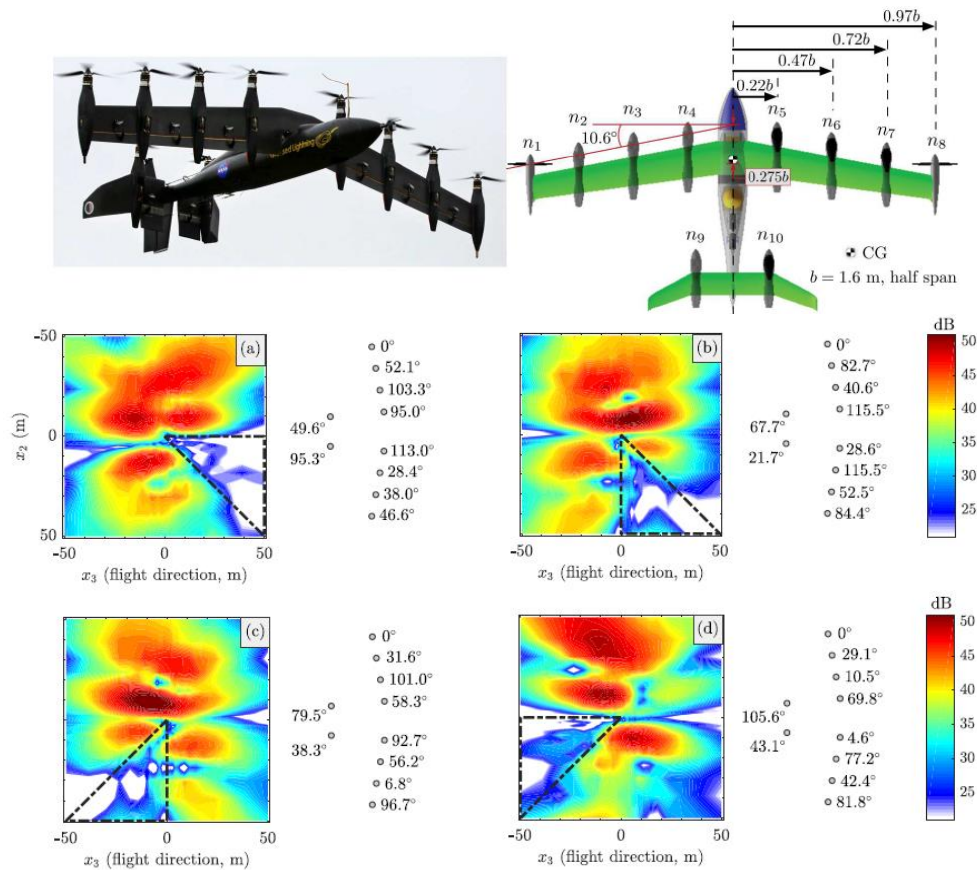


Figure 44: (Top) GL-10 in (a) hover mode and (b) top view of the forward flight configuration; (Bottom) Example of directivity modification of the blade passage frequency on the ground plane via relative propeller phase control, for the GL-10 layout at 5,000 RPM, $J = 0.6$, $\alpha = 0^\circ$. The outlined regions are the observers given to the optimization for noise minimization, and the relative phase, ψ_r , of each propeller is given in degrees in the direction of rotation.

5.2 Laminar flow

On most of today's aircraft, airflow is turbulent on almost the entire wetted surface. The result of this condition is a viscous drag which is larger than the one that could be obtained by forcing laminar boundary layer on the whole surface of the airplane. In order to force laminar boundary layer, or, at least, promote it on a large portion of aircraft wetted surfaces, two different approaches can be adopted: Natural Laminar Flow (NLF) and Laminar Flow Control (LFC) (see Figure 45). With the first concept, laminar boundary layer is kept solely by shaping the surface in such a way as to produce a favourable pressure gradient. With the second one, airflow laminarity is preserved by applying distributed suction over the surface. Another concept exists, which makes use of both the approaches: with Hybrid Laminar Flow Control (HLFC) one combines the NLF and LFC concepts. In fact, HLFC makes use of a moderate amount of suction at the leading edge, in order to counteract an adverse pressure gradient, combined with a more extended unsucked region in which a favourable pressure gradient is obtained through a suitable shaping of the aircraft surface. To a certain extent, the HLFC concept could be seen as an optimization of the LFC one, in the sense that it requires a much-reduced sucked region in order to keep the airflow boundary layer laminar [67].

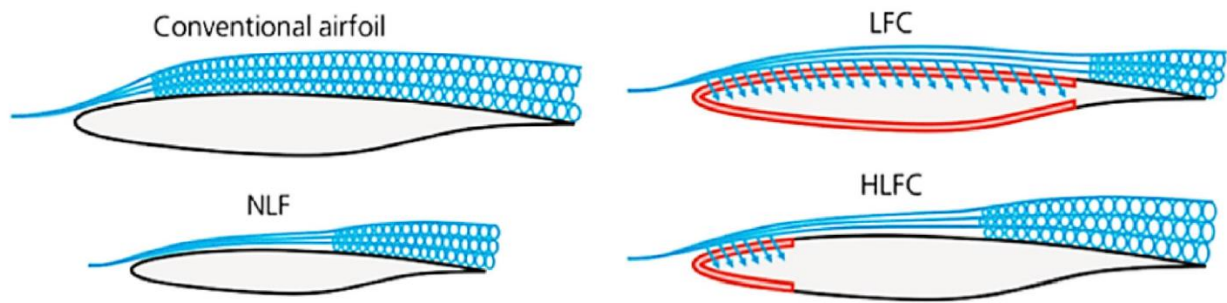


Figure 45: Schematic difference between NLF, LFC and HLFC [68].

For an airplane wing, three different instability mechanisms, leading to transition from laminar to turbulent boundary layer, can be distinguished:

- **Tollmien-Schlichting waves** – It is the most common way by which a laminar flow transitions to turbulent. They are streamwise unstable waves which arise in boundary layers, so are driven by viscous effect on the surface of a body. On a swept wing, they usually occur in the mid-chord region.
- **Attachment-line contamination** – It is essentially provoked by the boundary layer of the fuselage, which, propagating from the junction between the fuselage and the wing inner panel, ends to contaminate the boundary layer of the latter, provoking the transition from laminar to turbulent flow.
- **Cross flow instability** – It was first discovered during early studies on swept wings. This instability occurs in the region of high-pressure gradient of a swept lifting surface, for which boundary layer velocity profiles are three-dimensionally warped. For this reason, when projected into the direction perpendicular to the outer flow, a crossflow profile can be obtained, which is inherently unstable since having at least one point of inflection.

Figure 46 shows which are the transition mechanisms on a swept wing and which region of a lifting surface they affect the most. More specifically, the mechanism through which transition occurs on a swept wing can depend on the size of the sweep angle at the leading edge. For lower leading-edge angles transition is usually dominated by Tollmien-Schlichting waves, while cross flow instability dominates for higher values. Figure 47 gives an overview of the results obtained by different studies investigating the possibility to control turbulent transition. As a result, forward swept wings (FSW) seem to behave, for a transonic application, much better with respect to cross flow instability. This can be associated with their lower leading-edge sweep angle with respect to a backward swept wing (BSW) with the same 50% chord line angle (which is the location at which shocks usually occurs for transonic wings).

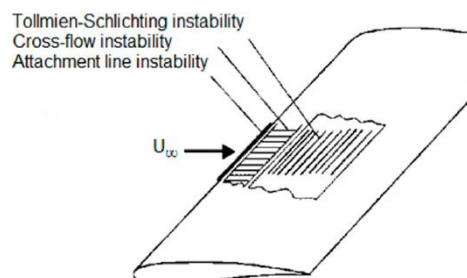


Figure 46: Transition mechanisms on a swept wing [69].

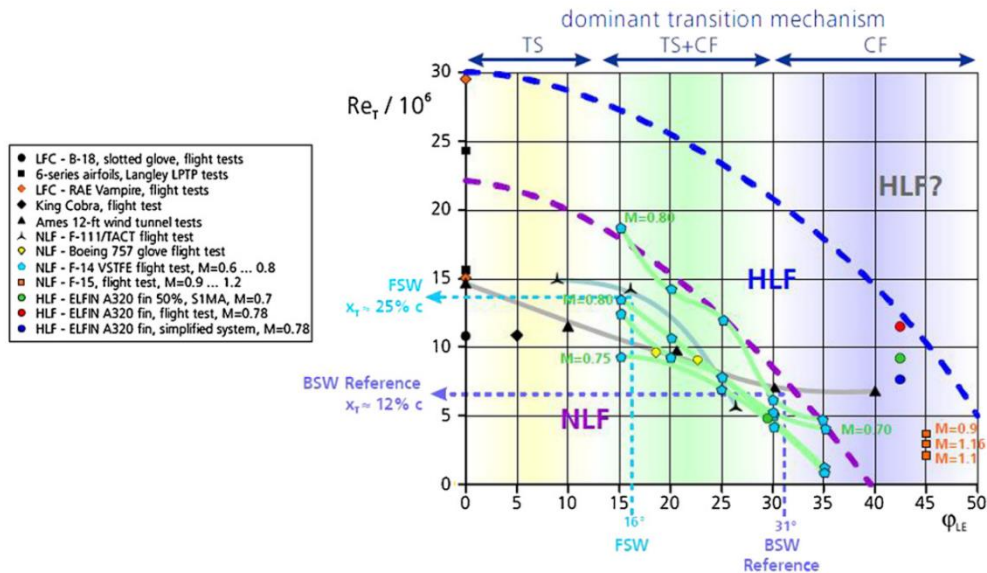


Figure 47: Dominant laminar turbulent transition effect for forward swept and backward swept wings [70].

The following sub-paragraphs focus on giving an overview on the so far performed research studies both for Natural Laminar Flow and Laminar Flow Control, providing, whether possible, information on actual flight tests and current applications of these technologies.

5.2.1 Natural Laminar Flow

One way to achieve laminar boundary layer on a large portion of an aircraft component without adopting active control devices consists in appropriately shaping its surface, in order to obtain a favourable pressure gradient ($dp/dx < 0$) over the forward region, in order to delay transition. On the lifting surface and airfoils side, this usually results in a sharp leading edge profile, which implies as a direct consequence a reduction in terms of lifting capabilities for the forward portion of the airfoil section and so a deterioration in terms of high-lift and stall performances. Besides, because of the dominant role of cross flow instabilities for high swept wings flying at transonic speed and at high Reynolds number, the use of this technology seems to be limited to small regional aircrafts carrying less than 100 passengers, at least for conventional wing configurations and in absence of further flow control technologies.

The effectiveness of this type of technology has been successfully validated through several flight tests during the last decades, some of which were performed as part of the European Laminar Flow Investigation (ELFIN) project [71]. One of the main elements of the project consisted in a partial-span flight demonstration of natural laminar flow utilizing a foam and fiberglass glove over existing wing structure. The aircraft chosen for this test was a Fokker 100 transport aircraft, whose starboard wing was modified with a full-chord, partial-span natural laminar flow glove simply bonded to it, as shown in Figure 48.

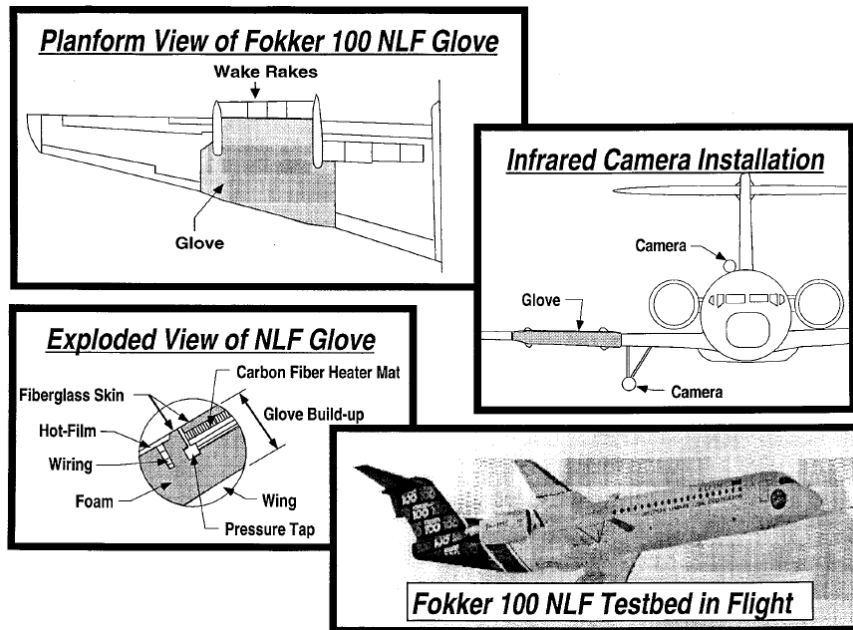


Figure 48: ELFIN project Fokker 100 natural laminar flow testbed [71].

Main objective of this test was to evaluate the reduction in drag associated with the natural laminar flow and to establish the upper limits in terms of transition Reynolds number for a given leading edge sweep angle. Flight tests were performed for a total of twelve hours, leading to results comparable with the ones resulted from wind tunnel tests, confirming predictions of **15% drag reduction**.

More recently, within the framework of the EU-funded Clean Sky I projects, more NLF demonstrators have been developed and tested. As part of the SFWA (Smart Fixed Wing Aircraft) project, the BLADE (Breakthrough Laminar Aircraft Demonstrator) demonstrator has been flight tested¹⁴. The outer wing of an Airbus A340 was substituted with a NLF wing, characterized by a lower leading edge sweep, in order to better control cross flow instabilities (Figure 49).

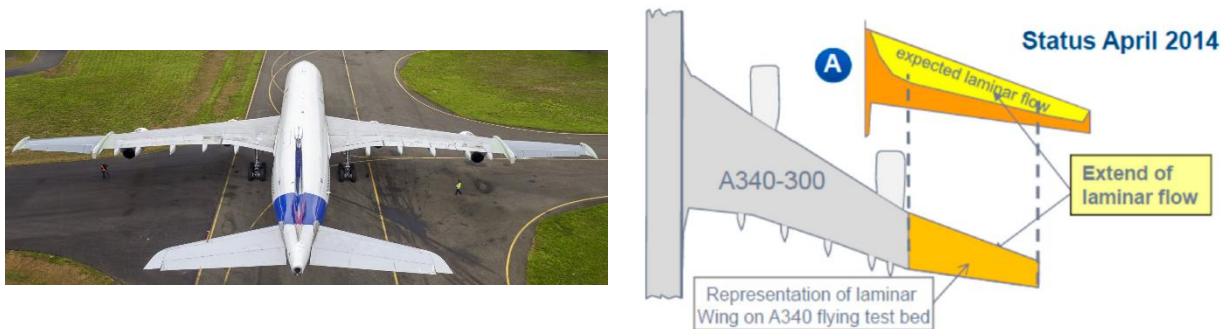


Figure 49: BLADE demonstrator.

Currently NLF has been adopted and realized only for light business jets such as the HondaJet [72,73]. Instead of adopting an existing NLF airfoil (as the ones developed by NASA for business jet applications), a new NLF airfoil has been designed and studied, in order to exactly match the requirements of the aircraft and to optimize the aircraft performance. The designed airfoil, SHM-1 (Figure 50), shows all favourable characteristics for such an application: high drag-divergence Mach number, small nose-down pitching moment, low drag for cruise, docile stall characteristics. All these achieved while keeping a 15% thickness, allowing to carry the necessary fuel without an increase in wing area.

¹⁴ G. Williams, "Progress and Achievements in CleanSky SFWA", http://www.forum-ae.eu/system/files/5-cleansky_sfw_forum-ae.pdf

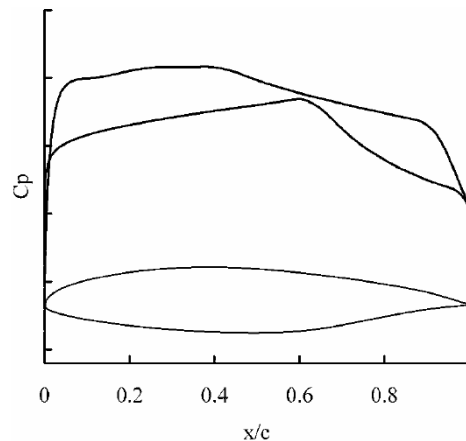


Figure 50: SHM-1 NLF airfoil shape and representative pressure coefficient distribution [73].

From flight tests and extensive wind tunnel experiments, an airfoil drag coefficient of 51 drag counts at $C_l = 0.26$ for $Re = 13.2 \cdot 10^6$ and $M = 0.66$, and 49 drag counts at $C_l = 0.35$ for $Re = 13.2 \cdot 10^6$ and $M = 0.27$ has been estimated. Besides, from transonic wind tunnel tests, a drag-divergence Mach number higher than 0.718 at $C_l = 0.30$ and 0.707 at $C_l = 0.40$ has been obtained. For the HondaJet, NLF has not only been pursued and researched for the wing. An NLF fuselage-nose shape has been extensively studied and developed, resulting in a reduction in terms of fuselage drag of the order of 10% compared to that of a turbulent-flow one.

5.2.2 Laminar Flow Control

Laminar Flow Control (LFC) is an active boundary layer flow control technique aiming to maintain the airflow over a surface laminar for chord Reynolds numbers much greater than the ones that usually characterize transitional or turbulent configurations. In highly swept wings that usually are required for flight at high subsonic and supersonic speeds, only suction can control sweep-induced crossflow disturbances which promote boundary layer transition. Most of the research so far has been on laminarization through flow active control by application of a combination of NLF and LFC, which is called Hybrid Laminar Flow Control (HLFC). In HLFC, suction is applied only at the leading edge of a swept lifting surface, in order to annihilate cross flow instabilities. The aft region of the wing is then appropriately shaped (as for the NLF technique) to control pressure distribution and stabilize mid-chord Tollmien-Schlichting waves. In theory, Tollmien-Schlichting instabilities could be controlled by suction even further downstream. The reason why this is rarely taken into consideration, at least in conventional aircraft configuration, lies in the weight penalty one would incur in installing a suction system in the area of the wing box, in addition to the reduction in total available volume for fuel tanks. Even in spite of this, introduction of active laminar flow control technology on a limited portion of wing area still adds, with respect to NLF, additional mass, power consumption and complexity to the aircraft. For this reason, the HLFC design requires multidisciplinary work on aerodynamics, structural engineering, production technology (closer tolerances), systems engineering, and airline operations (maintenance and damage repair, essentially). A HLFC installation would require a dedicated apparatus, comprising several systems. The following is a list of the systems that a HLFC aircraft would require. Except for the suction system, the remaining ones would be necessary for a NLF application too, although they are probably the less demanding in terms of power required and additional weight.

- **Suction system** – In order to keep the boundary layer on the leading edge of a swept lifting surface laminar, air must be removed from it through suction. Suction can be achieved both through the usage of a slotted wing surface or a perforated one, if a difference in pressure exists between the external surface and the chamber underneath the skin. Then the sucked air can be guided through an outflow or can be used by another aircraft system requiring air. In order to achieve the aforementioned pressure difference, two approaches can be followed: one making use of an active system based on an electric

motor-driven compressor, one exploiting the natural difference in pressure between the inflow and outflow positions. Active systems have been successfully tested both in wind tunnel and actual flight tests, but they obviously pose some problems in terms of increased system weight, power consumption, maintenance, cost and complexity. On the other hand, a passive system would not reach the same performances and the same laminar efficiency. Several studies [74][75] have been carried out in order to address the problematic of taking into account the design of HLFC suction systems during the preliminary aircraft design phase. Different sizing methodologies have been presented for an early estimation of components parameters, such as required power, mass and dimensions. Pe [74] also addressed the problematic concerning the number of compressors to be installed along with their positioning (Figure 51), concluding that for a long-range HLFC aircraft it is most beneficial, in terms of power usage and additional weight, to have one compressor for each side of a wing.

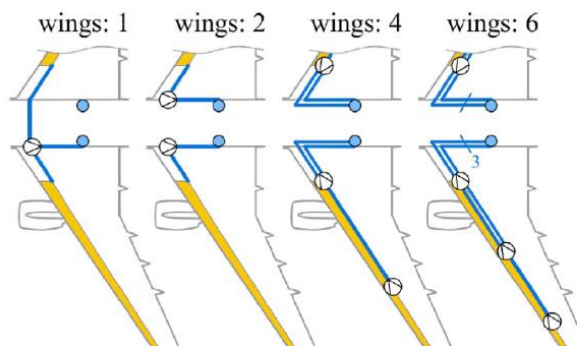


Figure 51: Pe [74] studies on HLFC suction system for a long-range aircraft.

- **Anti-contamination system** – In order to keep the flow laminar over the leading edge, very high surface cleanliness is required, since even small obstacles could undermine the effectiveness of the HLFC system and promote transition. Contamination of the leading edge area due to impact of insects has been extensively investigated in the past, even for NLF application for which such a system would be necessary too. It has been demonstrated that this type of contamination takes place below 500 ft, so actions must be undertaken before taking-off, at landing and taxiing in order to keep lifting surfaces clean. Several measures/concepts have been proposed during the last decades: paper coverings, scrapers/wipers, deflectors, soluble films, resilient surface, liquid spray systems. However, some of these solutions are too demanding in term of system complexity and additional weight, so have been regularly discarded. Krüger flaps have been proposed as a solution for such a problematic, at least for the wings, thanks to their potential shielding capabilities. The price to pay would consist in restrictions in the design freedom for the high-lift system, and thus a deterioration of high-lift performance.
- **Ice and rain protection** – In order to avoid the formation/growth of ice on aircraft surfaces, anti- and de-icing systems are regularly installed on main lifting surfaces. For HLFC application on tails and other aerodynamic components, an ice protection system should be installed to avoid ice blocking the suction holes, degrading the laminar boundary layer.
- **Monitoring system** – An HLFC aircraft should be provided with a monitoring system, which would start the functioning of the HLFC apparatus once the design altitude has been reached, inform the pilot about the malfunctioning of the system and/or of the anti/de-icing and anti-contamination systems, communicate with the fuel monitoring system in order to check the fuel consumption with respect to a laminar operation.

With respect to the last system, it is important to keep in mind the fundamental importance of such an apparatus. A failure of the HLFC systems would result in the inability to achieve the target fuel burn reduction, that, in turn, could imply the inability of the aircraft to reach the target destination due to not sufficient fuel reserves.

Several European and US based programs/research projects have performed flight tests involving HLFC technologies in order to assess its feasibility. In 1987, NASA and Boeing started a cooperative flight program on a B757 transport aircraft[71]. The main objectives of the flight test program were to perform high Reynolds number tests on HLFC technology, develop a database on the effectiveness of such a concept, test its integration with other aircraft systems (high-lift, anti-/de-ice, etc.). For these tests, the actual leading edge of the main wing of the B757 was replaced with a new construction, consisting of a micro-perforated titanium outer skin, subsurface suction flutes, and ducts to collect sucked air. Besides, the new portion of leading edge was also equipped with a Krüger flap, working as a shield against contamination from insects. Tests were performed at $M = 0.80$ and for $C_L = 0.50$. Effectiveness of the HLFC system in delaying the boundary layer transition was successfully demonstrated, with laminar flow extended much beyond the 50% chord, which resulted in a 6% drag reduction for the aircraft (Figure 52).

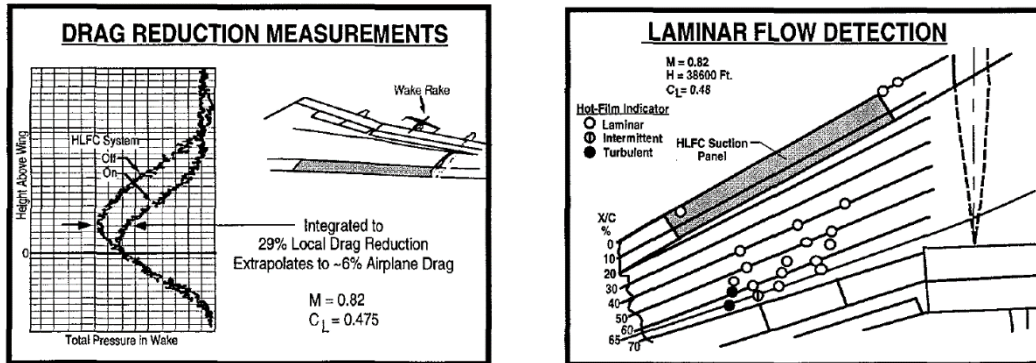


Figure 52: B757 HLFC apparatus and major accomplishment [71].

At the turn of the 1980s, Dassault tested HLFC technology on a Falcon 50 [71]. A perforated suction apparatus was gloved over the inboard structure, close to the fuselage. Suction was performed through an ejector/plenum arrangement. An anti-icing system was integrated into the design, also accomplishing the task of insect contamination avoidance. A Guster bump installation, in order to avoid attachment line contamination, was also tested for several configurations. Tests confirmed the effectiveness of the integrated anti-ice/contamination avoidance system. The optimal Guster bump location for attachment line contamination avoidance was found to be 300 mm from the side of the fuselage. For this configuration, and with boundary layer suction active, the test article was observed to become fully laminar (Figure 53).

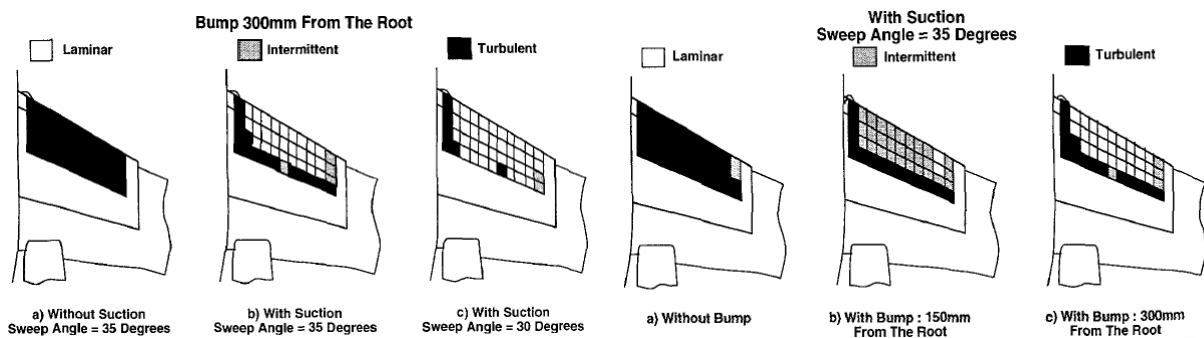


Figure 53: Dassault Falcon 50 HLFC testing results [71].

In 1998, another HLFC demonstration was prepared, this time under the leadership of Airbus [76]. For this experiment, the vertical tailplane of an Airbus A320 was equipped with a complex HLFC system. The experiment was a big success, since an extensive laminarization of the boundary layer over the vertical tail surface was observed. But the overall complexity of the system would have discouraged any aircraft manufacturer to put it into series production. Nevertheless, the positive results of the test have pushed the DLR to continue the study on such a technology, bringing to a simplified concept characterized by a much less complicated suction system, called

the ALTTA concept [77] which is represented in Figure 54. The ALTTA concept has been tested in 2014 within the frame of the VERSUS project, again on the vertical tail of an A320 and, this time, through wind tunnel tests. It will be flight demonstrated within the EU project AFloNext.

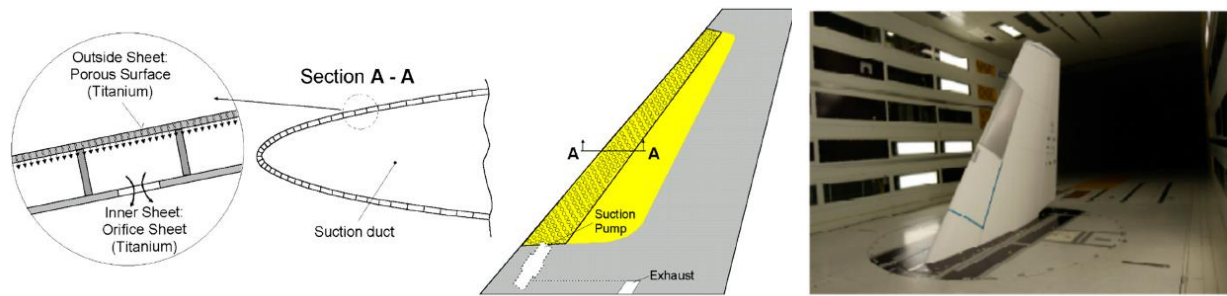


Figure 54: Scheme of the ALTTA concept system [77] and wind tunnel tests.

Boeing is currently testing HLFC for the horizontal tail and for the vertical fin of the 787-9, at least accordingly to several news articles. A passive suction system has already been patented by them in 2011.

Risse [78] has proposed in his work a way to include HLFC on wings and tails in the preliminary overall aircraft design. The basis of this work has been the integration of a preliminary design methodology for hybrid laminar flow control systems into an existing aircraft design framework. The framework in which this has been performed is MICADO [79], a multidisciplinary requirement-driven design software composed by a series of program modules dedicated to different tasks, including optimization. The approach through which HLFC systems design has been included into the existing framework is physics-based. A quasi-three-dimensional wing design approach and a database of optimized HLFC airfoils for different design conditions are used to incorporate HLFC aerodynamics into overall aircraft preliminary design. Drag is estimated through a transition prediction code, taking into account cross flow instabilities too. The chosen spanwise and chordwise distribution of the suction orifice, along with the pressure distribution coming from the aerodynamics computations allows to perform an automatic estimation of the power requirements and of the masses of the suction system. The suction system architecture is assumed to be the one of the ALTTA concept and is schematized in Figure 55 (which is almost identical to the one in Figure 54). It consists of:

- A micro-perforated thick metal sheet;
- Stringers parallel to constant chord lines, dividing the double skin into several chambers;
- An inner metal sheet with throttle orifices;
- A plenum with constant under-pressure.

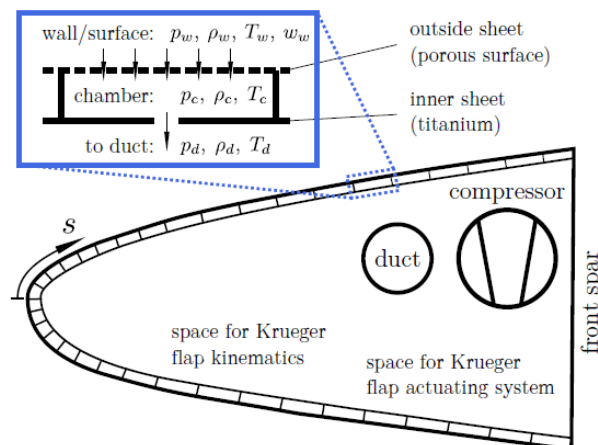


Figure 55: Risse [78] simplified suction system.

In Ref. [78] a quantitative assessment of HLFC at aircraft level is also provided. Since HLFC shows its full potential on long distance flights, a conventional turbulent long range aircraft configuration has been selected as reference, characterized by a design range of 8150 nmi, a design passenger number equal to 470, and a cruise Mach number of 0.85. The reference design, performed through the MICADO framework, has been then compared to the design coming from HLFC integration. In particular, three HLFC configurations are compared (HLFD-0, HLFD-1, HLFD-2), characterized by different values for the cruise Mach number (0.85, 0.80, 0.80, respectively) and the outboard leading edge sweep (34° , 34° , 28° , respectively). Besides, two different design approaches in terms of HLFC integration have been examined, one involving retrofitting of laminar flow technologies (D1), one taking into account the resizing of aircraft components (D2). Then comparisons have been performed in a step-wise fashion, in order to identify the different design influences. Figure 70 shows design evolution and impact on mission block fuel as a percentage with respect to the reference, with the vertical dashed line marking the influence of the single primary effects (left), and the impact of an integrated design (right). Here two additional scenarios have also been taken into account, both linked to the loss of laminarity during the mission: one at the 50% of the design range, the other for the whole length of the mission. From the figure it is well clear how a resizing of the aircraft for HLFC would imply greater benefits in terms of fuel burn reduction (more than 1%). Figure 75 shows instead the relative percentage changes of key design parameters. It can be observed how propulsion system and geometry are kept constant for the retrofit design (D1).

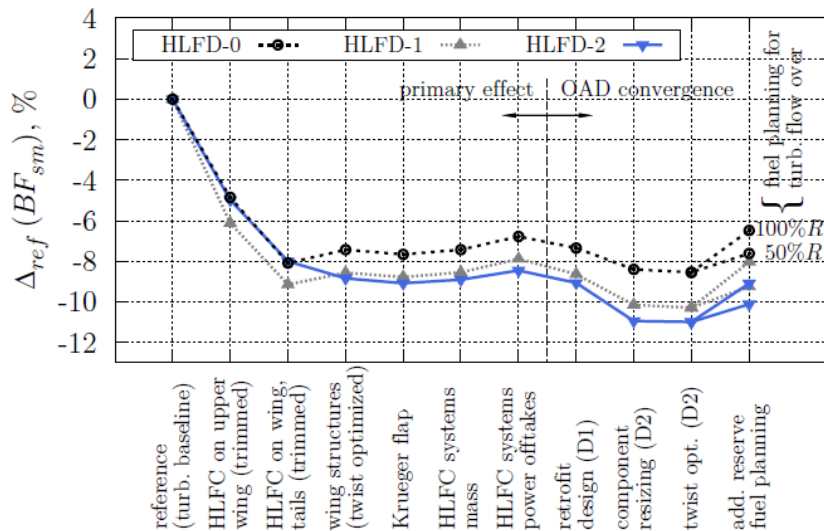


Figure 56: HLFC integration and design evolution, impact on block fuel [78].

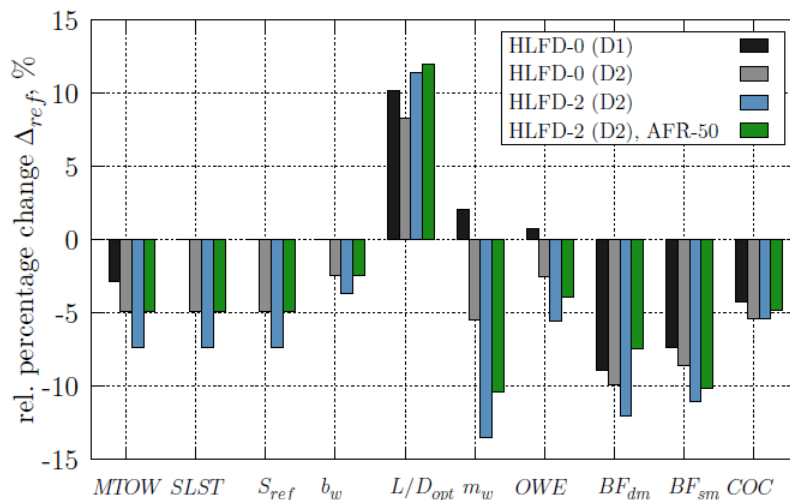


Figure 57: Relative changes with HLFC integration and comparison of key design parameters [78].

5.2.3 Riblets

The previous paragraphs addressed the problematics of keeping the boundary layer flow laminar for as much as possible in the chordwise direction. Laminar flow control could be theoretically used to extend laminarity even further the mid-chord region, as highlighted by [69], but this would come at a high cost in terms of required power, weight penalty, and direct operative costs. Since at this stage complete LFC seems not to be feasible, even when laminar flow control is successful a significant proportion of skin friction drag due to turbulence remains. An improvement in this sense could result from the usage of techniques reducing the turbulent drag.

Riblets are small surface protrusions, aligned with the direction of the flow, which confer an anisotropic roughness to a surface (Figure 58, left). There are also other passive techniques to be used in order to reduce the skin friction in turbulent boundary layers, such as dimples (Figure 58, right), but several tests performed during the last years have shown little or no improvements in terms of turbulent drag reduction, along with an higher cost associated with their operation. On the other hand, riblets potential has been successfully proven, both in laboratory and during actual flight tests.

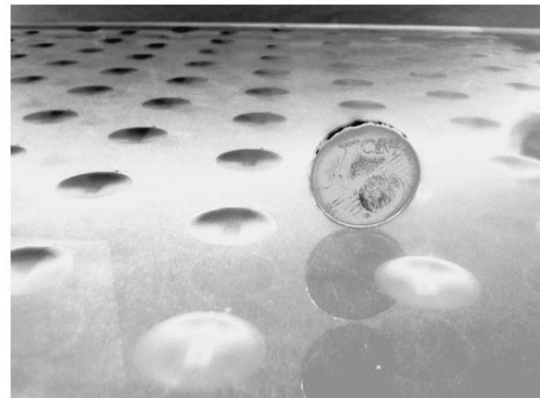
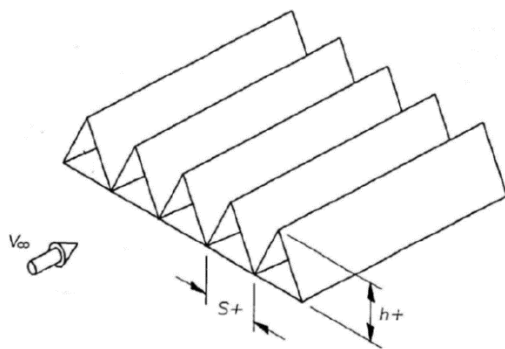


Figure 58: Riblets [80](left) and dimples [81](right).

The correct explanation of the underlying physics of riblets is still a subject of discussion and a topic of research. It has been shown that riblets induce a displacement of the turbulence eddies with respect to the mean flow, leading to a reduction of the momentum transfer to the wall with a consequence drag reduction [82]. However, this mechanism is confined to a region which is very close to the surface and, in case the riblets are large enough to interact directly with the turbulence structure, they could even lead to an increase in drag [80].

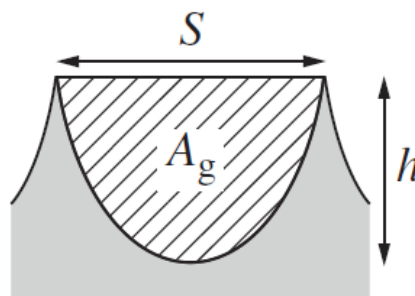


Figure 59: Schematic of riblets cross sectional area [83].

Garcia-Mayoral and Jiménez [83] have found that the riblets' groove dimensionless cross sectional area, A_g^+ , is the most suitable parameter to characterize riblet performance with respect to different non-dimensional parameters, such as riblet spacing, s^+ , or riblet height, h^+ . In fact, the adoption of $l_g^+ = \sqrt{A_g^+}$ collapses riblets experimental data into a compact group of similar curves, meaning that A_g^+ can be used to better identify an arbitrary family of riblets. Garcia-Mayoral and Jiménez have found that the best estimate for optimum drag reduction is $l_g^+ \approx 11$, but have

also confirmed that drag reduction is heavily affected by riblet spacing, size, and orientation, which, in some cases, could even produce a drag increase.

From an aircraft perspective, Catalano et al. [80] have investigated the effects of the application of riblets to a wing-body configuration of a typical regional turbopropeller airplane (Figure 60). Regarding the configuration taken into exam, the wing has been equipped with NLF optimized airfoils for cruise condition, with the twist being optimized for low-speed performances. Different assumptions have then been made in order to assess the effect of riblets in combination with NLF: riblets have been applied with the assumption of fully turbulent flow and in case the flow is assumed laminar for a large portion of the wing thanks to NLF technology. Three different aircraft configurations have been analysed, in order to better determine the zones of the aircraft in which the effect of riblets is more effective: one with riblets only on the wing, one with riblets applied on both the wing and the fuselage, and one with riblets applied on the whole aircraft. Finally, three different scenarios have been taken into account: cruise condition with fully turbulent assumption, laminar cruise condition, and fully turbulent climb/descent. RANS simulations have been performed in order to assess the effects of NLF and riblets, with a proper boundary condition to simulate the effect of the latter. Tab. 1 reports the results of the performed analysis in terms of saved weight percentage with respect to the weight obtained at the end of the cruise phase for the clean configuration. Two different design missions have been examined, one with a cruise phase of 350 nmi, and one of 900 nmi.

	Clean	Riblets wing (%)	Riblets body (%)	Riblets wing and body (%)	NLF (%)	NLF and Riblets wb (%)
100 $\Delta W/W_f^c$ (900 nmi mission)	0	3.75	1.74	7.38	9.86	16.03
100 $\Delta W/W_f^c$ (350 nmi mission)	0	1.6	0.74	3.15	4.20	6.82

Tab. 1. Percentage saving of weight for a design mission with cruise phase of 900 nmi and 350 nmi [80].

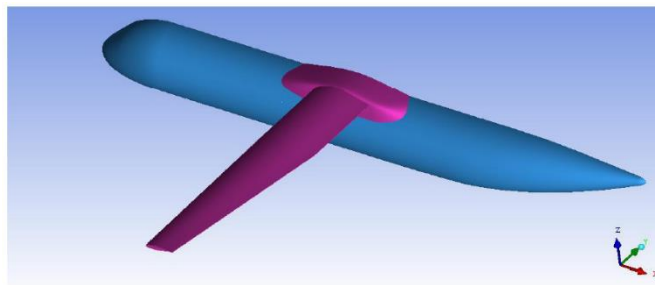


Figure 60: Aircraft configuration examined in [80].

From the table reported above it is possible to state that NLF technology can allow to save much more weight than riblets, but, at the same time, the usage of riblets can provide a sensible contribute in drag decrease. Besides, from the data reported in Tab. 1 it is easy to conclude that riblets on wing are much more effective than riblets on fuselage.

Regarding actual flight investigations with riblets applied on aircraft surfaces, several tests have been performed during the last decades. In the 1980s, McLean et al. [84] tested the effect on drag reduction of a riblet film glued over the upper surface of one wing of a T-33 jet trainer (Figure 61, left). Different 3M¹⁵ riblet films (in terms of spacing and height) were used on a portion of wing surface extending from the 7% to the 83% of the local chord. Tests results reported, for a flight

¹⁵ <http://www.3m.com>

Mach number equal to 0.70, that the presence of riblets actually contributed to slightly change the velocity profile on the wing surface, causing a lower velocity gradient (Figure 61, right). Results from two flights showed a skin friction drag reduction of 6-7%, in a range of s^+ varying from 10 to 15, while not significant effect of h^+ (at least for the riblet films tested) were observed.

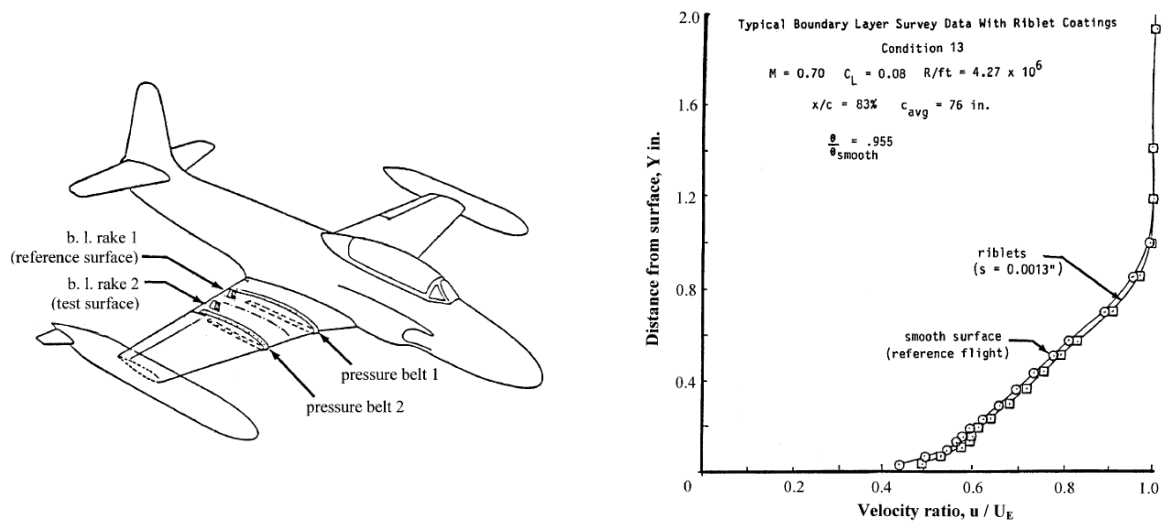


Figure 61: T-33 jet trainer riblet testbed (left) and velocity profile on wing for M = 0.70 (right).

In Ref. [85] Szodruich reported a flight evaluation of riblet performance on an Airbus A320. For this test, about 70% of the aircraft surface was covered with riblets. In order to estimate the total drag reduction, fuel burn savings were estimated during flight tests. According to Szodruich, for a Mach number range of 0.77-0.79, a 2% in total drag reduction was obtained, a really encouraging result considering it came from actual flight tests performed on a marketed commercial aircraft.

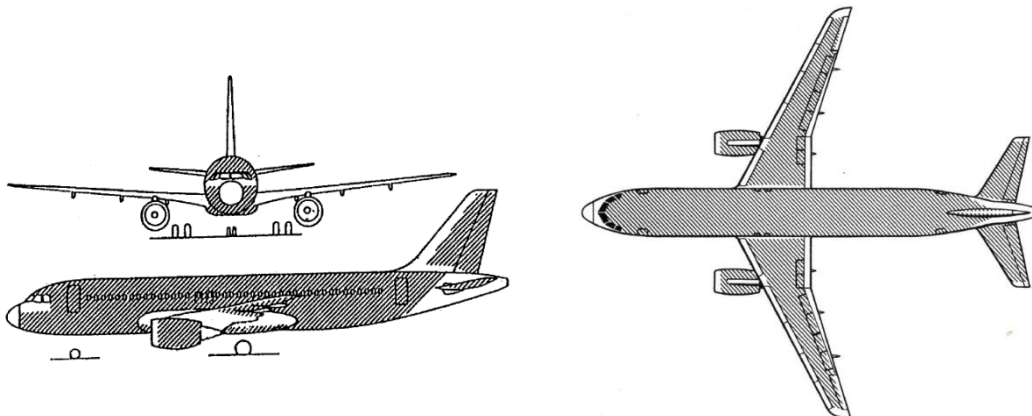


Figure 62: A320 riblets testbed [85].

As highlighted before, riblets pose some serious aerodynamics issues, such as their performance in off-design conditions. Other than that, several additional considerations must be made. Riblets, in fact, imply additional operative costs: maintenance of riblet shape and adhesiveness over operational life is required. Hydraulic fluids, dirt, insects, and hail can easily compromise their performance, and time required to install, remove and re-apply is surely not a negligible cost for an operator.

5.3 High Aspect Ratio Wing

Improving an aircraft aerodynamics efficiency is directly related to drag reduction, either parasite drag or induced drag. Technologies for parasite drag reduction have been already presented in Sec. 5.1.4 and Sec. 5.2. Induced drag is directly affected by the wing aspect ratio. It follows that

an ultra-high aspect ratio wing, with values well beyond the limits of actual operative commuters, would improve the aircraft aerodynamics efficiency. Moreover, by using an Ultra-High Aspect Ratio (UHAR) wing, laminar flow could be achieved more easily, because of the reduced cross-flow component.

Using an UHAR wing as a mean to improve an aircraft efficiency could be considered as the easiest and most straight-forward solution. However, there are some drawbacks in this immediate solution. Increasing the wing aspect ratio means either to enlarge the wingspan or either to reduce the wing area. Both have their pros and cons. A higher value of the wingspan triggers the need for aeroelastic considerations. In high span wings these phenomena, together with wing loads, require a sophisticated wing structure which, in turn, shall not bring a high weight penalty. Practical issues, ranging from new manufacturing technologies up to everyday ground operations and constraints should also be considered a-priori in such a solution. With this purpose, innovative aircraft concepts such as the Strut-Braced-Wing (SBW) [86] or Truss-Braced-Wing (TBW) [87] may be designed and optimized aimed to improve the wing aerodynamics, structural efficiency, flight performance, and pollutants emissions. Usually, long range aircraft fly at transonic speed fly at a lift coefficient lower than short range aircraft. The latter, in addition, spend a significant part of their flight in climb and descent, performing short cruise segments. Climb and descent are both characterized by higher lift coefficient. Therefore, even if for long range aircraft drag reduction has a larger impact on fuel burn, it is evident that the larger benefits in decreasing induced drag can be obtained on commuter aircraft.

The ultra-high aspect ratio wing configuration is expected to be prone to aeroelastic issues with specific reference to wing elasticity influence on loads distribution, effectiveness of roll control as well as on aircraft static and dynamic stability. Therefore, the preliminary stage of aircraft design cannot neglect the multi-disciplinary interaction between aerodynamics, structures, stability and control. As the simple cantilever wing layout is unfeasible for a wing aspect ratio as high as 20, strut-braced or truss-braced wing configurations must be considered. These configurations should provide fuel burn reduction between 10-20% [87,88] compared to a conventional cantilever wing (for a long range aircraft with additional innovative technologies such as riblets and natural laminar flow). Lacking similar aircraft configurations in service, the classic preliminary design methods cannot comply with such a task. Therefore, low- and medium-fidelity methods, such as vortex or doublet lattice methods, should be applied to investigate the aerodynamics, stability and control of a set of ultra-high aspect ratio wing configurations. In parallel, trade-off flutter, divergence and control-reversal analyses should be carried out to define a "safety domain" of stable structural arrangements for the wing [89].

Recent investigations on a regional aircraft with a typical mission profile of 300 nmi have shown that doubling the aspect ratio with a conventional layout will increase the operative empty weight of about 40% the fuel burn of about 10%. The effect of reducing the induced drag has been exceeded by the increase in weight. The UHAR wing becomes attractive if the design manufacturing technology is such that there is at least a 30% structural weight saving with respect to a conventional cantilever wing, as reported in Figure 63.

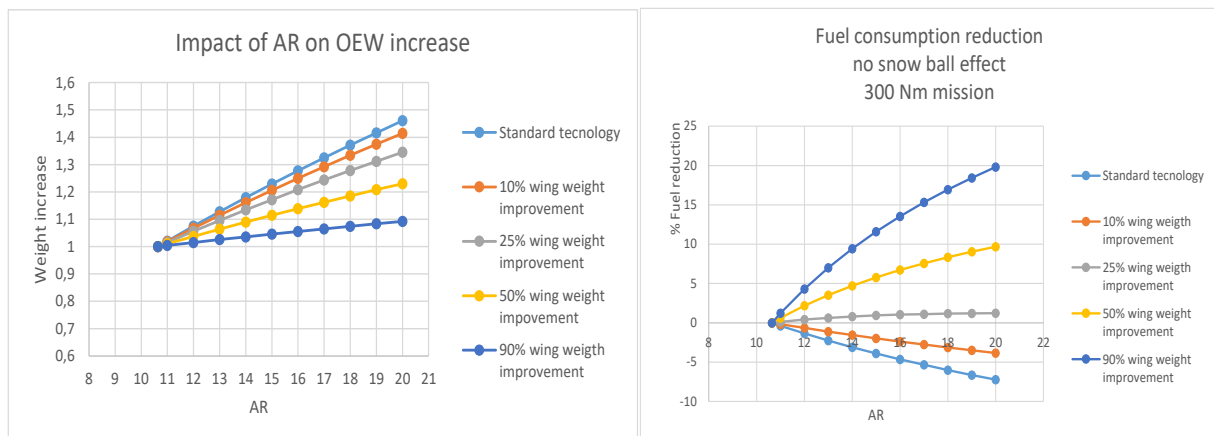


Figure 63: Example of potential weight increase and fuel burn variation due to aspect ratio variation.

5.4 High lift Device

Further improvement in aerodynamics are related to the design of high-lift devices. In SAT, Piaggio Aero and Evezkor are working on the design of such system, improving the design, hence the low speed performance.

Together with methods and tool improvement, a better high-lift device design can lead to a whole aircraft improvement.

High-lift systems, which include wing flaps and slats, are under development for small aircrafts in a first Clean Sky 2 research phase. After optimising the aerodynamic and integration design, these devices will be classified based on their high lift architectures to shortlist the best design. The EU-funded **MOTHIF**¹⁶ project will use a specifically designed and manufactured wind tunnel model for testing variable positions of flap and for different angles of attack. Along with the flap separation control jet blowing system installed at the main wing box trailing edge, this will be installed in the VKI subsonic wind tunnel and tested at the required Reynolds number. The project is on-going and results are not yet available. An example of active control on high-lift device is shown in Figure 64.

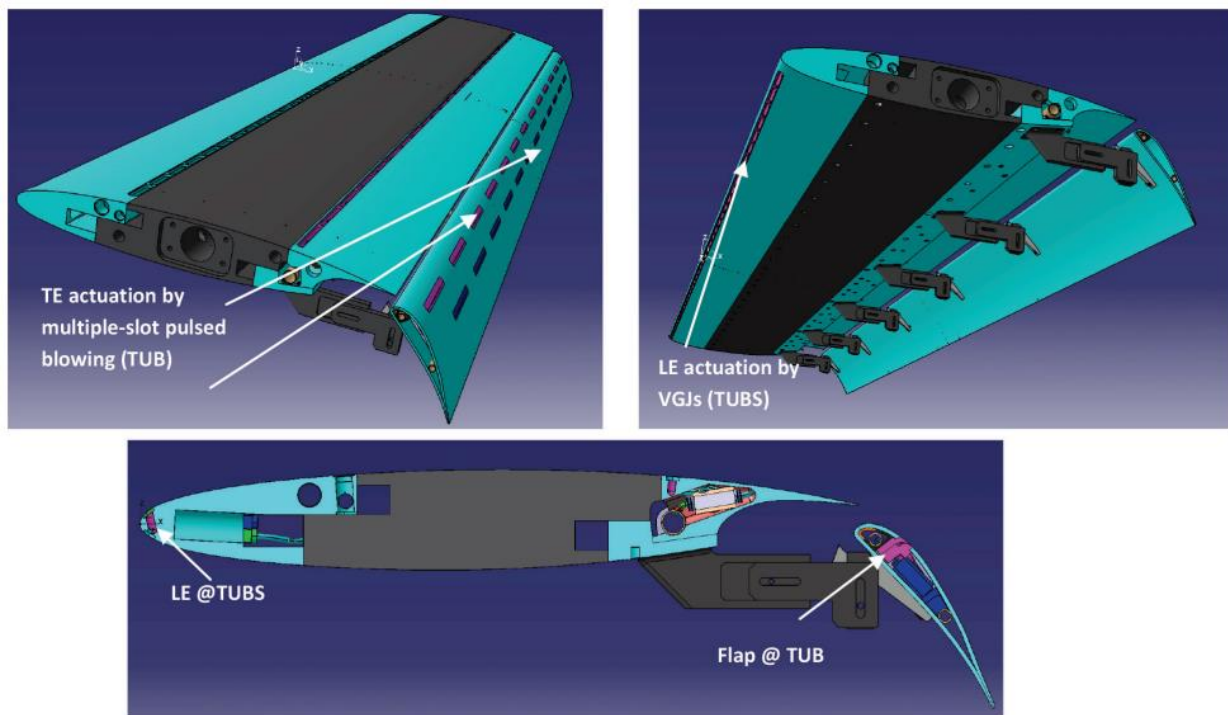


Figure 64: Actuation systems implemented on the DLR F15 model[90]

¹⁶ <https://cordis.europa.eu/project/id/865267>

6 Airframe

As a matter of facts, airframe directly affects the aircraft weight. That is the reason why a lot of new technologies were introduced in the last decades to pave the way towards low carbon air vehicles. New materials, along with new process technologies have been widely investigated with the aim to get to a lighter airframe. However, from one hand there is still a lack of understanding in new materials and almost each novel concept introduced (e.g. composite materials) has many drawbacks preventing their full exploitation in terms of weight saving and introducing strict maintenance procedures. On the other hand, airframe design is a matter of weighting structure configuration with aerodynamic loads and performances. As a direct consequence, the configuration designed is not always the best structural layout possible. Many factors affect the airframe design and multi-disciplinary analysis is strongly needed.

Moving from material and layout characterization, the most promising key enabling technologies are reported afterwards focusing the attention on how and how much they can impact the design at aircraft level. As a matter of facts, airframe directly affects the aircraft weight. That is the reason why a lot of new technologies were introduced in the last decades to pave the way towards low carbon air vehicles. New materials, along with new process technologies have been widely investigated with the aim to get to a lighter airframe. However, from one hand there is still a lack of understanding in new materials and almost each novel concept introduced (e.g. composite materials) has many drawbacks preventing their full exploitation in terms of weight saving and introducing strict maintenance procedures. On the other hand, airframe design is a matter of weighting structure configuration with aerodynamic loads and performances. As a direct consequence, the configuration designed is not always the best structural layout possible. Many factors affect the airframe design and multi-disciplinary analysis is strongly needed.

Moving from material and layout characterization, the most promising key enabling technologies are reported afterwards focusing the attention on how and how much they can impact the design at aircraft level.

6.1 Smart Intelligent Composite Structures

One of the major concerns of aerospace and transportation engineering during the last years has been related to efficiently adopt composite materials to increase vehicle performance and safety with energy savings. Composite materials have been indeed widely adopted with the aim to design stiffer and lighter components. That is mostly because they ensure tailoring the properties of the structure according to the specific load to be withstood achieving the optimal ratio between strength/stiffness and weight. In addition, composite materials allow one-piece barrel manufacturing with an incredible weight saving due to unneeded connections. However, there are many other aspects preventing their full exploitation which directly reduce the benefits that pushed up the composite quotation as key enabling technology.

For instance, random events such as certain low velocity impacts, may induce barely visible or not visible failure due to the complex mechanics behaviour of such anisotropic and multilayer structure. Impact induced damage in stiffened composite structures is usually accommodated with constrained design and strictly maintenance tasks which increase operational costs above all else and decrease the advantages for which composites have been massively introduced. To overcome such drawbacks, an integrated structure providing monitoring of critical components appears the most promising solution. A condition-based approach could be able to relax the maintenance strategy minimizing aircraft downtime as well. Moreover, the design constraints would be avoided with a further increase of structural performance resulting in a more environment friendly aircraft. Although the latter possibility is a very long-time perspective, for the first goal Structural Health Monitoring (SHM) systems, providing continuous or on demand information about the structural efficiency, appear to be the key technology.

Aircraft health monitoring system aims at enhancing flight safety and at the same time reduce maintenance and operational costs. A system that enables automatic detection, diagnosis, prognosis and mitigation of adverse events arising from component failure, can be conceptualized in an integrated vehicle health management system. The current practice of scheduled maintenance increases the cost of maintenance steeply, especially in the case of an aircraft operating beyond its designed service life. That is to say, preventive (or scheduled) maintenance

requires a deep and strict inspection task program that could be relaxed by moving to predictive (or on condition) maintenance. However, adopting condition-based philosophy is only possible through an effective and reliable health monitoring system. The aim of a health Monitoring system is to detect and diagnose initiation of any defect, to analyse its effects and to trigger maintenance workflows in order to maintain aircraft safety. That is possible through capturing data by a network of sensors and analysing them by using data analytics algorithm aiming at providing diagnosis and prognosis in a reverse engineering approach. Health monitoring systems are employed on both structures and systems. SHM characteristics deeply approached in the present section, essentially looks at the structural integrity by monitoring damage emerging and growing within airframe and assessing its remaining useful life. System health monitoring, approached in a following section looking into the case of landing gear, looks at functional aspects and any degradation in performance triggering maintenance tasks or replacement of affected components.

6.1.1 Composite Damage Mechanics

Moving into details, composites are some of the most critical type of materials with respect to fatigue, where the crack initiation may be due to accidental damage as well. For reasons inherent in their internal structure, they suffer much more than any other conventional metallic material of problems related to damage. Typical for composites are matrix cracking, delamination, fiber fracture, interfacial debonding. These kinds of damage, especially those accidentally and suddenly induced and then occurring in fatigue problems, are very critical. The most problematic aspect is that damage can be produced even by events involving very small values of energies. As an example, delamination at interfaces between different oriented adjacent plies might occur as a result of impacts with external objects involving energies of the order of some Joules. Typically, these low velocity impacts produce so small damage within the material that they cannot be detected through a simple or detailed visual inspection because they are characterized by small external indentation (not visible or barely visible damages). The damage tolerance approach involves the use of inspection procedures and structural design concepts to ensure safety, rather than the traditional correction factors used for ultimate loads [91]. The overall damage tolerance database for a structure should include information on residual strength characteristics, sensitivities to damage growth and environmental degradation, maintenance practices, and in-service usage parameters and damage experiences. However, a sort of "defect" factor based on degree of detectability has been the basis for establishing minimum damage tolerance residual strengths for composite structures in requirements proposed for inclusion in [92]. These strength requirements are identical to those for metal structure having critical defects or damage with a comparable degree of detectability. Requirements for cyclic loading prior to residual strength testing of test components are also identical. The application of this philosophy is thus introducing **knockdown factors** affecting the design of composite structures. New methods of investigation have been developed to reduce the gap between theoretical and practical benefits, including SHM. As discussed afterwards, both composite design and aircraft maintenance strategies are definitely affected and could both benefit by integrating SHM capabilities.

Impact damage to composite structures is unique in that it may not be visible or may be barely visible, making it more difficult for a repair technician or aviation worker to detect that damage [93]. Impact induced damage is indeed a very complicated phenomenon, requiring the basic mechanics and damage mechanism understanding. Some concerns have been raised when damages have to be detected in composite materials especially due to such complex mechanics. The impact behaviour of composite materials has been studied experimentally by many authors [94] and the complexity of the physical phenomena demands detailed investigation to numerical modelling making difficult to extend analytical solutions to complex structures [95]. The low velocity impact damage in laminated composite plate structures can be recognized as a debilitating threat; it has a significant effect on the strength and durability of the laminates; it is an inevitable event and needs appropriate design solutions to be addressed [96]. As a matter of facts, a lot of work is still necessary to improve the modelling of the damage developing during impact on composite laminates to better assess numerically their residual mechanical characteristics in order to optimize their design [97].

In composite structure, the damage caused by an impact event is typically more severe and even less visible than in metals. As a result, composite materials are sensitive to many aspects of in-service use for which it is difficult to provide design data. While subjected to out-of-plane loading or minor objects drop, like tools during assembly or maintenance operation, composite laminates reveal a brittle behaviour which may lead to significant damages. These damages are classically divided in two groups:

- intralaminar damage, i.e. the damages developing inside the ply like matrix cracking, fibre/matrix debonding or fibres breakages, and
- interlaminar damage, i.e. the damages developing at the interface between two consecutive plies, namely delamination.

Such a hidden damage is particularly dangerous because drastically reducing the residual mechanical characteristics of the structure. The reduction in compression after impact (CAI) strength due to the low velocity impact is for instance of particular concern. Generally, the loss in strength may be up to 60% of the undamaged value and typically industrial designers limit compressive strains to the range of 3000 to 4000 microstrains [98]. This significant reduction in design allowable is also a result of the fact that testing coupons cannot simulate the behaviour of larger realistic structures because their dynamic response to low velocity impact may be quite different and it is not economic to perform impact tests on relatively large panels so as to evaluate impact behaviour and damage development. In addition to the compressive strength, the impact damage can decrease also the fatigue strength of a composite.

Composite structure failure is often caused by the development of different damage mechanisms which begin locally. In fibre-reinforced laminates, delamination is the most common damage mode. It is where the fibre-reinforced laminate behaviour differentiates from that of metallic structures inducing a primary concern in composite aircraft design. Delamination is caused by high interlaminar stresses and relatively low interlaminar strengths of such composites, that show also very low through-thickness strength. The delamination usually occurs between layers with different fibre orientations. Two adjacent layers with different fibre orientation introduce a mismatch of flexural and extensional rigidity through the thickness that combined with the low resistance of the matrix, lead the composite material to be very sensitive to separation of these interfaces. For these reasons, a major source of delamination damage is from low-velocity impact where usually matrix cracks develop first in the plies (shear or bending cracks) and delaminations then grow from these cracks at the ply interfaces. The delamination indeed rarely occurs as an independent damage mode; when a shear or bending crack in a layer reaches an interface between two layers oriented in different ways it is unable to easily penetrate the upper layers and it can spread like delamination. Relevant efforts have been spent in the past years to understand how delaminations arise within the composite laminates. The investigation conducted in [99] demonstrated indeed that the delaminations only occur when there is a change in ply orientations and develop mostly alongside the direction of fibres in the lower ply of the interface. The size, shape and distribution of delaminations utilizing several evaluative techniques is investigated in [100], where the classic "peanut" shape is found at almost every interface through-the-thickness. Several additional studies have revealed this characteristic shape and the complexities of the related mechanics [101].

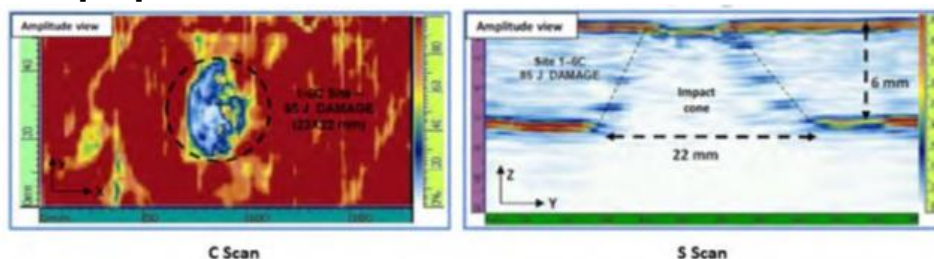


Figure 65: Low velocity impact damage. Typical peanut shape in the plane of the plate (left) and conical distribution of delamination through the thickness (right).

Nevertheless, the improved knowledge achieved in the last years, a major concern regards the detectability of damage. The impact induced damage evolution in composite laminates can be divided into two stages: (i) bending or shear stresses initiate the micro cracks in matrix, (ii) propagation of the micro cracks into the nearby interface yields to the delamination. The two kinds of damage, matrix crack and delamination, are connected and their relationship is responsible for the damage mechanism occurring under low velocity impact. These phenomena results in a very small surface indentation even when the through thickness damage is greater than an emerging flaw due to the mixed crack-delamination evolution. The structure of a damage typically obtained while a composite structure is subject to low velocity impact is showed in Figure 65, where a classic ultrasonic non-destructive evaluation (NDE) is depicted. Specifically, it regards the case of a 6mm CFRP plate designed for a lower wing panel of a commercial aircraft and loaded with a low velocity impact of 85J using a drop weight machine with one inch tip. The peanut shape and the relevant extent of damage is evident from the c-scan image (in plane view of the damage). Furthermore, the s-scan (section view of the damage) shows how the laminate is corrupted through the thickness with several delaminations arising among several layers resulting in the typical impact cone due to the complex failure mechanics (cracks-delamination mixed failure). However, although the conformation of the damage appears evident, the only visible item is the indentation on the upper surface which is of the order of few hundred microstrains and quite not visible.

6.1.2 Composite Damage Tolerance Approach

As a matter of facts, actually the complexities of composite response to low velocity impacts and the detectability of emerging damages require the design of structure to be appropriately addressed. Basically, in a damage tolerance approach, the presence of hidden failures due to barely visible damages is accounted during the design, generally accomplished by limiting the design strain level for ultimate and limit combined load design criteria [102]. Another common design approach limiting the benefits of composites is operated to preserve the collaboration of reinforcements. In this context, the typical problem regards the stiffened composite structures where the stringers adopted for reinforcing thin walled structures may be affected by not visible disbondings even when subjected to low energy impacts. As in the case of delamination, the punctual load leads to complex damage mechanics resulting in the separation between the stringer and the hosting structure preventing the collaboration between parts with a dangerous drawback for loading absorbing. Hence, disbonding stoppers are usually included into the design to avoid separations between stiffeners and skin above the maximum size ensuring safe structural collaboration [102]. As a matter of facts, connectors are indeed necessary where the introduction of composites would avoid or limit any type of connection between different parts to reduce weight as well as manufacturing and maintenance costs. This rough damage tolerance approach therefore breaks down the benefits encouraging composites introduction. There are indeed two primary damage tolerance requirements described in [103]: (i) damage growth characterization, and (ii) residual strength capability. The certification demands the demonstration of required levels of static strength, durability and damage tolerance as well as the ability to predict stiffness properties. Demonstration of compliance for composite structure includes sustaining design ultimate loads with damage at the threshold of visual detectability (barely visible impact damage, BVID) and sustaining design limit loads with clearly visible damage. In addition, it must be demonstrated that levels of damage smaller than those that reduce the residual strength to design limit load capability will not experience detrimental growth under operational loading conditions. For instance, considering the applied strains, materials and design concepts, a no-growth approach for damage tolerance has been adopted in the case of Boeing B777 empennage [91]. This approach is based on demonstrating that any damage that is visually undetectable will not grow under operational loads. This means that structures with undetectable damage must be capable of carrying ultimate load for the operational life of the airplane. The advisory circular [103] includes acceptable means of compliance in the following areas: (i) effects of environment

(including design allowables and impact damage); (ii) static strength (including repeated loads, test environment, process control, material variability and impact damage); (iii) fatigue and damage tolerance evaluation; (iv) other items - such as flutter, flammability, lightning protection, maintenance and repair. According to such items, the no-growth behaviour of B777 CFRP structure has been demonstrated in numerous subcomponent tests. Following the typical building block approach in use within aeronautical field, two full-scale cyclic load tests have been performed inserting damage sites during several test sequences. In addition, the full-scale tests demonstrated the following characteristics required for damage tolerance compliance [91]:

- manufacturing anomalies allowed according process specifications will not grow for the equivalent of more than two design service lives;
- visible damage due to foreign-object impact will not grow for the duration of two major inspection intervals (i.e. two "C" checks, 4000 flights per "C" check);
- the structure can sustain specified residual strength loads with damage that can reasonably be expected in service;
- the structure can sustain specified static loads ("continued safe flight loads") after incurring inflight discrete-source damage.

To demonstrate residual strength capability, the test box has been further damaged with visible impacts. Visible damages are those that are easily detected by scheduled maintenance inspections. Fatigue testing representative of two inspection intervals again verified the no-growth approach. Tests are also conducted to provide certification data for failure modes not readily predicted by currently accepted analysis methods. For example: strength after barely detectable impact damage, called threshold of detectability (TOD) impact damage in FAA advisory material; flaw growth from TOD impact damage; strength after detectable damage; flaw growth rates from detectable damage; lightning strike resistance; flame resistance.

Summarizing what is emerging analysing a real certification stage of an aeronautical composite structure, during the design phase, it is necessary to demonstrate that not visible and barely visible damages occurring at every time do not affect the safety of the aircraft between adjacent inspection checks. To detail how a safety design may be affected by unforeseen events, the typical trend of residual stress/strain versus impact energy level is schematized in Figure 2 A first low energy range is connected to not visible damages as it is not inducing any failure (namely below the energy level ensuring the onset of a hidden failure). Then, the residual strain/stress deeply decreases while the impact energy level ensures a slightly increasing damage which is barely visible. That failure is indeed characterized by a through thickness delamination where not any indentation is visible (inner visibility) or together with a slightly visible indentation (external visibility) which is not always appreciable by visual inspection. Then, the damage appears increasingly evident according to the energy level. That is the limit for ultimate design stress or strain where any safety factor is not considered yet.

Furthermore, as above mentioned, the damage is not the only event introducing knockdown factors. Other aspects to be accounted are reported in Figure 67, whose scheme shows how they define the allowable design region merely with a reduction of allowable stress/strain. Composite structures are indeed sized using limit allowables, which results appreciably lower than material ultimate due to the introduced tolerance (see Figure 68). According to Boeing design manuals and military handbook [91], the design limit allowable $\sigma_{d.l.a.}$ can be calculated for first approximation introducing a scatter to the ultimate material allowable $\sigma_{m.u.a.}$ as follows:

$$\sigma_{d.l.a.} = 0.5 \sigma_{m.u.a.}$$

This definitely means that a huge amount of weight reduction expected introducing composite materials is wasted. That is where the SHM introduction may provide more relaxed design, limiting the allowables to the residual stress or strain associated to the minimum damage detectable with an integrated system (i.e.: the system target) capable to identify emerging flaws where any other detection is not possible. As a matter of facts, the standardization and reliability required to move

from the damage tolerance to a condition-based design actually makes far from application the integration of SHM technology during the structural design to avoid knockdown factors due to detection of inner visible damages.

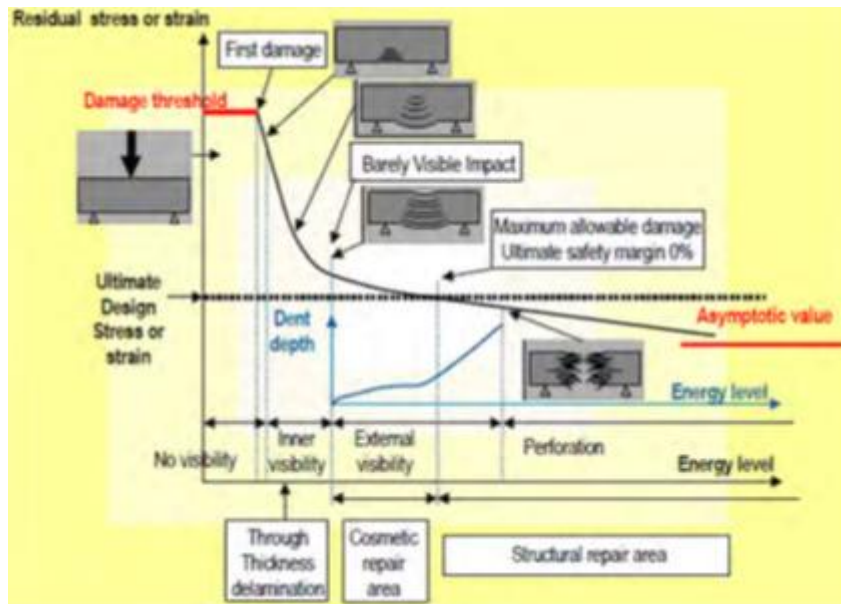


Figure 66: Schematic representation of residual strain versus energy level and derived design constraints.

However, due to the results that this type of system may potentially achieve, SHM appears to be the only way to design high performance and lighter components reaching the advantages expected fully up to now. For these reasons, the condition-based design is referred here as long-time perspective of SHM. Instead, the short-time perspective introducing SHM is related to the damage assessment procedure adopted during lifetime and connected again with damage tolerance approach which is based on scheduled inspections to ensure safety.

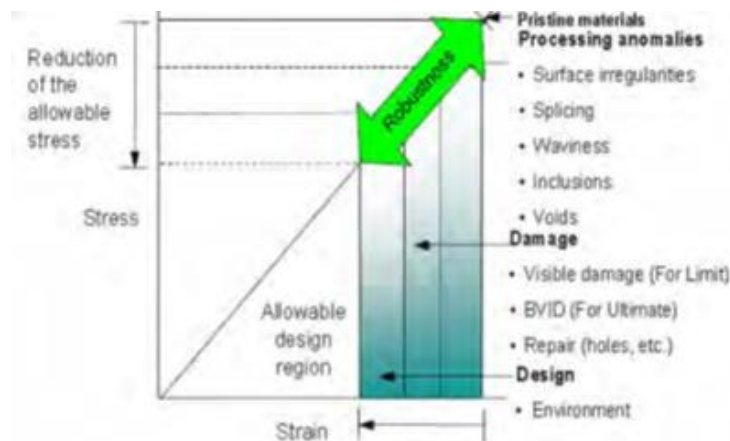


Figure 67: Schematic representation of scattering factors constraining the composite design.

The Paris law or similar approaches are useful to define the remaining life of structure, but the particular evolution of the crack in structures subjected to cyclic loads requires a skilful inspection planning. As a matter of facts, extreme conditions in which aerospace structures are expected to work lead to continuously check the ability of the component to support the expected loads and it is primarily a flight safety consideration. Damage tolerance ensures the structure can continue of carrying the agreed-upon regulation loads despite any damage or degradation (e.g. impacts induced failures). As indeed defined in the previous section with the example given by the Boeing B77 empennage, the damage tolerance is defined in connection with the prescribed checks no

matter the growth approach is. Consequently, the concern with damage tolerance is ultimately with the damaged structure having adequate residual strength and stiffness to continue in service safely at least until the damage can be detected by following scheduled maintenance inspections.

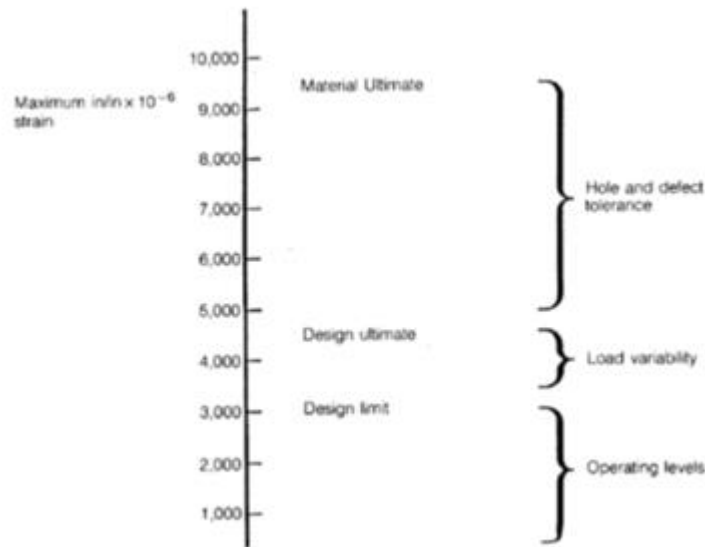


Figure 68: Typical design allowables for carbon fibers reinforced plastics (CFRP).

The focus of damage tolerance evaluations should be on ensuring safety in every unforeseen event, not solely on likely scenarios of damage, like that tested within B777 program. As a consequence, an important part of a structural development program is to determine the damages that the structure is capable of carrying at the various required load levels (ultimate, limit, etc.). This information can be used to develop appropriate maintenance, inspection, and real-time monitoring techniques to ensure safety. Structure certified with an approach that allows the presence of a damage no matter the damage growth is, must have associated in service inspection techniques, which are capable of adequately detecting damage before it becomes critical. In addition, if the damage growth is allowed, it must be predictable such that inspection intervals can be reliably defined.

In this context in-service inspection procedures play a major role so that structural regions and elements are classified with respect to required non-destructive inspection (NDI) and NDE sensitivity. Inspection intervals are usually established on the basis of crack growth information assuming a specified initial flaw size and a detectable crack size, the latter depending on the level of available NDI/NDE procedure and equipment. Cracks larger than that are presumed to be discovered and repaired with a defined confidence level. That is the target of the NDE equipment usually assessed with Probability of Detection approaches [104]. Furthermore, the inspection intervals must be such that an undetected flaw will not grow to critical size before the next inspection. Due to their key role, the use of NDI/NDE techniques and the establishment of appropriate inspection intervals have progressed considerably especially in the case of composites.

Non-destructive testing methods deal with the identification and characterization of damages without altering (destroying) in any way the component inspected, whether they show inner or external visibility. Due to their characteristics, they provide a cost effective approach to investigate condition of a single component or for the in service inspections of complex systems [105]. In the field of composites, numerous techniques are adopted, including ultrasonic testing [106], thermographic testing [107], infrared thermography testing [108], radiographic testing [109], visual testing [110], acoustic emission testing [111], acousto-ultrasonic [112], shearography testing [113] and electromagnetic testing [114]. As described above, each one of these methods has advantages and drawbacks, addressing specific problems in several types of flaw to be detected

and different parts. As a consequence, although the great potentialities of several NDT techniques, some of their inherent limitations still persist. First of all, NDI/NDE inspection sensitivity and reliability while inspecting actual airframes are far from the standards within laboratory tests which include simpler coupons. However, the major concern of current NDI/NDE practices is that they cannot provide a continuous assessment of the structural condition. To practically perform NDI/NDE inspections, the aircraft has to be taken offline, disassembled in some parts and scanned. This process is time consuming and expensive, making necessary a detailed scheduling and preventing on demand inspections. The implementation of a SHM system could improve such situation due to the permanently attached transducers allowing structure interrogations as often as needed even when and where the accessibility is not possible. The potential benefits introduced by operating SHM within aircraft inspections are detailed in the next section, where specific examples are given to justify the cost benefits achievable by introducing condition-based monitoring with integrated structures.

6.1.3 Benefit of SHM System Within Aircraft Life Cycle

Unlike NDE inspections, the on-demand interrogations of a SHM system based on permanently attached sensors are done always in the same way, making possible to build an historical database and acquire change information to assist in the system reasoning process. Advanced signal processing methods can be used to detect characteristic changes in the material state and make that state-change information available to the prognosis reasoning system. The concept of change detection can be used to characterize the material state by identifying critical features that show changes with respect to a reference state that is stored in the information database and updated periodically. When this is performed in coordination with existing NDI/NDE practices, the structural health monitoring information performed between current inspection intervals can provide supplementary data that would have a densifying effect on the historical information database. Another advantage of implementing SHM systems is related to the nonlinear aspects of structural crack propagation. Most of the current life prognosis techniques are indeed based on linear assumptions rooted in laboratory tests performed under well-defined conditions. However, actual operational conditions are far from ideal, and incorporate a number of unknown factors such as constraint effects, load spectrum variation, and overloads. These effects are within the nonlinear fracture mechanics and make the prediction very difficult. However, the dense data that can be collected by an SHM system could be used as feedback information about the crack-growth rate and could allow the adjustment of the basic assumptions to improve the crack-growth prediction laws.

Structural health monitoring could have a major contribution to the structural diagnosis and prognosis not only increasing the safety by introducing a continuous monitoring. As a matter of facts, the introduction of an effective SHM system may completely change the maintenance strategies increasing safety level of operations. The damage assessment process is really complicated by the necessity of inspections targeted to ensure safety according to the damage tolerance design criteria. The complex environment in which aircrafts work, driven by the business of the operator, lead to the necessity of scheduled inspections between several flights which minimize the downtime. Actually, the damage assessment process is based on different levels of inspection, as depicted in Figure 69, and oriented to release the aircraft or to require its repair. The turn-around operated by the aircraft captain is the first way to detect damages by visual inspection. However, the first detailed inspection is operated by the Level 1 inspectors according to rigorous visual inspection criteria and it is usually available at larger airports. When the release is not obtained during this phase, the inspection operated using sophisticated NDT approaches is required to obtain the release or repair response. However, the Level 2 inspectors, in charge of such type of inspections, are available only in certain bases and it is necessary to move the aircraft in most cases. As a matter of facts, the inspection procedures are complicated and introduce often relevant downtime. In this context the principal aim of SHM is to reduce operative costs moving from the actual maintenance approach based on two different levels of inspection

towards a condition-based philosophy exploiting an autonomous and integrated sensing system for achieving the release of the aircraft or its repair request.

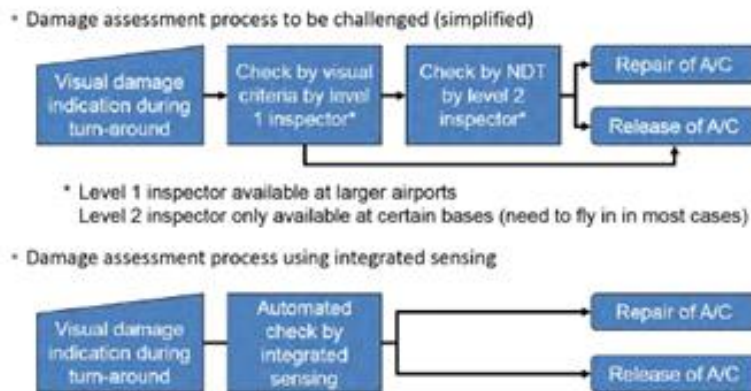


Figure 69: Damage Assessment process based on NDE and SHM capabilities.

According to the IATA benchmark for direct operating costs per flight depicted in Figure 70, the 17% of the operative costs of a recent aircraft are demanded to maintenance tasks and they can increase up to 25% for aging vehicles. **In the case of the 19 pax aircraft De Havilland Canada DHC-6 Twin Otter, the maintenance costs (based on a combination of labour costs and parts costs) are about 21% of the total direct operative costs while airframe and propeller maintenance cost assumes an annual utilization of 1200 flight hours (FH) and a cycle to FH ratio of 2, which is the typical mission of that aircraft.**

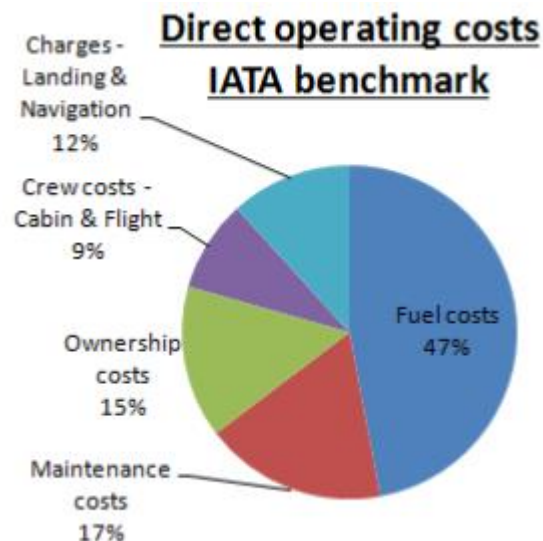


Figure 70: Cost breakdown for commercial aircraft.

The scheduled maintenance levels for a commercial aircraft are reported in Table 11 with typical frequency and man hours required for each of them. This summary easily explains the complexity of maintenance procedures, step by step heavier, to ensure safety of aircraft lightweight structures. The check A is usually performed overnight every 500-800 flight hours (FH) at an airport gate while the check B requires 1 to 3 days at an airport hangar to be completed. More complex but very crucial is the Check C, usually performed less than every 2 years requiring 1 to 2 weeks of work in a maintenance base. Instead the check D is operated usually every 6 years, where the paint may be needed to be completely removed for further inspection on the fuselage skin. For this reason, it requires a suitable maintenance base and about 2 months of work. Such data are variable and depend indeed on how much the aircraft is devoted to maintenance, as reported in Table 11 for the check C.

Check Type	Frequency	Man hours
A	500-800 FH	20-50
B	4-6 months	150
C	20-24 months	6000
D	6 years	50000

Table 11: Scheduled maintenance levels for commercial aircraft.

The cost of a check C depends on the maintenance required (it may be light or heavy) starting from 60k\$ for a small narrow body aircraft up to 1M\$ for a wide body aircraft [54]. Again, considering the case of the 19 pax aircraft De Havilland Canada DHC-6 Twin Otter, the maintenance programme contemplates the check C is performed after 4000-6000 FHs and is usually anticipated by 48 scheduled inspections of 100-125 FH interval. Only the C-check could cost up to 30-40 k\$ (the C-check lifetime plan is about 5-6% of the direct operative cost of that aircraft) while the total maintenance cost needed before is approximately equal to 100-120 k\$.

A/C Type	Interval	C-Light Cost (\$)	C-Heavy cost (\$)
B737-800	20 months	120k – 160k	220k – 320k
B747-400	18 months	600k – 800k	1.0M – 1.2M
B767-300ER	16-18 months	450k -550k	600k -700k
B777-300ER	16-20 months	375k – 475k	550k – 650k
A320-200	18 months	150k – 180k	250k – 350k
A330-300	18 months	375k – 475k	550k – 650k
E190	6000 FH	70k – 90k	110k – 180k
CRJ-700	4000-6000 FH	60k- 80k	100k – 170k
DH TwinOtter	4000-6000 FH	20k – 28k	30k - 40k

Table 12: Approximate costs for C-check inspection for a variety of aircraft categories.

Starting from these considerations, to reduce such costs it is possible to limit non-destructive inspections and disassembly of aircraft just in case of negative response claimed by a SHM system. It is indeed estimated that in this way SHM allows to reduce a relevant percentage (**up to 3-4% maintenance costs**) of operative costs for airlines by modifying the damage assessment process (short-time perspective). As a consequence of such aspects, the introduction of a reliable SHM system can increase the safety (continuous monitoring) reducing costs (maintenance just in time).

About the latter perspective, it is possible to quantify such reduction estimating inspection costs and SHM system benefits instrumenting the door surrounds of a passenger airplane with 2 doors. The area under investigation is about 3m² and the standard design flight goal of the fuselage is about 100k FH. The costs of inspection and instrumentation can be divided in NDT inspections, SHM weight, sensor installation and sensors cost. The former is demanded for actual maintenance operation and consists of inspection for barely visible damages (BVID) and visible damages (VID) operated by L2 level inspector. Each inspection may cost around 22k\$. The other costs are demanded for SHM based maintenance by avoiding any NDT inspection. For instrumenting one door surround are needed about 3kg of sensors, 7kg of electronic parts and 16kg of cables and miscellaneous, for a total mass of 26kg per door. The operational cost derived by further introducing 1kg is about 0.07\$ per each FH. The sensor installation cost depends on how the sensor are bonded: (i) bonded on the cured structure or (ii) co-cured. In the first case the cost is about 26k\$ per each door surround ensuring 200M FH of durability while it decreases to about 8k\$ for a cobonded installation. This means 58k\$ or 16k\$ for instrumenting all door surrounds of the fuselage. the sensors will cost approximately 12k\$ per door, with a total cost of 24k\$. For an aging airplane is estimated that 1000 damages will occur on the fuselage operating for 500k FH. About 75% of these damages occur at door surround and 80% of these damages have a dent depth within 0.3mm and 1.3mm and they require inspection. For a composite it can be assumed that $d < 0.3\text{mm}$ is not visible, $0.3 < d < 1.3$ visible but less

than the allowed size and $d > 1.3\text{mm}$ visible but with non-admissible damage. In conclusion, the occurrence of damage requiring inspection is $1.1 \cdot 10^{-3}$ per FH. The resulting cost for inspecting door surrounds is about 2.4M\$ per 100k FH. **According to the estimation given above, a fuselage integrated with sensors around the doors will cost in the worst case about 0.438M\$ with a benefit of about 1.9M\$ if no inspection is carried out while continuous monitoring the structure.**

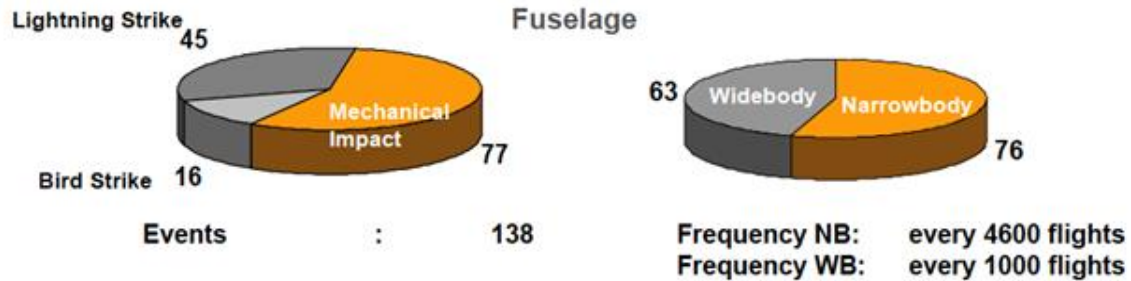


Figure 71

Figure 72: Damage occurrence on a composite fuselage for wide and narrow-body aircraft (courtesy of Lufthansa Technik).

It is possible to quantify the reduction of costs even considering a composite panel with an area of 1 m^2 and making a few assumptions again for the benefit and cost calculation. For the former let us consider that:

- Impacts which are not visible are within allowable damage size
- Impacts occurring which are visible but within allowable damage size
- Special detailed (NDT) inspection after visual impact detection required
- Special detailed (NDT) inspection by L2 inspector: one day for arrival time including 9 hours inspection effect Aircraft on Ground (AoG costs) for about 45k\$. In addition, inspection cost can be approximately calculated as 240\$ per Man Hour resulting in about 2k\$ for the prescribed inspection and a total cost of 47k\$

For the Cost calculation:

- Additional weight of SHM system causes costs of 0.07\$ per FH and kg
- The design goal for the selected wing is 100000 FH
- No maintenance costs are needed for SHM system

Sensor installation based on secondary bonding techniques could need approximately 50 Man Hours (1 MH = 150 \$) to install 50 Sensors on 1 m^2 of composite panel (at structural assembly) with a total installation cost of 7500\$. The Hardware of the SHM system can be broadly divided in:

- Sensors = $50 \times 30\$$ (Duraact) = 1500 \$
- Acquisition/generation channels = $50 \times 100\text{€}$ = 5000 \$
- Data acquisition/analysis unit = 2000 \$

With a total HW cost of approximately 16000\$.

The mass added by the SHM system introduces operating costs approximately equal to 0.07 \$/kg/FH. The total weight added on-board can be broadly divided in:

- Cables: $100\text{m} \times 7,5\text{ gr/m} = 0,750\text{ kg}$ (reduced cables length can be obtained by "hubs" like "piezocubes")
- Sensors: $50 \times 2\text{gr} = 0,100\text{ kg}$
- Connectors: $50 \times 10\text{gr} = 0,500\text{ kg}$

For a total mass of about 1,350 kg. that is introducing about 9450\$ (1,350 x 100000 x 0,07) of costs for the designed useful life of the airframe. Under that hypothesis, the overall SHM system cost about 25450\$ for each square meter.

To make a benefit vs. cost comparison let us consider that the costs depend on the number of damage occurring that requires L2 inspection and 1day aircraft on ground, which costs about 51 k\$. Let us assume unknown the occurrence of relevant damage ($P(E)$ Damage/FH), then the benefit can be computed as:

$$\text{Benefit} = 100000 \text{ FH} \times P(E) \text{ Damage/FH} \times 47\text{k}\$$$

$$\text{Benefit} > \text{Costs} \quad \text{if} \quad P(E) > 25/(47 \times 100.000) = 0.53\text{E-}5$$

Just to give an impression, probable events which are likely to occur at least one time during the operational life of a number of airplanes of the same type corresponds to a probability of occurrence $P(E) > 1\text{E-}5$ FH. That is to say, considering 40m² surface wing of a 19 pax aircraft, 20 impacts during the whole lifetime are enough to have benefits achieved costs for instrumenting the wing. However, it is statistical identified that up to 1300 impacts due to bird strike may occur at wing surface with damage requiring inspection occurring in many of that cases [115].

The impressive benefit obtained based on certain assumptions([116], [117], [118]) and affected by an uncertainty of 10% does not account the cost for SHM maintenance and the inspections required for clarifying some system responses (combined NDE-SHM). However, also including scatter factors, the promising benefits introduced by integrating SHM during damage assessment process (short-time perspective) are remarkable and not negligible. **Extending this calculation to the whole aircraft with a scatter factor equal to 4, it is possible to achieve about 4% reduction of maintenance costs, that is to say, about 0.8% of direct operative costs.**

In addition, SHM must be considered during the structural design: monitoring, inspection and damage detection become an integral part of structures at the design level reducing the knockdown factors introduced by actual damage tolerance approach (long-term perspective) for further decrease operational costs. Considering the limitation schematized in Figure 3, the damage tolerance approach introduces about 15% reduction in allowables calculation due to damage, whose contribution can be divided among safety factors need to address holes and repairs (which decrease the material allowables because of stress intensity factors around the affected region) , visible damage and barely visible damage if one is considering ultimate or limit load, respectively. That is to say, the thickness of the structure will be increased of about 15% to address the presence of a damage which can be statistically expected among two C-Check intervals. The use of continuous monitoring technology, warning the presence of damage immediately after occurring, can reduce this gap significantly. Imprinting that wing and fuselage takes approximately 8-14% and 7-12% of the maximum take of weight and considering the effect on the design limit allowable only, **in the worst case the maximum take-off weight can be directly reduced of 0.75%**. That is where SHM directly reduce take-off weight. However, then it enables the snowball effect with further reduction of weight and costs.

As a matter of facts, actually SHM appears the major key enabling technology to design safer and lighter airframes.

6.2 On Condition Maintenance of Aircraft

Structural Health Monitoring deals with the analysis of structural performances in view of on condition maintenance as well as integrated oriented design. However, a health management system is a complex environment in which the diagnosis is the crucial but not the only critical task to perform. Different stages can be identified, and likewise different methodologies can be exploited to perform different tasks. The underlying concept is to record the response of a structure when excited by a diagnostic or ambient input, process and analyse the response to extract features affected by defect and relate such parameters to defect characteristics. A typical SHM system consists of transducers for actuation and sensing. The actuator is usually excited by a signal generator for generation of diagnostic input while the sensors acquire data to be

transmitted to a data acquisition system. In few cases the ambient excitations replace the diagnostic input and all transducers are used to detect the response of the structure to such external loads. From this distinction, it is possible to broadly group several methods in:

- active SHM;
- passive SHM.

In both cases the data are analysed by a post-processing unit to predict and estimate damage. Therefore, an efficient SHM system requires transducers, signal processing for several purpose and algorithm providing damage reconstruction/information.

Generally, a SHM system may provide a multi-level diagnostic, depending upon the information collected and the algorithm adopted to interpret test data sets. It mainly deals with diagnostic phase and should be supported by a prognosis tool predicting the remaining life span of the structure to obtain a self-sensing smart structure with a condition-based lifetime strategy. The health management system can be broadly divided in four different steps [119]:

- damage detection, oriented to identify mostly the presence of the damage when a certain metric overcomes a defined health threshold (decision making output);
- damage localization, which deals with the identification of the more probable location of the detected damage (position output);
- damage dimension assessment, aimed to provide the extension and/or severity of the flaw (severity output);
- remaining life, which deals with the prognosis of the current expected lifetime of the component considering the dimension of damage and the prescribed load history (prognosis output).

The first three outputs constitute the diagnosis of a comprehensive SHM system while the last one is the prognosis demanded as input for the management of the monitored component in order to deliver aircraft release or repair (see Figure 69). From this breakdown, it is possible to define the multi-level diagnostic necessary for condition monitoring approach. The crucial issue is the damage detection, whose reliability affects the remaining steps. The target of the system, i.e. the minimum detectable size with a defined confidence level (usually approached extending to SHM the Probability of detection analysis [104] is crucial for application purpose. Regardless the detection capability of the metric, the quantification of a SHM system [120] is strongly affected by the decision level adopted for the identification which needs a careful unsupervised [121] or supervised [122] analysis of data and it should be optimized in view of the aircraft lifetime management [123]. Moreover, the relation between signal response and flaw size can be primarily assessed approaching a statistical analysis to correlate the specific feature to the damage dimension and/or severity [124]. Thus, the system provides simultaneously the presence and the severity of damage scenario. To finally assess the location of hidden flaw, a dedicated algorithm should analyse the (non-censored) data sets available after decision making.

As a matter of facts, a comprehensive diagnostic output may be simply achieved but it is crucial to: (i) chose a signal response that is sensitive to such a hidden flaw as well as increasing with the severity of damage and (ii) estimate at least the position of damage as a spatial point using a reconstruction algorithm. However, a critical point in the context of this work is in the type of damage scenario induced by low velocity impacts which may be different depending on the impact location. Typically, delaminations mostly arise between adjacent layers of flat multilayered composites while disbondings appear in stiffened composites between thin walled structure (skin) and stringer. Consequently, a SHM methodology aiming to discover and characterize impact induced damages should be able to monitor both events.

In addition to that, an operational load monitoring is strongly required to estimate loads and overloads and update the remaining useful life accordingly [125]. The value of information [126] given by such adaptive prediction tools can be used to manage even scheduled maintenance

tasks and avoid useless inspections or costly replacement and repairs with an increased return of investment respect to the integration of SHM only capabilities.

Previous research projects related to similar topics focused on the development of structural health monitoring, usage monitoring and operational load monitoring methodologies. However, to get condition maintenance approaches into practice, it is crucial to adapt and implement such methodologies, assess the reliability of the self-monitored system, define the minimum requirements for the system and define an operation strategy according to the previous aspects. Hence, it is worth developing strategies for addressing the actual maintenance philosophy including structural health monitoring, usage monitoring and operational load monitoring diagnostics in order to make condition monitoring enables increased asset availability and hence a higher return on investments while ensuring safety.

The European Union itself is deeply involved in research programs dedicated to mature, validate and demonstrate the technologies that best suit the environmental goals set for regional aircrafts, that will enter service from 2020 onwards, performing low-weight aircraft configurations in which the continuous monitoring is a key concept. The "Green regional Aircraft (GRA)" project¹⁷ recently funded within "Clean SKY" platform under the FP7 program, is indeed aimed to reduce CO₂ and NO_x emissions through lightweight architecture, efficient energy management and increased aircraft availability through more efficient maintenance (repair, longer lifetime etc.). However, a crucial aspect emphasized by the recently funded project "Smart Intelligent Aircraft Structures (SARISTU)" under the FP7 program¹⁸ is to limit the integration cost of SHM systems by moving the system integration as far forward in the manufacturing chain as possible. In this manner, SHM integration becomes a feasible concept to enable in-service inspection cost reductions. This concept can be transferred to smaller aircraft easily when the aim is mostly the environment protection because it will enhance economic return for the operator as well.

It is quite complex to provide a defined TRL for such an approach, but the aim of the future projects should be to move from an unproven concept (SHM system, which is standing as idea because the testing of the required technologies have been tested only) to the complete formulation of the concept, which will be optimized in terms of direct operative costs (DOC) and emissions and verified by means of requirements compliance.

The SHM system development, including employed technologies and methodologies, assumes a crucial role for the enhancement of maintenance strategies of commercial aircrafts. Modern aircraft can be mounted with a large number of sensors collecting information regarding aircraft operations and system condition. Coupled with maintenance event and logistics data, aircraft and system health diagnostics and prognostics can be developed, tested, and further validated, allowing for the adoption of a predictive approach towards aircraft maintenance and logistics. The output of these models/methodologies will be employed to feed into an efficient maintenance packaging and schedule optimisation framework for adaptive aircraft fleet maintenance management. The implementation of SHM within maintenance strategies allows moving to an "on-condition approach" the actual scheduled inspections and making scheduled the inspections actually unscheduled (due to new warning and prognosis capabilities). As a philosophy the SHM based maintenance is pro-active more than reactive as the actual maintenance approaches. The result is expected to move from a "preventive" to a "predictive maintenance" with the aim to obtain a cleaner, safer, and cheaper aircraft.

Predictive maintenance, diagnostics and health monitoring could eliminate unscheduled groundings, by making maintenance schedule intervals more frequent to avoid Aircraft On Grounds (AOGs) and the associated operational interruptions, ultimately eliminating them. Data or monitoring can tell that some parts do not need a scheduled check, but a full transition to this

¹⁷ Clean Sky 1 GRA - Green Regional Aircraft. [Online]. Available: <http://www.cleansky.eu/green-regional-aircraft-gra>

¹⁸ SARISTU - Smart Intelligent Aircraft Structures. [Online]. Available: <http://www.saristu.eu/>

model will need much greater experience. With more history, examples and regulatory confidence, the maintenance manual could become a dynamic document for each specific aircraft with every check and interval based on its operational history (depending on the past, current and future health of the aircraft).

However, SHM implementation within maintenance strategy requires the settling of various aspects mostly related to aircraft and damage types as well as level of safety ensured by the actual maintenance scheduling. For this reason, the actual approach is the focus for investigating the effective advantage of SHM based maintenance. Scheduled maintenance is a combination of different inspections categorized as transit check and A/B/C/D checks, respectively. From the transit to the D check, the time to perform the maintenance tasks is increasingly longer as the time interval between two following checks. The transit check, which can be done in half an hour, is performed even after each flight, but only obvious damage is checked by "walking around" inspection.

The other checks are performed in a time interval depending upon how the aircraft is devoted to maintenance. Just to provide an example, the A-check on Boeing B-737 (metal-based aircraft) is performed every 100 flight-cycles, and it normally takes about one week. During the A-check, only general visual inspection is performed. Instead the B-check is increasingly inserted in following A-checks. Since the internal surrounding structures are required to be removed starting from a C-check, this is the key point enabling request for SHM system standardization within maintenance programs. Instead, introducing SHM system for replacing actual D-check tasks may require SHM to be integrated within design of aircraft and the expected requirements may be not feasible for actual maintenance program modification.

SHM system standardization at C-check level reduces time to remove interiors, inspection costs and reduces risks of other damages while removing interiors. However, it is crucial to define the inspection level until which the SHM should operate as well as the framework of detection. To obtain a reasonable assumption, let us consider the B737 aircraft, whose C-check is characterized by a massive detailed visual inspection (DVI) up to 80-90 % of AOGs time. The remaining downtime/costs are related to NDI requested by maintenance operators for further analysis and calculation of maintenance engineers who release the aircraft or request for further repair. Hence, it can be envisioned to apply SHM at replacing visual inspection (general and detailed) and NDI (much more expensive) levels while engineers continue working as maintenance supervisors (for release/repair). On the other hand, it is necessary to fix standards to be achieved in terms of:

1. Hotspots Monitoring;
2. Global monitoring (analogous to human neural network);
3. Event detection.

The items 1 and 3 seem to be those more convenient and mature to get into practice SHM based life-management of aircrafts. Methodology standards/requirements must be established accordingly.

Aircraft and damage types are even crucial for standardization of continuous monitoring. The key points to be continuously inspected and characterized for a metal-based aircraft are:

- a. Joints and fittings;
- b. Bearing behavior;
- c. Crack growth;

Otherwise, for a composite-based aircraft it is crucial to monitor and characterize:

- d. Impact induced damage;
- e. Delamination and disbonding growth;
- f. Optimal crack-stoppers placement;

In addition, it is necessary to categorize the "non-identification" of maintenance-critical parts (e.g.: shear fittings of central wing box), where the request for NDE inspection and further monitoring

or anyway replacement should be established as convenient options. As a matter of facts, procedure standardization has to be achieved accordingly.

Regardless the specific field of application, SHM system standardization requires a monitoring approach, which should be continuous respect to the damage tolerance perspective. This means that damage may occur at airframe level and the structure must comply and withstand operative loads until next inspection (C-Check level). To replace conventional inspection with SHM, it is worth achieving its same safety level enhanced by a more continuous inspection. To account how much continuous should be the active monitoring, it is worth grouping three reference times:

- Interrogation Time; the time required to interrogate the aircraft with SHM capabilities provided by a multi-type and multi-purpose sensor network (MTMPSN);
- Available Time; on ground downtime useful for SHM inspection between two flights;
- Time to Inspection; target time for the inspection of the whole aircraft;

The interrogation time depends upon the area covered by sensor nodes, the type of monitoring and the time needed for each interrogation. For a certifiable SHM system, it is supposed here that the SHM interrogation cannot be activated in flight (online) but only on-ground (on demand). For this reason, the interrogation time cannot be covered with one single interrogation, but it needs for multiple interrogation slots, each of them covering a subpart of the aircraft. Those time slots cannot be greater than the available time to prevent altering the aircraft mission (Direct Operative Costs would increase). In addition, to ensure the safety level provided by actual maintenance, the Time to Inspection should not be greater than check-A interval (e.g. 100 flights for B737 aircraft). To enhance the safety as well as the accuracy of the SHM diagnosis, OLM can be enhanced by an event detection methodology (passive only) employed on-board (on-line/real-time) to detect unforeseen events during the time to inspection interval according and enhancing damage tolerance perspective. The benefit deals with the online and real time monitoring of impacts, which could induce damages at a random point which will be revealed by inspecting the concerning area within the interrogation time. Such a hybrid approach requires an on-board/on-ground procedure standardization, requirements definition and cost/benefits optimization.

Another key point for the standardization of the SHM based maintenance requires updating the Structural Repair Manual (SRM) with a network of self-powered wireless sensor nodes. Theoretically, the maintenance operator identifies the damage, compares that damage with the allowable and then repairs the component according to what SRM prescribes. The allowable depends upon position and dimension of damage and it is usually present in the SRM for standard damages. Maintenance engineers approve such a standard repair. Otherwise they investigate non-conventional repairs together with manufacturing engineers (for technical approval) when the damage scenario is not prescribed by the SRM. As a matter of facts, identification, allowable damage and repair are key aspects in the actual maintenance procedures and can be replaced respectively by: (i) SHM diagnosis for a specific damage, (ii) database of allowables for damage type and position and (iii) data analytics for repair diagnosis and suitable action. The question to be further investigated is to integrate SHM for the field of non-prescribed damages when the engineers have to a key role to enable correct assessment and repair procedures. All those aspects will be deeply investigated to obtain a certifiable SHM system.

As above discussed, several perspectives are available for SHM system at aircraft level. A standardization process relating technological level and SHM system capabilities (category) should be investigated as envisioned in Figure 73. The trend is moving from such a low level SHM system, where the maintenance tasks are partially or totally performed according to the MDR, to the overall management where the diagnosis and repair is postulated by means of SHM and augmented by prognosis and predictive analytics (full automation). Minimum requirements for the certifiable system at all high levels will be investigated.

Starting from these standpoints and the methodologies available with reliability agreeing means of compliance, a possible SHM based maintenance strategy, is depicted in Figure 81 and proposed within Clean Sky 2 – Regional Aircraft Project¹⁹. It consists of two main parts:

- An on-ground data analysis system with plug and play or WiFi capabilities. The SHM interrogation with further data analytics is performed on the central aircraft computer and on-ground. The time to inspection is set for replacing A-check.
- A real time monitoring system based on passive event detection. The relatively low costs and weight envisioned suggest considering a monitoring continuously performed on board which enables a proactive inspection for load monitoring and unforeseen damage during time to inspection.

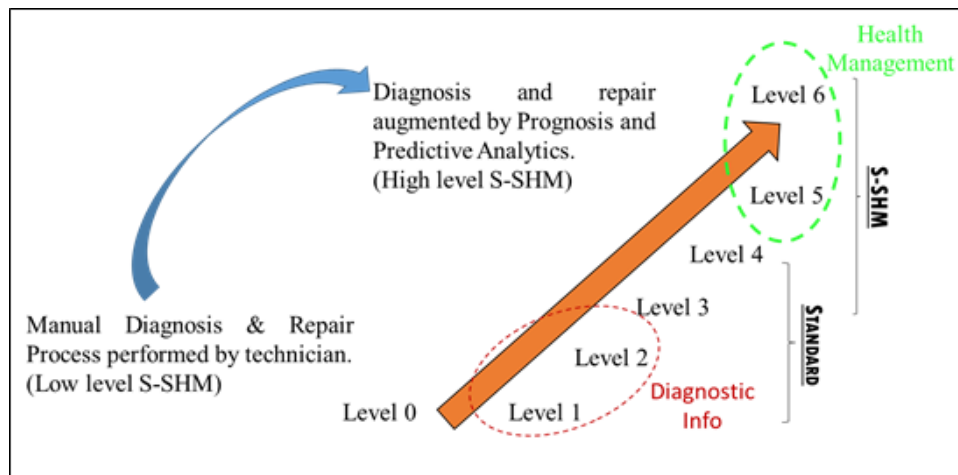


Figure 73: Technological level and SHM system category. Adopted scenario for categorization.

The dual output will consist of: (i) a simple diagnostic information about operative loads and impact loads, which can be compared with allowables every time, and (ii) a comprehensive SHM output performed at global/local level during the time to inspection (set close to the A-check time interval). Every health information during the time to inspection (high level SHM) is thus compensated with event detection (low-level SHM) to achieve a continuous monitoring of the aircraft.

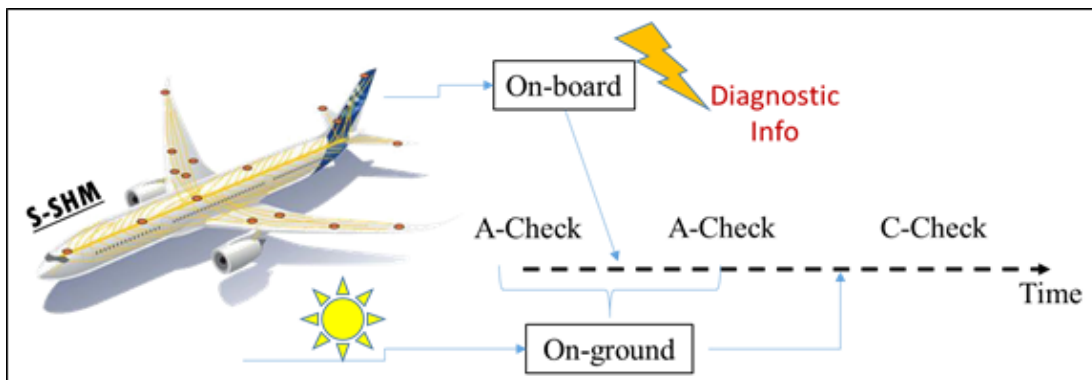


Figure 74: Hybrid SHM system approach for efficient replacing of maintenance tasks. In the schematization, the sun shows the pristine condition (calm and quite status) while the lightning represents and unforeseen and sudden impact.

From above consideration, it is worth defining:

- Maintenance strategy; the analysis depends on the strategy adopted in terms of SHM level and depth of diagnosis/decision (minimum requirements). The test case, including

¹⁹ Clean Sky 2 RA - Regional Aircraft. [Online]. Available: <https://www.cleansky.eu/regional-aircraft>

details about all parts to be monitored as well as maintenance critical parts, should be fixed to work on one or more strategies.

- b. Standardization; the standardization for implementation of health management requires:
 - a. The standardization of SHM techniques in terms of durability, reliability and Probability of Detection;
 - b. The establishment of fault tree and Structural Repair Manual updating;
 - c. SHM adjustment to maintenance critical parts.

The maintenance strategy can be finally investigated with a multidisciplinary design optimization approach where the SHM system impact on the aircraft lifetime is defined in terms of direct operative costs and emissions. Semi-empirical approaches can be used to define the trends with variable SHM system capabilities. In this way it is possible to achieve the best solution in terms of investment return and pollution impact. It is understood that monitoring the whole airframe and all the system may not be the best solution.

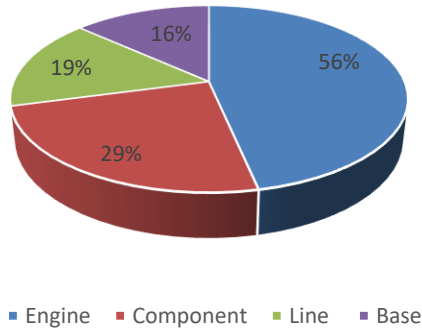
To estimate such an investment return given by the adoption of such an on-condition maintenance, let us consider the typical operative costs induced by maintenance on a 19 pax aircraft. The use of this kind of aircraft requires Direct Operation Costs Per-Flight Hour approximately equal to:

1. Fuel Cost: \$345
2. Airframe and Propeller Maintenance: \$140
3. Engine Restoration Cost: \$180
4. Total Direct Operating Cost: \$665

Scheduled maintenance events, which are required and predetermined by the manufacturers specifications, can be predicted and costs controlled since they can be performed close to home base at pre-negotiated rates. Unscheduled events are more difficult to manage and happen on the road such as a blown tire, bird or lightning strike. Larger fleet operators will have a network of pre-approved maintenance facilities around the World, reducing the costs and improving safety. Some aircraft types will have maintenance programs in place for more predictable costs. Much like an insurance plan, you pay into a pool each hour you fly and when maintenance is required, it is paid out of that pool. That is to say, it is difficult to predict the real cost, but it is possible to establish the rough order of magnitude for costs under ideal conditions. Namely, the benefits introducing health management can be accounted as the minimum possible ones. For the above mentioned examples, airframe and propeller maintenance cost assumes an annual utilization of 1200 flight hours (FH) and a cycle to FH ratio of 2. It is based on a combination of labour costs and parts costs. Approximately the health management system will allow to skip scheduled maintenance and reduce the cost of unscheduled maintenance moving scheduled maintenance towards predictive approaches and unscheduled maintenance towards scheduled philosophies. Instead, the material cost will remain approximately unchanged (Actually, several times, parts not still completely deteriorated are replaced earlier to avoid a very time close inspection.). Considering a 150\$ cost per MH, the maintenance cost will be statistically given by:

- Material cost = 30%
- Labour cost = 70%

In addition, the ratio between the labour cost due to maintain engine and airframe (Line and Base) is about equal to 1 (see Figure 75).



(a)

Fiscal Year	Line Labor%	Line Material%	Line Outsourced%
2007	64%	18%	18%
2008	70%	16%	14%
2009	59%	17%	25%
2010	65%	18%	17%
	65%	17%	18%

Fiscal Year	Base Labor%	Base Material%	Base Outsourced%
2007	33%	30%	37%
2008	46%	28%	26%
2009	36%	33%	31%
2010	50%	25%	25%
	42%	29%	30%

(b)

Figure 75: Maintenance cost (a) and Labor cost (b) breakdown.

Introducing the new concept philosophy, the C-Check will be accurately performed while the A-check will be replaced in favour of automatic health monitoring. The C-check impacts approximately 23% of the maintenance costs. Furthermore, **assuming again that on condition (predictive) maintenance will reduce only half of the inspections, the overall return of investment will be approximately equal to 13.5% ($0.7 \times 0.5 \times (1 - 0.23) \times 0.5$) reduction of maintenance costs which are approximately equal to 2.7% reduction in direct operative costs.** The benefit will be reduced by the cost and weight introduced by the health management system but there is enough margin to keep a valuable return of investment.

6.3 Integrated Landing Gear Health Management

As demonstrated above, integrated health management is one of the few technologies that will help in reducing operational cost while increasing safety. In addition, it also moves away from conservative design philosophies. The health management requires a multi-disciplinary approach bringing together advanced principles of mechanical engineering, sensor technologies, signal processing and data analytics. Aircraft landing gear, which has not been considered in the previous discussion, is one of the most critical aircraft systems with a maintenance task programme requiring much effort, almost like engines. The health of the landing gear system depends on the proper functionality of each component. Several parts can have many failure modes and potential failure can be detected through the analysis of data collecting by distributed sensors. While some failure modes can be critical, others may only degrade the performance. The failure can be classified as [127]:

- a. Incipient – hard to detect;
- b. Slow progressive – hard to detect;
- c. Intermittent;
- d. Cascading;
- e. Fast progressive

System health is monitored measuring deviation of useful parameters affected by the failure monitored. The remaining useful life is specified by the number of duty cycles and should be predicted on the base of the value of information given by the health management system. Few probable failures of a landing gear systems are [128]:

1. Failing to retract;
2. Failing to extend;
3. Failing to get-up locked after retraction;
4. Failing to get down-locked after extension;
5. Exceeding retraction/extension time limits;
6. Failing to give indications in cockpit of down locking, transit and up locking.

A retraction activity is possible only when the following conditions are met:

1. Aircraft hydraulics power and electrical power are "ON";
2. All weight-on-wheel switches are "OFF";
3. Select landing gear "UP" on the landing gear selector switch;
4. Hydraulic pressure flows correctly;
5. All down locks are unlocked;
6. Actuator stroke retract the landing gears individually

Hence, a failure of retraction can be due to any of the reasons summarized in Table 13.

In addition to all those aspects related to retractable system architecture functionalities, the landing induce overloads to the main structure and is subject to critical fatigue failure. As a matter of facts, landing gear represents a costly maintenance item and this fact pushed many manufacturers of small aircraft to opt for non-retractable landing gears to limit maintenance to landing load induced damage (e.g.: Tecnam P2012, DH Twin Otter, Cessna Caravan, etc). This design is approved without any concern even at the cost of accepting huge drag resistance increasing. Setting an integrated health management system at landing gear level can thus reduce maintenance costs of retractable systems by implementing predictive philosophy and reduce drag at aircraft level.

The technical benefits regarding the implementation of the health management system to a landing gear system are the ability of the system to monitor the operational and standard functional status of the landing gear system; provide the necessary warnings to insiders in the event of functional anomalies following limited landings, hard landings, landings in particular critical conditions or reaching fatigue life.

Failure	Detection Mechanism	Hardware Availability	Comments
No Hydraulic Power	Sensed by a pressure transducer in the system	Already available in the current system	Need to get the information from existing avionics system
No Electric power	Sensed by system voltage sensor		
Weight on wheel signal failure	Sensed through electrical signal which needs to be tapped		
Failure of Down locks	Sense the signals from Down locks		
Gear unlocked, but not going up to up lock	Sense signal from Up lock		
Retraction failure	Time intervals between selector switch operation, down lock release and up locking for each gear is beyond limits		
Electro-selector switch failure	Identify through solenoid voltage	New sensor need to be deployed	New data to be captured
Electro-selector valve failure	Identify through pressure in "UP" line		

Table 13: Landing gear failure modes and detection mechanisms [128].

In fact, it is precisely in terms of maintenance that it is possible to discuss about benefits since the system is capable of acting as a counter of the real fatigue life of the gear components and therefore of the real fatigue of the landing gear with respect to the theoretical fatigue loads (foreseen by the aircraft operator and in accordance to the applicable aeronautical legislation) with which the system has been qualified and approved. Thus, it allows to intervene constructively and proactively in the ordinary maintenance program, being able to extend in its current maintenance intervals, with considerable savings in terms of time and maintenance costs while returning an increased safety level as well. In particular, the benefits obtained are:

- reduction of global development costs;
- reduction in the number of fatigue tests and operating costs;

- increased reliability of the landing gear system;
- higher flight safety;
- reduction of maintenance costs through the elimination or simplification of scheduled and preventive maintenance "tasks", avoiding replacements of still intact parts and frequent inspection tasks.

6.3.1 Maintenance tasks for a landing gear system

As mentioned in the previous section, land gear systems are among most complex aircraft systems to be inspected during lifecycle management. To give an impression, the following considerations refer to a nose landing gear of a 19 pax aircraft according to standard procedures, therefore without any monitoring system integrated within the structure. Scheduled maintenance for this landing gear consists of the following tasks:

1. Every 100 FHs: check that there are no external leaks, breakages, cracks, and the static attitude of the aircraft is guaranteed
2. Every 600 FHs: check the correct tightening torques, and check that there are no external leaks, breakages, permanent deformations, and the static attitude of the aircraft;
3. Every 1800 FHs or 6 years, perform Eddy current on the body (there is no need to completely disassemble the truck), and visual inspection only on the shock absorber rod, checking for the absence of corrosion and the condition of the chromed surface;
4. Starting from 1800 FHs or 6 years, perform the same inspection as in the previous point every 600 FHs;
5. Every 12 years, disassembly for visual inspection of the structural components, replacement of the rubber / gasket kits, verification of the absence of corrosion, and condition of the chromed, cadmium-plated, anodized surfaces. Run NDT by eddy current on the body.

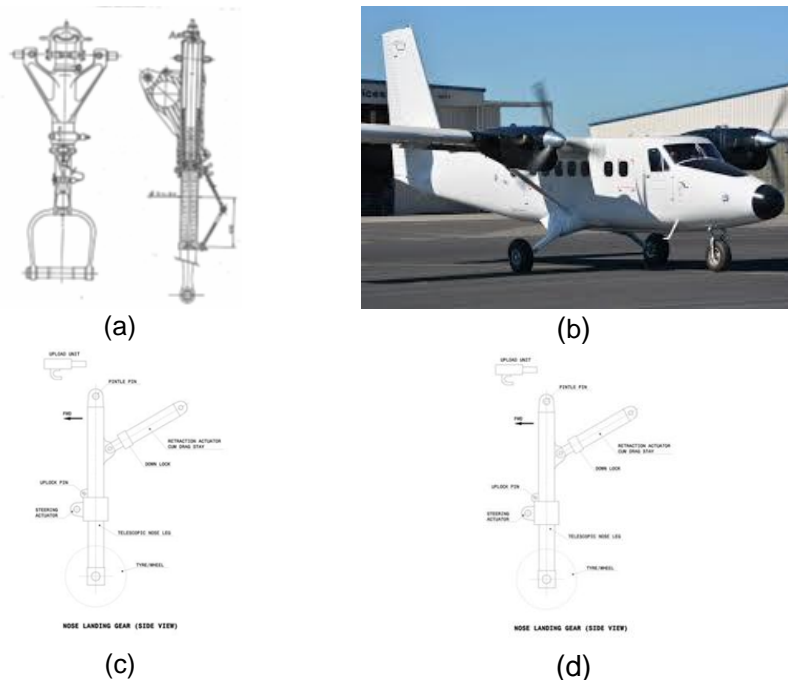


Figure 76: Typical Landing gear system of a 19 pax aircraft. Different views.

Operations 1) and 2) do not involve a significant commitment of time and costs and are therefore neglected as a precaution; for phases 3) and 4) the aircraft must be on ground, even if the complete disassembly of the landing gear is not necessary. Operation 5) involves complete disassembly. If the landing gear returns for general overhaul, as agreed with the customer, it is necessary to completely disassemble and proceed to the inspection phases provided in the maintenance manual. If the trolley returns due to a malfunction, before disassembling it is necessary to carry out a complete functional test which consists of:

- deformation test;
- seal tightness test;
- check of operation of the charge valves (oil and nitrogen);
- polytropic execution by hydraulic press;
- testing the "anti-shimmy" system;

Instead, during the revision it is necessary to:

- Disassemble the landing gear completely;
- paint off the painted components;
- perform and ensure thorough cleaning of all parts;
- carry out visual inspection to verify that there are no evident signs of wear, deformation, indentations, corrosions, scratches, surface state of the chromed and cadmium-plated or anodically oxidized parts and check the integrity of the gaskets. This inspection must be carried out mandatorily on all the components of the shock-absorbing part (rod, piston, gasket holder, cylinder, oil scraper, leak plug (metering pin), etc, ...)
- Non Destructive Testing as follows:
 - Penetrating liquids on the compasses (torque links)
 - Penetrating liquids on the stem;
 - Magnetoscopy on the articulation axes and on the wheel axle and valve seat, leak plug;
 - Penetrating liquids on the supports, bushings, spacers;
 - Penetrating liquids on the container;
 - Penetrating liquids on the shock piston;
- Rework and replacements with new parts:
 - Replace all parts that do not pass the visual inspection test;
 - Replace all the rubber / gasket kits, and the "consumables" (standard small parts, screws, washers, nuts, braking wire, cotter pins, spacers, plastic elements);
 - Rework the areas of the non-compliant parts in compliance with the tolerances required by the construction drawings and the maximum increases shown therein;
- Restoration of special processes (chrome plating, cadmium plating, anodic anodizing, etc.) and of the roughness required on drawing;
- Re-painting of the painted components;
- Re-assembly;
- Verification of the correct application of the tightening torques and functional gaps required by the project;
- Perform full functional test according to applicable test report;
- Carry out finishing operations (identification plate, braking wire, paint retouches, etc ...)
- Storage.

The previous action list gives an impression of the complex maintenance the landing gear is going through. Based on that task, in the following section it is reported a calculation regarding the maintenance costs associated to a classical land gear and the same landing gear integrated with health management system.

6.3.2 Cost benefits integrating health management system

As previously made for the airframe structures, several hypotheses can be made to estimate the return of investments in implementing an Integrated vehicle system even for landing gear systems [117], [118]. To find out the benefit is important to estimate the costs given by both classic system (inspection costs) and integrated system (system cost and added weight cost).

Inspection costs for classic landing gear: An accurate NDT requires an L2 category technician, for a cost of approximately 15k\$, including the costs of taking the aircraft on the ground. The whole cost of inspections is 15k\$ after the first 1800 FHs and every 600 FHs thereafter, and therefore for 100k FHs (design life) it will be approximately $100000/600 \times 15k\$ = 2.5M\$$.

Costs for integrating health management system: the monitoring system adds a mass to the aircraft that has to be included in computation of the direct operative cost. The weight can be estimated as follows:

- Sensors: 0.5kg,
- Electronics: 8kg,
- cables and other items; 5kg

For a total of 13.5kg per landing gear and a total weight added to the aircraft which corresponds approximately to 40.5 kg. The cost of the mass added to the aircraft can be estimated as 0.07\$ per FH per kg. Those values return an impact on direct operative costs of approximately 283k\$ for 100k FHs if no cost is associated with the maintenance of the monitoring system. In addition to that cost, it is necessary to consider the integration costs as:

- Sensor installation: 5k\$ per landing gear (worst case, 50 man hours, MH, necessary) for a total of 15k\$
- Cost of sensors: 4k\$ per landing gear for a total of 12k\$
- Electronic cost: 80 k\$

The integrated landing gear will impact the direct operative cost of the aircraft as follows: 283 k\$ + 15 k\$ + 12 k\$ + 80 k\$ = 390 k\$. Although the estimate is approximate and although it envisages having to restore some components of the SHM system, the benefit in terms of cost reduction in the life cycle is evident.

However, let us consider also the costs could be needed to maintain the monitoring system. If the landing gear returns for general overhaul, the operations described in the previous paragraph are estimated to affect approximately 15 k\$ per landing gear and therefore 45 k\$ for the aircraft. If they are inspected four times, they will require about 90 k\$ costs. Hence, the total maintenance of the landing gear system integrated with health management system during 100FHs will have a cost equal to:

$$390 \text{ k\$} + 90 \text{ k\$} = 480 \text{ k\$}$$

That is equal to 1/5 of the corresponding inspections and maintenance without any SHM and OLM approach mounted. The benefit can be calculated as:

$$\text{BENEFIT} = 2.5\text{M\$} - 0.48\text{M\$} = 2.02\text{M\$}$$

Which is valid for a life cycle, or one hundred thousand flight hours (FH), That results in approximately 80% saving of costs. Even considering that half of the inspection tasks only can be skipped, a 40% saving is still obtained.

Given all the above considerations, introducing a health management system for aircraft landing gear can make more advantageous introducing retractable configuration for this aircraft category because of the reduced maintenance costs. In addition, the landing gear induced drag and noise could further reduce costs and emission strongly. That is to say, integrated health management of aircraft landing gear is a future challenge but even a key enabling technology for this category of aircraft in order to achieve a near-zero emission vehicle.

6.4 Aeroelastic Tailoring of Distributed Propeller Wing

Distributed propulsion is barely a new concept and has captured the attention of major players in the aviation landscape to increase propulsion system efficiency along with better aerodynamic flow. However, such a non-conventional aircraft requires updated configuration to be effectively introduced in commercial aviation. Within the scope of the exploration of commuter aircraft key enabling technologies, it is crucial to mention the need for new and better preliminary design approach which can strongly improve the impact of such a non-conventional architecture on the aircraft weight. That is also useful to address the potential outcomes after the implementation of such innovative concept on the selected aircraft configuration.

For preliminary design concepts, it is necessary to understand the performance limits, and the overall physical reconfiguration that an airframe experiences when switching to distributed

propeller propulsion. One of the main goals is to define the effect of implementing distributed propulsive technologies in commuter aircraft. Furthermore, when referring to the preliminary aircraft design model, it is essential to have a better understanding of how to include these subsystems and a proper analysis in the preliminary design phase of the aircraft model. In general, the framework of the pre-conceptual design concepts is very much dependent on several key parameters such as the principal dimensions, aerodynamic parameters, weight, propulsion system characteristics, and flight performance. The following main aspects will require refinements: geometric-modelling capabilities, propulsion module, aerodynamics, performance analysis, weights, and mission definition. In particular, the mass breakdown analysis requires estimation models on weight of each aircraft component in order to compute the Operating Weight Empty and Maximum Take-off Weight.

The design of an efficient aircraft featuring new technologies has always represented a substantial challenge for aircraft designers, especially when the proposed novel concept challenges the existing knowledge base, and the accuracy of normally used empirical methods and statistical data collected from previously constructed aircraft. During the development of new aircraft, the structural mass of an aircraft has a big influence on the overall performance and cost development of the aircraft at the initial design stages. Reducing the structural mass has the effect of lowering the operating empty weight, allowing the aircraft to fly higher payloads at a greater range. The wing of a modern transport aircraft is one of the heaviest structural components, and therefore a particular focus has always been placed on the accurate estimation of wing structural mass. This is even more important in the case of distributed propulsive technologies, where the mass distribution (and the overall mass consequently) is highly affected by the position and mass of the engines. In particular, the use of tip mounted propellers can make quite challenging the design and the result can be far from optimal. That is where an accurate preliminary tool can be quite crucial to improve the design layout and return the optimal configuration without attempting to much resources and expensive experimental trials.

Generally, different methods are available in literature to estimate the mass of the airframe as well as the overall aircraft weight. It is possible to broadly divide those methods according to the approach adopted in:

- empirical and semi-empirical methods;
- analytical and quasi-analytical based methods;
- finite element-based methods.

Empirical methods consist mostly of statistical evaluation based on existing aircraft. Although great and valuable results have been obtained by Raymer [129], Roskam [130], Torenbeek [131], whose empirical mass estimation methods are still in use, the implementation and accuracy level of statistical-based methods in predicting aircraft mass depends primarily on the amount and quality of the data available for existing aircraft, in addition to how closely the presented aircraft matches the design and configuration concept, mission profile and weight of the aircraft under investigation. These conditions make statistical-based methods of limited practical use to the designers of an innovative design concept, where the novelty is in the configuration or the material used.

Semi-empirical methods, on the other hand, are used when a simplified geometrical layout of the aircraft configuration becomes available. These methods are used to estimate the mass of the primary structural components of an aircraft using analytically based equations that combine geometrical parameters, load factors and aircraft design speeds, adjusted using statistical data correlations derived from the weight breakdowns of existing aircraft [132]. Moreover, some experience was needed to account for any special features of the design. Although semi-empirical methods improve the accuracy of the wing mass prediction compared to statistical-based methods [133], the effect of the internal wing structural design configuration, like the number and location of spars, stiffeners and ribs, still cannot be evaluated at this stage.

Purely analytical methods make use of analytical structural analysis to provide a mass estimation. However, they are rarely found in the literature due to the complexities involved or limited to single aircraft components. Even in analytical formulation, statistical and or experimental data can be used to improve elementary structural analysis of simplified models in order to compute the material amount required to resist the applied loads. Although the attempts to derive sophisticated strength/stress relations [134], analytical and quasi-analytical methods available cannot be

considered completely accurate for establishing final design masses. As a matter of facts, the design requires holistic approaches able to account for aerodynamic effects and aeroelasticity. To overcome these limits, several approaches have been introduced using beam model representation and analytical methods for the analysis and sizing of the wingbox structure, while considering the effects of static aeroelasticity [135].

Nowadays, Finite Element Methods (FEM) have been used as a general-purpose approach and are able to provide useful data for mass estimation as well. Different attempts have been made in the literature to define accurate modelling strategies with low computation efforts needed [136]. Although the major advantage of numerical simulation is the possibility to introduce as many details as needed in the model, including non-linear behaviours, they may increase the computational costs, or may not be available at the preliminary design stages [137].

As a consequence, current approaches based on FEM are quite heavy and usually adopted to obtain a final optimization of the structure. Those approaches can be intended also to produce mass values for comparison and optimization purposes rather than for mass estimation on its own. However, a dedicated investigation is required to deal with optimization approaches. The finite element based structural optimization methods use finite element analysis and design optimization techniques to estimate the structural mass of aircraft when minimizing weight or maximizing aerodynamics performances.

Moving from empirical methods to finite element methods and passing through analytical approaches, different results may be achieved according to the fidelity of the method. On the same way of the previous classification, it is possible to group several adopted techniques according to the level of estimation achieved [138]:

- class I methods;
- class II methods;
- class II & ½ methods;
- class III methods.

Class I methods are also known as fractions methods, because the mass of each aircraft component is defined as a fraction of the maximum take-off mass of the aircraft. To establish ratio of the mass of a particular component (e.g. wing) to the aircraft mass, a number of existing aircraft designs of the same class and category as the aircraft under study are usually analysed. Typically, these techniques are used at initial stages of aircraft design process. In addition to coefficients obtained by statistical analysis of existing aircraft, Class II methods further include aircraft parameters such as design speeds, load factors, geometrical dimensions, configuration aspects, into sets of empirical equations to calculate mass of every fundamental aircraft component.

Class II & ½ methods are based on estimation of the mass of material, required to withstand loads applied to a particular aircraft component. In order to calculate the required amount of material, basic strength/stiffness analysis is applied to simplified structural model of the load-carrying component. The use of statistical and experimental data may be considered to improve performance of these methods. The further outcome achieved is because these methods further allow studying the influence of particular design decisions on the estimated mass of aircraft component or group of components. Finally, Class III methods allow the refinement of the mass breakdown prediction by incorporating FEM to calculate the aircraft primary structure. Other analytical and empirical methods integrate the approach because required for the secondary and non-structural masses on the aircraft structural loading.

Moving back to the specific application, it is worthy achieving further advancements in the establishment of accurate Class II&1/2 methods and Class III methods to optimize the airframe design. In particular, those approaches require advancements in setting formula for aero elastic compensation while dealing with high aspect ratio aircraft and distributed propeller wing. The use of high aspect-ratio paves the way to the application of really flexible wings, which may undergo to very high deformation due to the low twisting resistance of the outer wingbox. In addition, the presence of tip propeller mounting may generate dynamic instability reducing strongly the flutter velocity. This is such an under covered topic in the literature and the knowledge of the mechanics of structures under such a complicated wing configuration is quite needed to address the optimal configuration in terms of weight penalties and aerodynamic improvement. While the high aspect ratio can be compensated by introduced a strut, actually the engine mounting over the wingspan may be a big issue due to lower flutter speed expected when moving the engine outboard.

However, Mardanpour and Hughes [139] demonstrated that engine placement at certain location has the potential to increase the flutter speed. That may be induced in two ways. One is the location where lower frequency flutter mode could be relegated to a higher frequency mode and the other is the location where the fluid structure interaction is decreased. Both criteria could be met at the area of minimum kinetic energy of the mode. That is to say, engine placement at the area of minimum kinetic energy of the modes has the potential to decrease fluid-structure interaction and enforce the structure to flutter at a higher mode [140]. In case of the high-aspect ratio wing presented by the authors, the area of minimum kinetic energy density of the bending and torsion modes of the wing, in the absence of engines, gravitational, and aerodynamic forces, is may present different minimum level. While the first bending mode has a minimum value at the root, the second bending mode shows the minimum kinetic energy density outboard of the 85% span, and for second torsion mode this minimum moves to the region between 70% and 90% span. To further explore this possibility, the authors performed the same analysis for two-engine and four-engine configurations. In the first case, the point of the minimum kinetic energy is just outboard of 60% span [141].

In case of the four-engine configuration, for engine placement forward of the elastic axis, the unstable mode contains a combination of first, second, and third bending modes [142], and when the engines are placed around 60% to 80% span, there is a noticeable increase in flutter speed. This area is close to the area of minimum kinetic energy of the first three bending modes.

Summarizing the results, it appears that dealing with the classic two engine configuration, the maximum flutter speed is obtained at 60% outboard while the tip mounted engine would reduce the flutter speed around 15% (see Figure 77). That is where further mass is needed to compensate that effect and return to the previous flutter speed. However, the negative effect of the tip mounted engine can be compensated by installing another engine onto the wing, whose mass is equal to that of the tip mounted engine. Furthermore, if that adjunct mass is located around the location of minimum kinetic energy, a 25% increasing of flutter speed is experienced. This opens a new challenge in preliminary design of distributed propeller aircraft which deals with aeroelastic tailoring of wing. Keeping flutter speed constant while introducing outer wing propellers would mean keeping the benefits of distributed propulsion at all.

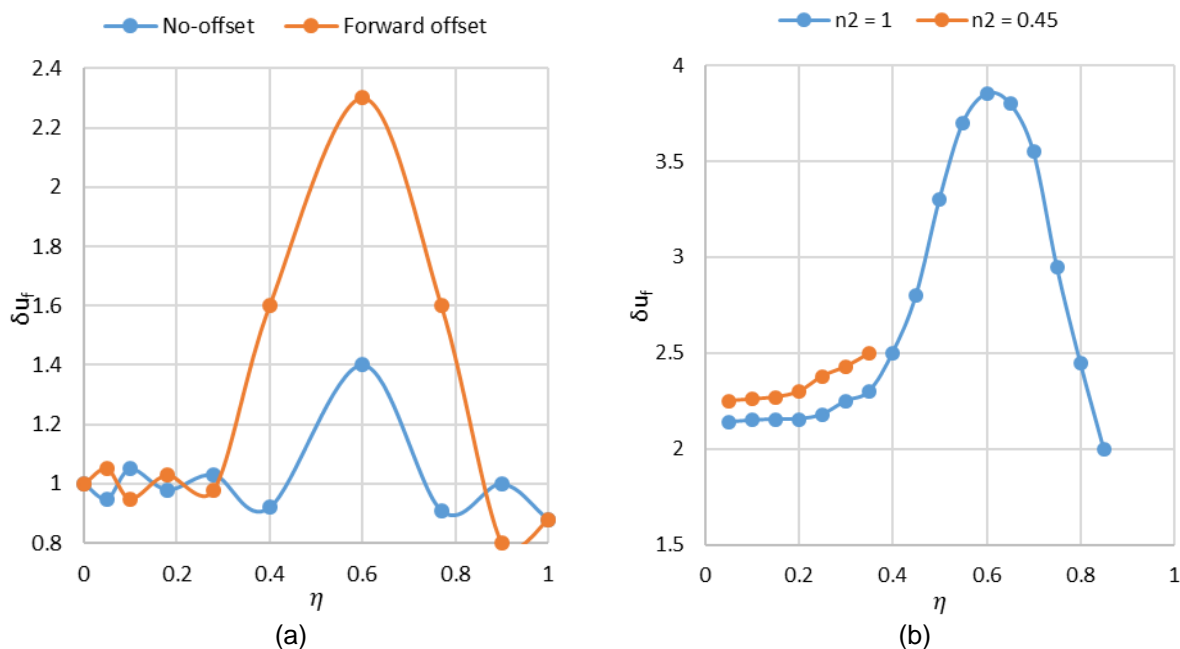


Figure 77: Flutter speed for engine placement along the span for two values of chordwise offset (a) and Normalized flutter speed in 4 engine configuration with one fixed (η_2) and one movable engine (η_1).

Another important issue is related to the coupling of engine modes and wing modes, which may result in very critical instability. That is the case of the X-57 Maxwell, a prototype aircraft designed by NASA from the two-propeller Tecnam P2006T. Respect to the father aircraft, the X-57 has reduced wing area along with an additional twelve wing-integrated propellers [143]. The objective

behind 14 propellers is that in low speed flight, such as take-off and landing, the downwash of the smaller 12 inboard propellers would help the wing generate lift in what would otherwise be stall conditions. Under high speed flights, such as in cruise, the X-57 will be operating with only the two larger outboard propellers active.

As with any new aircraft, it is imperative that any aeroelastic instabilities do not occur inside the flight envelope. However, a particular concern for the X-57 has been the potential for whirl flutter. This aeroelastic instability is caused by the propeller aerodynamics, which drives the airframe/pylon motions to become unstable. The design went through a multi-step analysis where different wing version were investigated thoroughly. In particular the whirl flutter stability analysis revealed that improvement can be obtained without compromising the airframe too much. The critical issue is the pylon mount flexibility, which allows the engine pitching mode to enable whirl flutter. Between several wing design version different changes were carried out to achieve flutter safety [144]. The second version showed two substantial changes in the structural design and model. The close spacing observed for the first two modal frequencies of the first version design was an aeroelastic concern, more from a wing flutter perspective than from a whirl flutter perspective (for what mentioned above). This led to incorporation of unidirectional fibers in the spar caps. The second important development was that the design of the tip nacelle geometry, structure and propulsion system had advanced including a firewall that served as a faceplate for mounting the motor for the tip propeller. This faceplate provides much of the structural stiffness between the propeller system and the nacelle, strongly influencing the in-plane behavior. In addition, the firewall was stiffened in the third version design, substantially reducing the faceplate deformations, and increasing engine mount rigidity.

Summing, the design of X57 Maxwell demonstrated that both wing aero elastic concern and whirl flutter instability can be addressed by tailored aeroelastic properties of the wing. It is worth noting that structural optimization may lead to improved stability performances at the cost of a very low weight increase. That is to say, the necessity of preliminary tools including such critical aspects for distributed propeller aircraft is quite crucial to enable the full exploitation of aerodynamic advantages induced by this unconventional configuration.

6.5 Strut-braced Wing

Strut-braced wing configurations have been used both in the early days of aviation and today's small airplanes. Adopting thin airfoil sections required external structural wing support to sustain the aerodynamic loads. However, external structures cause a significant drag penalty. Gradually, it was understood that the external bracing could be removed, and lower drag could be achieved by replacing the wing-bracing structure with a cantilever wing with an appropriate wing-box and thickness to chord ratios. However, along with the idea of the cantilever wing configuration with its aerodynamic advantages, the concept of the truss-braced wing configuration also survived. This is due to the tireless efforts of Pfenninger at Northrop in the early 1950s and his continuation of these efforts until the late 1980s. Using a strut or a truss offers the opportunity to increase the wing aspect ratio and to decrease the induced drag significantly without wing weight penalties relative to a cantilever wing. Also, a lower wing thickness becomes feasible reducing transonic wave drag and, hence, resulting in a lower wing sweep. Reduced wing sweep and high aspect ratios produce natural laminar flow due to low Reynolds numbers. Consequently, a significant increase in the overall aircraft performance is achieved [145].

A number of strut-braced wing aircraft configurations have been investigated in the past. Kulfan and Vachal from The Boeing Company performed preliminary design studies and evaluated the performance of a large subsonic military airplane [146]. They compared performance and economics of a cantilever wing with a strut-braced wing configuration. Two load conditions, a 2.5-g maneuver and 1.67-g taxi bump were used to perform structural analyses. Their optimization and sensitivity analyses showed that high aspect ratio wings with low thickness to chord ratios would result in a significant fuel consumption reduction. For the cantilever configuration, a ground strike problem arose during taxiing. This issue was resolved by adding a strut to the wing structure. Moreover, the analysis indicated that the strut-braced wing configuration requires less fuel (1.6%) and results in lower take-off gross weight (1.8%) and lower empty weight (3%) compared to the cantilever wing configuration. Cost comparisons showed that, because of a lower

take-off gross weight, the operating costs of the strut-braced wing configuration were slightly less than those of the cantilever wing configuration.

Park from The Boeing Company compared the block fuel consumption of a strutted wing vs a cantilever wing [147]. He concluded that the use of a strut saves structural wing weight. However, the significant increase in the strut thickness to cope with strut buckling increased the strutdrag. Therefore, because of a higher fuel consumption compared to the cantilever case, the strut did not appear practical for this transport aircraft. Another study on strut-braced wing configurations was conducted by Turriziani et al. [148]. They addressed fuel efficiency advantages of a strut-braced wing business jet of aspect ratio 25 over an equivalent conventional wing business jet with the same payload and range. For the strut-braced wing design, the combined wing/strut weight was higher than for the cantilever wing. However, the strut-braced wing configuration reduced the total aircraft weight due to the aerodynamic advantages of high aspect ratio wings. Further studies showed fuel weight savings of 20%.

The strut-braced wing concept offers the possibility to reduce wing thickness without the penalty of an increased structural weight by reducing the bending moment acting on the wing. However, a reduced wing thickness together with shorter wing chords result in smaller wing-box dimensions, thus significantly reducing wing-box torsional stiffness and rendering the wing more sensitive to aeroelastic problems such as increased static aeroelastic deformation or reduced flutter and divergence speeds. However, different approaches highlighted the possibility to remedy the problem of increased aeroelastic deformations by employment of the moment induced on the wing by a strut. Previously investigated strut-braced wing concepts considered the strut to be rigidly attached to the wing. Therefore, strut buckling during negative load factors was a major design issue, rendering the strut very heavy to overcome this buckling constraint. To avoid strut buckling, the authors in [149] proposed an innovative concept to have the strut active only during positive load factors. For negative load factors, the wing acts like a cantilever wing, rendering the strut buckling constraint unnecessary. Furthermore, this arrangement allows one to apply a defined strut force at the 2.5-g manoeuvre design load instead of the statically indeterminate one obtained from a rigid strut attachment. This way, the strut force as well as strut position can be optimized to achieve the maximum benefits out of the design concept.

Generally, the calculations provided by the literature reveal the significant influence of the strut on the bending material weight of the wing. The strut enables one to design a wing featuring thin airfoils without weight penalty. It also influences the spanwise redistribution of the aerodynamic loads and the resulting deformations. Increased weight savings are possible by iterative resizing of the wing structure using the actual design loads. As an advantage over the cantilever wing, the twist moment caused by the strut force results in increased load alleviation, leading to further structural weight savings.

Although the design may be challenging for commercial aircraft of a certain dimension, small aircraft can strongly benefit from a strut braced configuration. To look into those benefit, a simple calculation is reported afterwards, considering the effect on the bending alleviation induced by a strut. While remaining valid all the aspects mentioned before towards application of strut braced configuration and other aerodynamic aspects pointed out in the relative section, it is worth noting that calculations made afterwards take in consideration the structural aspects only to estimate the possible weight saving achievable keeping the same wing characteristics. It is understood that weight alleviation can be then adopted to further increase the aspect ratio of the wing.

In this context, a preliminary calculation is carried out to estimate the weight alleviation introduced by the strut. In this case two different configurations have been considered (see Figure 78):

1. Cantilever beam with uniform load distribution q ;
2. Strut-braced beam with connection at one third of the wing span and load distribution q .

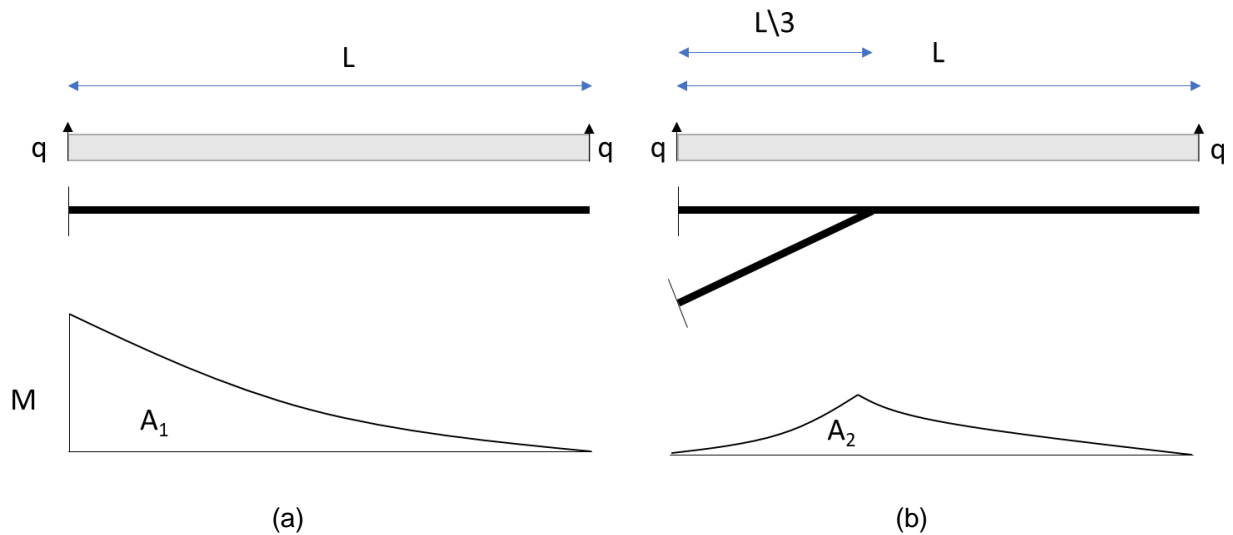


Figure 78: Cantilever beam model (a) versus strut-braced beam model.

To estimate the weight ratio and give a first impression of the effect of the strut, the bending moment is estimated for both examples and the area under the weight is considered directly proportional to the area under the bending. As a consequence, the weight ratio is considered proportional to the ratio between those area as explained afterwards. Firstly, A_1 and A_2 are approximately calculated as:

$$A_1 = 0.167 qL^3; \quad A_2 = 0.111 qL^3$$

The weight alleviation can be then estimated as 33.5%:

$$\Delta W = \frac{A_1 - A_2}{A_1} = 0.335$$

The bending moment is absorbed by the spar caps and the upper and lower panel. Neglecting the effect on the stiffened panels, it is possible to estimate the bending moment withstood by the caps as 80% of the total bending moment. Using a preliminary wing design algorithm, the caps have been estimated to be the 14% of the overall wing weight which is equal to 8-12% of the max take-off weight. **Considering the relation chain, the strut-braced configuration can alleviate the maximum take of weight of about 0.48%.** In addition, a further alleviation can be introduced by the lighter panels while the strut introduces a small penalty, which can be considered negligible as well.

Besides the static alleviation factor, it is worth noting that the strut decreases the wing free length with a positive effect on aeroelasticity. In particular the aeroelastic penalty can be calculated for both configuration according to Torenbeek formula [131]:

$$\Delta W_{aer} = \frac{\rho g}{G} q_D \frac{b^3}{\frac{t^2}{c} \sqrt{1-M}}$$

The effect is proportional to b^3 with a weight penalty reduced by up to 70%. That contribution is estimated to be about 2% of the wing weight, which is approximately 8-12% of the maximum take-off weight. **Applying again a rational relation chain, the alleviation factor ranges between 0.1% and 0.2% of the maximum take-off weight.**

It is worth pointing out that the static and dynamic weight alleviation have been estimated by making suitable assumption on two wing configurations with same wing span. The weight alleviation can be compensated to increase the aspect ratio. That is to say, the MTOW is kept constant and the aerodynamic performances are improved.

6.6 Morphing Wing

The idea of changing the wing shape or geometry is far from new. The Wright Flyer, the first heavier than air aircraft with an engine, enabled roll control by changing the twist of its wing using cables actuated directly by the pilot. The increasing demand for higher cruise speeds and payloads led to more rigid aircraft structures that are unable to adapt to different aerodynamic conditions, characterizing a typical mission profile. Actually, the real issue about implementation of morphing technology is intrinsically related to the high elasticity required for smoothly change the shape of the wing which cannot be easily implemented without facing structural stability problem. That is the reason why high lift devices have been widely adopted so far. Unless aeroelastic problems, they ensure proper functionality when higher lift is required without compromising the primary structure rigidity. However, they work properly only in fixed conditions and cannot be used to smoothly adapt the aircraft aerodynamics. **That is where morphing structures can decrease the parasite drag up to 22% and poses the challenge even for smaller aircraft [150].**

Morphing structures have been investigated within a large number of research activities over recent decades. Morphing wings matching the optimal aerodynamic shape at any flight condition is one of the most challenging aeronautical application. Current projects aim to achieve technology maturation for the structural-mechanics and materials aspects. More in detail, the change in shape of the metal wing structures has always attracted the scientific community. In this regard, based on specific application needs, multiple unconventional architectures have been idealized and built up. A first remarkable distinction within the adaptive systems can be made according to two macro-groups of interest: mechanized and compliant architectures. The first one implements morphing through rigid roto-translation of linkages interconnected by kinematic chains [151]. The sizing is led so that each kinematic sub-component withstands the external stresses foreseen in the real operating conditions; the actuators and the transmission lines must allow the correct kinematic behaviour of the system, ensuring the achievement of target shape-configurations. The available mechanical torques are chosen to balance the aerodynamic loads while minimizing power consumption [152].

On the other hand, the compliant mechanisms, reach the required shapes through the deformation of structural elements. In this case, in order to guarantee a more uniform shape change, the mechanical resistance characteristics must be appropriately distributed throughout the system. Compared to compliant mechanisms, 'robotized' architectures provide a more practical solution to the paradox of morphing a structure which has to be considerably stiff to safely withstand external loads and at same time, enough flexibility to accommodate different shapes with a small amount of actuation energy. Fewer actuators are typically required to control the morphing process which expected benefit expected at system level drives the definition of additional mass, volume, force, and power required by the actuation system. In force of this consideration, it naturally follows that the adoption of mechanized structures becomes quite mandatory when dealing with large aircraft applications and/or when multi-modal morphing functionalities have to be assured.

Although mentioned benefits provided by the use of morphing technology on an aircraft are mostly for high speed flight conditions, the use of morphing technology at low speed conditions, namely take-off or landing, can also be the source of significant performance improvements. As already mentioned, high lift devices can be considered as belonging to the family of morphing systems, and the performance level obtained by a system made of a single slotted Fowler flap and a slotted leading edge slat is almost the maximum achievable level without active flow control. The drawback is that heavy complex mechanisms are necessary to set the elements at their position. When stowed, some external fairings are considered to hide the mechanics in order to minimize both friction and lift induced drag components in cruise conditions. However, the selection of a high lift system depends on the performance required for take-off or landing conditions, with the main one being the maximum lift and the stall angle. The specificity of high lift systems is that, depending on the needs, one system has to be used [153]. If there is a need to increase the stall incidence, a leading-edge device has to be used. If lift has to be increased at a given flight angle, the use of a trailing edge device is necessary, but, in that case, the stall angle generally decreases. Both systems can be combined for both maximum lift and stall angle increases. For both types of devices, morphing technology can be considered.

As a matter of facts, morphing technologies remain a key enabling technology for all aircraft categories where the emission is the first key driving design constraint. However, many challenges from airframe standpoint remain open and require improved system and much effort to achieve a step forward, looking at potential application of such technology to innovative green airliners. For instance, in morphing applications, where large shape changes are expected (e.g. STOL configuration), the design of a suitable skin is a huge challenge and a key issue. The skin has to withstand the aerodynamic pressure loads, while being sufficiently compliant for the underlying morphing structure. In addition, the weight required for morphing actuators or necessary to opportunely stiffer the structure is currently reducing the benefits coming from introducing morphing technologies.

6.7 Novel composite technologies, nanomaterial and multi-functional materials

Improving material properties has been an increasingly challenging application since many years. However, the introduction of composite technologies opened many ways to improve material performance by improving criticalities and without affecting the overall weight or even reducing the weight impact of the resulting component/system at aircraft level. Generally speaking, the composite performances are highly demanding, and they are currently able to withstand high loads in harsh environments, too. However, there are some lacks that can be improved by introducing improved manufacturing technologies. In addition, the tailored manufacturing of fully composite made structures paved the way to the introduction of multifunctional materials with improved performances obtained by introducing different or novel materials within the structure. Hereinafter, three different key enabling technologies are introduced briefly describing how they can affect positively the aircraft design towards a near-zero emission air vehicle.

6.7.1 Automatic Fibre Placement

Composite manufacturing is a very challenging technology since replicability is not ensured in its nature. Involving layout assembling of resin and fibres and fibres with different direction or even sheets and cores in sandwich structures, the final product likely fails to ensure very low tolerance. In addition, different stages of manufacturing and the need to obtain tailored components, return high costs due to repeated processes and rejection of components that do not result in line with the specifications. In particular, manufacturing processes require the detailed monitoring of some parameters such as temperature and pressure which can even compromise the mechanical properties of the final product. Instead, the automatic fibre placement with Out of Autoclave manufacturing [154] that is able to return tailored configuration with lower expensive process and better quality of component. In particular the use of automatic placement of fibres ensure to guarantee the positioning of dry fibres without using prepreg materials. All in all, it returns a specific tolerance requirement. Some advantages can be listed as:

- Lean Manufacturing;
- Simplified Configuration;
- Tailored Material Configuration / Weight Reduction;
- Longer Material Shelf Life;
- Controlled resin to fibre content;
- Low void content;
- Suitable for large part production and sandwich structures;
- Low Energy Consumption;
- Special heated tools allow to build any composite shape;

Particularly promising is the manufacturing of coupons as much complex as possible by rapid automated dry preforming process (AFP) followed by Liquid Resin Infusion (LRI). However, it is rather difficult to address some challenges yet:

- manufacturing process parameters setup;
- development of a system for online monitoring of LRI process parameters;
- technology characterization;
- Allowable determination along with flammability and conductivity, thermal and lightning strike properties.

Nonetheless, the use of novel and more reliable manufacturing technology can reduce the knock-down factors, reducing the gap between material and design allowables. In addition, the costs and emissions of production lines can be reduced with a strong impact on both cost of the aircraft and its overall emission. That is to say, new emerging technologies can strongly impact the aircraft design of near-zero emission aircraft and are good candidate as key enabling technologies.

6.7.2 Carbon Nanotubes

Carbon fibre reinforced polymer (CFRP) composite laminates are increasingly being used in aerostructures because of its superior strength to weight ratio when compared of metallic materials. However composites show some criticalities in lower electrical and thermal conductivities and, generally, they need the development of new approaches to anti-icing/de-icing, lightning strike protection, and, has already widely described above, potentially structural health monitoring. Moreover, CFRP laminates have poor through-thickness strength and interlaminar fracture toughness, which make them susceptible to delamination under relatively low-energy impact events. To address these demands, the introduction of carbon nanotubes (CNTs) in structural fibre-reinforced polymers, to imbue the composite with multifunctional properties (e.g. enhancing electrical/thermal conductivity, structural health monitoring), has received much attention in recent years. Maintaining, and preferably enhancing, the structural integrity of the composite is imperative and the addition of carbon nanotubes (CNTs) within the resin is a promising option due to their outstanding mechanical, thermal, and electrical properties [155]. Thus, CNTs are considered an ideal candidate to provide multifunctionality to advanced hierarchical CFRP composites [156]. Within a hierarchical composite structure, CNTs can be distributed in the entire matrix, placed around the individual fibres, or distributed between plies. The last option allows to accurately control amount and orientation of the CNTs, what is of paramount importance since different and multiple functionalities can be provided in specific directions and locations, increasing the design options for integrated systems in CFRP multifunctional composites. The highly conductive CNT webs are drawn directly from specially grown CNT forests produced by chemical vapour deposition (CVD) [157]. As a matter of facts, the nanotubes webs can be interleaved with plies of carbon fibre to tune the thermal and electrical properties of the laminate with negligible weight penalty. Despite their negligible weight and thickness, the introduction of CNT webs may hinder the nesting between the carbon fibres of different plies, reducing the bridging effect and consequently the interlaminar failure attitude. Moreover, it has been observed that the interaction of CNTs with some epoxy resins has a major influence on interlaminar fracture toughness (ILFT). Bhanushali and Bradford [158], working with woven glass fibre reinforced polymer (GFRP) composites, found that ILFT was either marginally degraded or enhanced, depending on the orientation and number of layers of the CNT webs. Moving to practical benefits, a few examples can be remarked. The placement of an ethylenediamine-functionalised multilayer CNTw (0.2 g m^{-2}) between carbon fiber plies resulted in a 13% enhancement in the interlaminar Mode I fracture toughness, while providing an electrical conductivity of 10^3 S m^{-1} in the direction of the CNTs within the interleaved CNTw [159]. Another study investigated the same aspects by infusing CNC/epoxy mixture through plain-woven glass fabric (GF) reinforcement to develop hierarchical CNC/GFRP composites. The results show that CNC/GFRP composites exhibit significantly enhanced mechanical properties compared to the

GFRP control composite. The addition of 2 wt% CNC to GFRP yielded increases of 56% in storage modulus, 50% in flexural modulus, 55% in flexural strength, 14% in tensile modulus and 24% in tensile strength. Morphological studies (SEM) confirm the strong anchoring of CNCs with GF and the EP interphase thin layer around the GF. These results show that CNCs can be effective for strengthening the interface in fibre-reinforced composites for structural applications [160]. The introduction of such a zero-weight reinforcement, strongly reduce some drawbacks of composite structure, inducing to close the gap between material allowables and ultimate and limit design allowables. **Reducing 5% of these values only for the wing could reduce up to 0.6% the Max take-off weight of the aircraft.** In addition to that, such multifunctional materials introduced can be adopted for de-icing and anti-icing purposes and SHM, further increasing the achievable benefits.

6.7.3 Structural Batteries

Another multifunctional property, that can be particularly suited for electric aircraft, consists in replacing load bearing components with such a structural battery. That can be achieved by a special layout where batteries are installed within the structure ensuring both energy storage and structural stiffness.

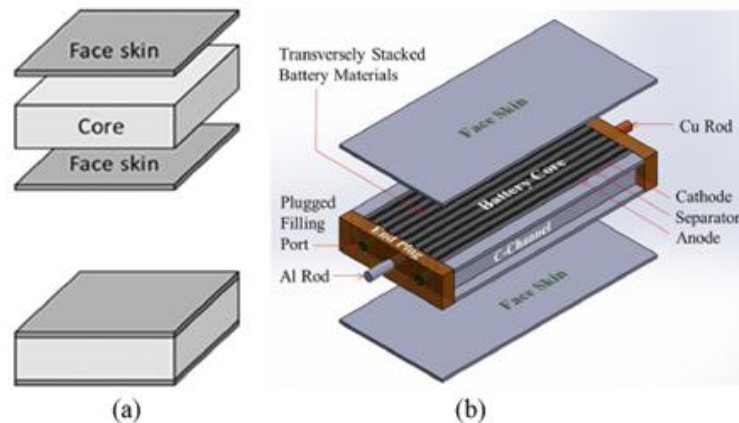


Figure 79: Schematic concept of sandwich structural battery: (a) sandwich panel with a foam core and two face skins and (b) sandwich panel with battery core and two face skins [161].

Multifunctional structural batteries are capable of storing energy while fulfilling a structural role in various applications such as satellites [162], spacecraft [163], unmanned air vehicles, and marine systems [164]. Lithium-ion batteries are particularly suitable for this application because of their high energy density, long cycle life, and environmental friendliness with zero emissions. Previous investigations have used two general approaches for developing structural batteries. One approach incorporates conventional lithium-ion batteries into composite structures [165], while the second develops structural electrodes [166], and even structural electrolyte [167] into lithium-ion batteries. Generally, both energy density and structural performance are needed for structural batteries in electric vehicles. That is a highly demanding characteristic and reduce the field of application. However, structural battery shows interesting promise for applications where sandwich structures and batteries are used [161]. In this last application, the authors demonstrated that measured bending stiffness showed only a 3% reduction upon filling with electrolyte and undergoing 50 charge–discharge cycles. Ex situ mechanical tests showed a significant (31%) decrease in lap shear strength of the E-120HP epoxy after exposure to the battery electrolyte for 3 months. However, the significant degradation did not cause any structural damage or leakage during the charge–discharge cycling of structural battery. Sandwich beam theory is able to predict the stiffness of the sandwich structural battery within 10% difference from the experimental bending stiffness, and it proves that the structural battery behaves as a sandwich beam and the battery materials are sharing in the load-carrying function of the sandwich panel



show that the shear deflection is only 2.5% in the midspan deflection, indicating that the battery core is very stiff. This approach has been recently proposed even for aircraft vehicle because shows promising results. Basically, it may reduce the weight of the batteries, which became part of the load carrying mass. In addition, lighter vehicle needs smaller batteries and electric motors enabling again the snowball effect. As a consequence, **this design could reduce the weight and cost of electric aircraft** and it is understood as a key enabling technology although much work is needed to achieve a reliable implementation within aircraft.



7 Design Tool Improvement

One of the key-aspect of new aircraft design success is the design tool improvement and their integration.

The following items must be accounted:

- 1) Multidisciplinary design and optimization (multi-fidelity, hierarchical, collaborative)
- 2) Model-based-system engineering approach (MBSE)
- 3) Higher-order fidelity tools (aerodynamic, structure, systems, powertrain, costs, maintenance, etc).

8 Certification Authority

Some comments on certification of aircraft energy storage and transmission have been made in the previous chapters. Basically, certification evolves around safety. For instance, regulations fix a limit of ± 270 V (540 V) for the maximum operating voltage of electric machines because of the Paschen effect (Sec. 4.1.5.1). Until authorities accept new insulation materials as a mean to operate in the kilovolt range, the operating voltage will be below such limit.

The discussion on the certification of an aircraft with distributed propulsion is more complicated. Current Federal Aviation Regulations (FARs) and Certification Specifications (CS) Part 23 dictate that any single engine aircraft or a multi-engine aircraft weighting less than 6000 lb that cannot meet certain critical engine out climb requirements must exhibit a stall speed of no more than 61 knots, unless certain other criteria designed to improve the crashworthiness of the aircraft are met [168,169]. The conditions at which the stall speed must be determined are explicitly stated in the regulations, and these conditions currently do not allow any credit for blowing from high-lift propellers (i.e., the stall speed must be determined without any positive thrust from the propellers). Additionally, the current regulations also only cover "reciprocating engine-powered airplanes" or "turbine engine-powered airplanes", so an electric aircraft with no reciprocating or turbine engine cannot be certified. Clearly, aircraft with distributed electric propulsion will require new regulations before they can be certified.

The aviation authorities and the aerospace industry as a whole are well aware of the limitations of the existing regulations in certifying new technologies and are working to improve the process. The advent of practical electric aircraft in recent years has been one of the factors leading to this realization. ASTM International's Committee F44 on General Aviation Aircraft²⁰ was established to develop consensus standards that will contain more flexible means of compliance than the existing Part 23 regulations, which should allow for new technologies such as electric propulsion to be certified. If these standards will be adopted by the aviation authorities, the possibility of certifying electric aircraft with high-lift propellers may become a reality.

Actually, no definitive statements can be made. The current regulations dictate a minimum threshold for a reference approach speed, V_{REF} , which depends on the stall speed of the configuration. Although the reference approach speed does not denote the speed at which an approach must actually be

own by a pilot, it does dictate how a manufacturer can represent the performance of the aircraft (and provides solid guidance for how pilots should actually fly an approach). Generally, the regulations specify that the reference approach speed is 30% higher than the stall speed (i.e., $V_{REF} = 1.3 V_{S1}$, unless the minimum control speed is higher).

Although the regulations do not explicitly state the reasons for maintaining a higher speed in approach, the 30% velocity margin likely exists to provide a sufficient buffer between the stall and approach speeds to account for both pilot error and factors beyond the pilot's control such as wind gusts and low-level wind shear. The pilot must be able to react to any changes in aircraft attitude or airspeed without stalling or otherwise losing control of the airplane (e.g., having insufficient control surface authority due to decreased dynamic pressure from a tailwind gust). This view is at least partially supported by the fact that the regulations for larger, transport category aircraft certified under Part 25 require a reduced velocity margin of only a 23% increase over the stall speed [168]. This reduction in the required margin is likely due to the higher approach speeds of transport aircraft. The impact of a sudden change in wind velocity of 15 knots, for example, will be less pronounced on a transport category aircraft approaching at 150 knots than a small aircraft approaching at 65 knots.

From a technical perspective, the 30% velocity margin dictated by FAR/CS §23.73 is likely more appropriately viewed as a lift coefficient margin. Since $C_L = L/(0.5\rho V^2 S)$ and the lift produced at the approach speed V_{REF} and stall speed V_{S1} must be the same, the lift coefficient at the approach speed must be $C_{L_{ref}} = C_{L_{max}}/1.3^2 \approx 0.59$ where $C_{L_{max}} = L/(0.5\rho V_{S1}^2 S)$. Therefore, the lift coefficient margin between the stall speed and approach speed is

$$(\Delta C_L)_{\text{margin}} = (1 - 1/1.3^2)C_{L_{max}} \approx 0.41C_{L_{max}} \quad (8)$$

²⁰ <https://www.astm.org/COMMITTEE/F44.htm>

The equation indicates that the required C_L margin between approach speed and stall speed varies with the aircraft's C_{Lmax} . An aircraft with a higher maximum lift coefficient is required to carry a larger margin than one with a lower C_{Lmax} . The required C_L margin for values of the maximum lift coefficient ranging from 1 to 5 is shown in Figure 80. For conventional general aviation high-lift systems that produce maximum C_L values of approximately 2, a C_L margin of approximately 0.8 is required. However, for novel high-lift systems such as those with high-lift propellers that could produce lift coefficients of 5, a C_L margin of over 2 is required. This margin is greater than the maximum lift capability of many current small aircraft. It is difficult - and arguably impossible - to justify that such high $(\Delta C_L)_{margin}$ values are actually necessary to maintain safety.

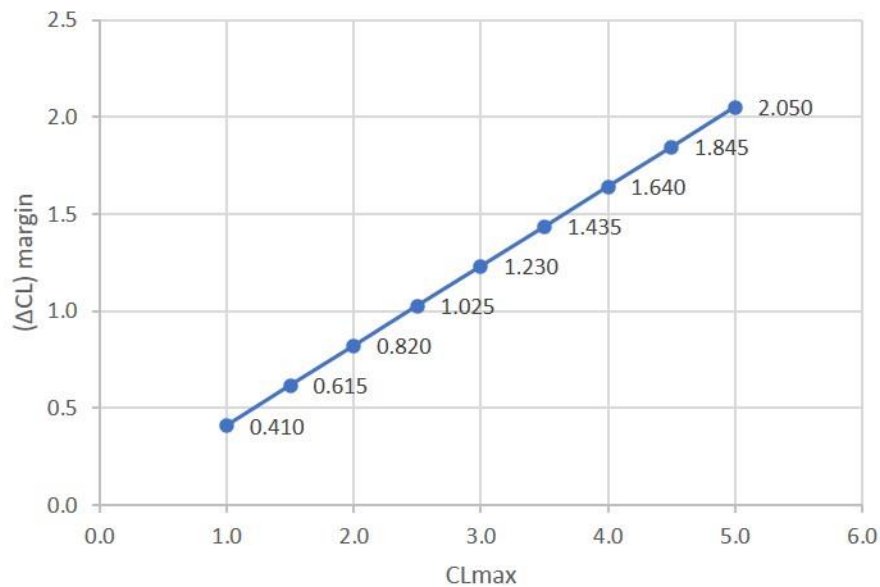


Figure 80: Lift coefficient margin in approach as function of max lift coefficient.

Conventional aircraft obtain the required C_L margin entirely by controlling the angle of attack, as the use of propulsive thrust to certify stall speed is currently prohibited. Therefore, the 30% velocity margin can be interpreted as an angle of attack margin, which is denoted as $(\Delta\alpha)_{margin}$. The angle of attack margin will more directly relate to the safety of the aircraft than a velocity margin because stall is much more closely related to the angle of attack than it is to velocity (the variation of C_{Lmax} due to Reynolds number is negligible).

Since every aircraft will have a different lift curve slope and maximum lift coefficient, the velocity margin does not equate directly to a single $(\Delta\alpha)_{margin}$. Instead, the angle of attack margin will vary for every aircraft, and these variations can be significant. Figure 81 indicates how the angle of attack margin varies for aircraft with typical lift curve slopes from 4 to 2π per radian over a range of C_{Lmax} values from 1 to 5.

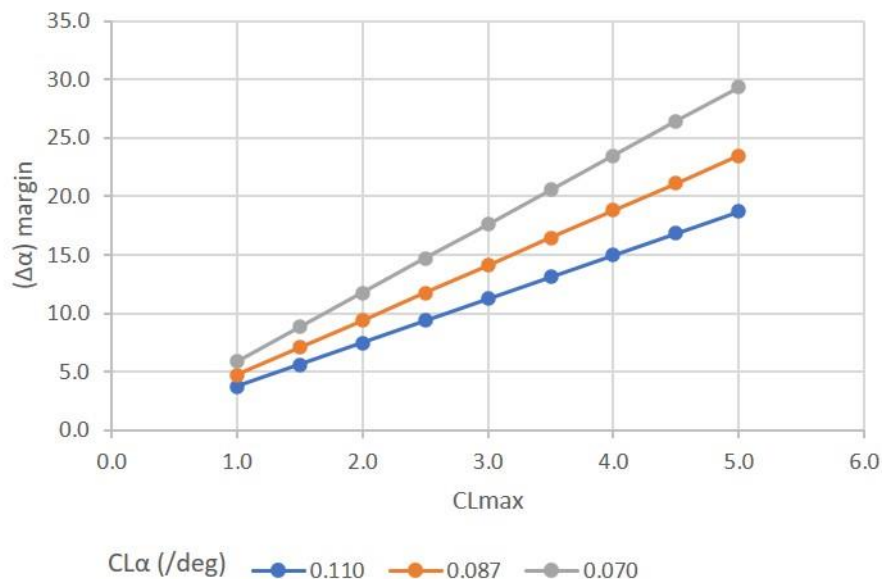


Figure 81: Angle of attack margin in approach as function of max lift coefficient.

As indicated in Figure 81, the angle of attack margin required by the current regulations can vary widely depending on the aircraft. The $(\Delta\alpha)_{\text{margin}}$ values for the cases in the figure range from 4° to 30°. The rationale for requiring such varied angle of attack margins is open to interpretation, but the author sees no solid safety reasons for requiring such large variations in $(\Delta\alpha)_{\text{margin}}$. It is assumed here that relative velocity margins were specified in the regulations rather than angle of attack or C_L margins primarily because velocity is much more easily measured than angle of attack or C_L . However, Figure 81 makes it clear that requiring all aircraft to maintain the same velocity margin does not equate to maintaining an equivalent level of safety (assuming that an angle of attack margin equates more-or-less directly with safety).

In defence of the existing regulations, conventional Part 23-certified small aircraft typically have maximum lift coefficients near 2.0, so the current regulations in practice have only required aircraft to maintain angle of attack margins ranging from approximately 5° to 10°. However, for new technologies or vehicle concepts that may enable very high maximum lift coefficients on the order of 5.0, the current regulations would

require angle of attack margins of approximately 15° to 30° or up to six times more than required for conventional aircraft. So long as approximately the same approach and landing speeds are being considered for these aircraft with higher $C_{L\text{max}}$ values, it is difficult to justify margins so much higher than with conventional technologies. This is another example of how existing regulations may not be appropriate for new technologies.

Apart from being able to generate much higher maximum lift coefficients, aircraft with high-lift propellers generate lift differently than conventional aircraft. Whereas a conventional aircraft in a specified configuration at a certain airspeed and altitude can only increase lift through increasing the angle of attack, aircraft with high-lift propellers can create additional lift at the same angle of attack through increasing the blowing from the props. The induced velocity from the propellers adds a new degree of freedom to produce lift and thus generate a safe C_L margin.

Because these two mechanisms for producing lift in an aircraft with high-lift propellers can be modified independently, it is helpful to decompose the total lift generated into two components: the angle of attack contribution and the blowing contribution. Mathematically, this relationship can be expressed as

$$C_L = C_L(\alpha) + C_L(\text{blow}) \quad (9)$$

where $C_L(\alpha)$ is the C_L contribution from the angle of attack (i.e., the lift coefficient without any blowing) and $C_L(\text{blow})$ is the additional lift generated by the high-lift propellers' slipstreams (i.e., the total lift less the unblown lift). Similarly, the total lift coefficient margin is comprised of a contribution available from the angle of attack, and a contribution from increasing propeller blowing. The discussion around Figure 81 assumed all the C_L margin would be required to come



from the angle of attack. Since high-lift propellers offer a new degree of freedom to generate C_L , the need for angle of attack margins on the order of 3 to 6 times conventional aircraft is not necessarily required to maintain the $(\Delta C_L)_{\text{margin}}$ values currently required by the regulations. However, as noted above in relation to Figure 81, the current regulations also require C_L margins that are likely higher than justifiable no matter how they are generated. This total lift margin can be created from any combination of an angle of attack margin and a blowing margin, but with the former greater than zero, since the reference approach speed must be always greater than the unblown stall speed of the wing to account for the case of a full system power loss. It is an open question if it is really necessary for an aircraft with a $C_{L_{\text{max}}}$ of 5 to have over 2.5 times the C_L margin of conventional aircraft and carry more margin than the lift capability of conventional aircraft [50].

9 Bibliography

- [1] *Commercial Aircraft Propulsion and Energy Systems Research*, The National Academies Press, Washington, DC, 2016. doi:10.17226/23490.
- [2] Della Vecchia, P., Malgieri, D., Nicolosi, F., and De Marco, A., "Numerical analysis of propeller effects on wing aerodynamic: tip mounted and distributed propulsion," *Transportation Research Procedia*, Vol. 29, January 2018. doi:10.1016/J.TRPRO.2018.02.010.
- [3] Patterson, M.D., Daskilewicz, M.J., and German, B., "Simplified Aerodynamics Models to Predict the Effects of Upstream Propellers on Wing Lift," in: *53rd AIAA Aerosp. Sci. Meet.*, American Institute of Aeronautics and Astronautics, Reston, Virginia, January 2015. doi:10.2514/6.2015-1673.
- [4] Borer, N.K., Patterson, M.D., Viken, J.K., Moore, M.D., Bevirt, J., Stoll, A.M., and Gibson, A.R., "Design and Performance of the NASA SCEPTOR Distributed Electric Propulsion Flight Demonstrator," in: *16th AIAA Aviat. Technol. Integr. Oper. Conf.*, American Institute of Aeronautics and Astronautics, Reston, Virginia, June 2016. doi:10.2514/6.2016-3920.
- [5] Stoll, A.M., and Veble Mikic, G., "Design Studies of Thin-Haul Commuter Aircraft with Distributed Electric Propulsion," *16th AIAA Aviation Technology, Integration, and Operations Conference*, No. June, 2016. doi:10.2514/6.2016-3765.
- [6] Epstein, A.H., "Aeropropulsion for commercial aviation in the twenty-first century and research directions needed," *AIAA Journal*, Vol. 52, No. 5, 2014. doi:10.2514/1.J052713.
- [7] EASA, "Certification Specifications and Acceptable Means of Compliance for Normal, Utility, Aerobatic, and Commuter Category Aeroplanes," Amendment 4, 2015.
- [8] Ranasinghe, K., Guan, K., Gardi, A., and Sabatini, R., "Review of advanced low-emission technologies for sustainable aviation," *Energy*, Vol. 188, 2019. doi:10.1016/j.energy.2019.115945.
- [9] Ruijgrok, G.J.J.J., and Paassen, D.M. van, *Elements of aircraft pollution*, Delft University Press, 2005.
- [10] Babikian, R., Lukachko, S.P., and Waitz, I.A., "The Historical Fuel Efficiency Characteristics of Regional Aircraft from Technological, Operational, and Cost Perspectives."
- [11] Felder, J.L., "NASA Electric Propulsion System Studies Outline," *NASA Presentation*, November 2018.
- [12] de Vries, R., Brown, M.T., and Vos, R., "Correction: A Preliminary Sizing Method for Hybrid-Electric Aircraft Including Aero-Propulsive Interaction Effects," *2018 Aviation Technology, Integration, and Operations Conference*, No. June, 2018. doi:10.2514/6.2018-4228.c1.
- [13] Orefice, F., Della Vecchia, P., Ciliberti, D., and Nicolosi, F., "Aircraft conceptual design including powertrain system architecture and distributed propulsion," in: *AIAA Propuls. Energy Forum - IEEE Symp.*, AIAA, Indianapolis, 2019: pp. 1–20. doi:10.2514/6.2019-4465.
- [14] Ciliberti, D., Orefice, F., Della Vecchia, P., Nicolosi, F., and Corcione, S., "An Approach To Preliminary Sizing Of Turbo-Electric Aircraft With Distributed Propulsion," in: *AIDAA XXV Int. Congr.*, Rome, 2019.
- [15] Cotton, I., Nelms, A., and Husband, M., "Higher voltage aircraft power systems," *IEEE Aerospace and Electronic Systems Magazine*, Vol. 23, No. 2, 2008. doi:10.1109/MAES.2008.4460728.
- [16] Michaelides, E.E. (Stathis.), *Alternative Energy Sources*, Springer, 2012. doi:10.1007/978-3-642-20951-2.
- [17] Strack, M., Pinho Chiozzotto, G., Iwanizki, M., Plohr, M., and Kuhn, M., "Conceptual Design Assessment of Advanced Hybrid Electric Turboprop Aircraft Configurations," in: *17th AIAA Aviat. Technol. Integr. Oper. Conf.*, American Institute of Aeronautics and Astronautics, Reston, Virginia, June 2017. doi:10.2514/6.2017-3068.
- [18] Bradley, M., "Design of Electric and Hybrid-Electric Aircraft," No. June, 2018.
- [19] Scrosati, B., and Garche, J., "Lithium batteries: Status, prospects and future," *Journal of Power Sources*, Vol. 195, No. 9, 2010. doi:10.1016/j.jpowsour.2009.11.048.
- [20] Gerssen-Gondelach, S.J., and Faaij, A.P.C., "Performance of batteries for electric vehicles

- on short and longer term," *Journal of Power Sources*, Vol. 212, August 2012. doi:10.1016/j.jpowsour.2012.03.085.
- [21] Zamboni, J., "A Method for the Conceptual Design of Hybrid Electric Aircraft," TU Delft, 2018.
- [22] Gallagher, K.G., Goebel, S., Greszler, T., Mathias, M., Oelerich, W., Eroglu, D., and Srinivasan, V., "Quantifying the promise of lithium-air batteries for electric vehicles," *Energy and Environmental Science*, Vol. 7, No. 5, 2014. doi:10.1039/c3ee43870h.
- [23] Blurton, K.F., and Sammells, A.F., "Metal/air batteries: Their status and potential - a review," *Journal of Power Sources*, Vol. 4, No. 4, 1979. doi:10.1016/0378-7753(79)80001-4.
- [24] Rajashekara, K., Grieve, J., and Daggett, D., "Hybrid fuel cell power in aircraft," *IEEE Industry Applications Magazine*, Vol. 14, No. 4, 2008. doi:10.1109/MIAS.2008.923606.
- [25] Santin, M., Traverso, A., and Massardo, A., "Technological aspects of gas turbine and fuel cell hybrid systems for aircraft: A review," *Aeronautical Journal*, Vol. 112, No. 1134, 2008. doi:10.1017/S0001924000002426.
- [26] Dunn, J.P., Fuel Cell Powered Electric Aircraft, US006568633B2, 2003. doi:10.4271/t-114.
- [27] Bradley, T.H., Moffitt, B.A., Mavris, D.N., and Parekh, D.E., "Development and experimental characterization of a fuel cell powered aircraft," *Journal of Power Sources*, Vol. 171, No. 2, 2007. doi:10.1016/j.jpowsour.2007.06.215.
- [28] Verstraete, D., Lehmkuehler, K., Gong, A., Harvey, J.R., Brian, G., and Palmer, J.L., "Characterisation of a hybrid , fuel-cell-based propulsion system for small unmanned aircraft," *Journal of Power Sources*, Vol. 250, 2014. doi:10.1016/j.jpowsour.2013.11.017.
- [29] Bradley, T.H., Moffitt, B.A., Fuller, T.F., Mavris, D.N., and Parekh, D.E., "Comparison of design methods for fuel-cell-powered unmanned aerial vehicles," *Journal of Aircraft*, Vol. 46, No. 6, 2009. doi:10.2514/1.41658.
- [30] Bradley, T.H., Moffitt, B.A., Mavris, D.N., Fuller, T.F., and Parekh, D.E., "Hardware-in-the-loop testing of a fuel cell aircraft powerplant," *Journal of Propulsion and Power*, Vol. 25, No. 6, 2009. doi:10.2514/1.40805.
- [31] Rhoads, G.D., Wagner, N.A., Taylor, B.J., Keen, D.B., and Bradley, T.H., "Design and flight test results for a 24 hour fuel cell unmanned aerial vehicle," in: *8th Annu. Int. Energy Convers. Eng. Conf.*, No. July, 2010.
- [32] Renouard-Vallet, G., Saballus, M., Schumann, P., Kallo, J., Friedrich, K.A., and Müller-Steinhagen, H., "Fuel cells for civil aircraft application: On-board production of power, water and inert gas," *Chemical Engineering Research and Design*, Vol. 90, No. 1, 2012. doi:10.1016/j.cherd.2011.07.016.
- [33] Njoya Motapon, S., Dessaint, L.A., and Al-Haddad, K., "A comparative study of energy management schemes for a fuel-cell hybrid emergency power system of more-electric aircraft," *IEEE Transactions on Industrial Electronics*, Vol. 61, No. 3, 2014. doi:10.1109/TIE.2013.2257152.
- [34] Motapon, S.N., Dessaint, L.A., and Al-Haddad, K., "A robust H2-consumption-minimization-based energy management strategy for a fuel cell hybrid emergency power system of more electric aircraft," *IEEE Transactions on Industrial Electronics*, Vol. 61, No. 11, 2014. doi:10.1109/TIE.2014.2308148.
- [35] Nicolay, S., Liu, Y., and Elham, A., "Conceptual design and optimization of a general aviation aircraft with fuel cells and hydrogen as propulsion system Conceptual Design and Optimization of a General Aviation Aircraft with Fuel Cells and Hydrogen," No. February, 2020.
- [36] Kim, K., Kim, T., Lee, K., and Kwon, S., "Fuel cell system with sodium borohydride as hydrogen source for unmanned aerial vehicles," *Journal of Power Sources*, Vol. 196, No. 21, 2011. doi:10.1016/j.jpowsour.2011.01.038.
- [37] Dudek, M., Tomczyk, P., Wygonik, P., Korkosz, M., and Bogusz, P., "Hybrid Fuel Cell – Battery System as a Main Power Unit for Small Unmanned Aerial Vehicles (UAV)," Vol. 8, 2013.
- [38] Herwerth, C., Chiang, C., Ko, A., Matsuyama, S., Choi, S.B., Mirmirani, M., Gamble, D., Paul, R., Sanchez, V., Arena, A., Koschany, A., Gu, G., Wankewycz, T., and Jin, P., "Development of a Small Long Endurance Hybrid PEM Fuel Cell Powered UAV," No. 724,

- 2018.
- [39] Yang, C., Moon, S., and Kim, Y., "A fuel cell / battery hybrid power system for an unmanned aerial vehicle †," Vol. 30, No. 5, 2016. doi:10.1007/s12206-016-0448-3.
- [40] Clean Sky 2, and European Commission, *Hydrogen-powered aviation*, No. May, 2020. doi:10.2843/766989.
- [41] Corchero, G., and Montañés, J.L., "An approach to the use of hydrogen for commercial aircraft engines," *Proceedings of the Institution of Mechanical Engineers, Part G: Journal of Aerospace Engineering*, Vol. 219, No. 1, 2005. doi:10.1243/095441005X9139.
- [42] Kim, H.D., Perry, A.T., and Ansell, P.J., "A Review of Distributed Electric Propulsion Concepts for Air Vehicle Technology," *2018 AIAA/IEEE Electric Aircraft Technologies Symposium, EATS 2018*, 2018. doi:10.2514/6.2018-4998.
- [43] SNYDER, and ZUMWALT GW, "EFFECTS OF WINGTIP-MOUNTED PROPELLERS ON WING LIFT AND INDUCED DRAG," *Journal of Aircraft*, 1969.
- [44] Patterson, J.C., and Bartlett, G.R., "EVALUATION OF INSTALLED PERFORMANCE OF A WING-TIP-MOUNTED PUSHER TURBORPROP ON A SEMISPAN WING.," *NASA Technical Paper*, 1987.
- [45] Deere, K.A., Viken, S.A., Carter, M.B., Viken, J.K., Derlaga, J.M., and Stoll, A.M., "Comparison of high-fidelity computational tools for wing design of a distributed electric propulsion aircraft," in: *35th AIAA Appl. Aerodyn. Conf. 2017*, 2017. doi:10.2514/6.2017-3925.
- [46] Veldhuis, L.L.M., "Propeller Wing Aerodynamic Interference," 2005.
- [47] Dimchev, M., "Experimental and numerical study on wingtip mounted propellers for low aspect ratio UAV design," *Thesis at Delft University of Technology*, 2012.
- [48] Sinnige, T., van Arnhem, N., Stokkermans, T.C.A., Eitelberg, G., and Veldhuis, L.L.M., "Wingtip-Mounted Propellers: Aerodynamic Analysis of Interaction Effects and Comparison with Conventional Layout," *Journal of Aircraft*, November 2018. doi:10.2514/1.C034978.
- [49] Borer, N.K., Patterson, M.D., Viken, J.K., Moore, M.D., Bevirt, J., Stoll, A.M., and Gibson, A.R., "Design and Performance of the NASA SCEPTOR Distributed Electric Propulsion Flight Demonstrator," 2016. doi:10.2514/6.2016-3920.
- [50] Patterson, M.D., "Conceptual Design of High-Lift Propeller Systems for Small Electric Aircraft Coceptual Design of High-Lift Propeller," *Dissertation at Georgia Institute of Technology*, 2016.
- [51] Deere, K.A., Viken, S.A., Carter, M.B., Viken, J.K., Wiese, M.R., and Farr, N., "Computational analysis of powered lift augmentation for the LEAPTech distributed electric propulsion wing," in: *35th AIAA Appl. Aerodyn. Conf. 2017*, 2017. doi:10.2514/6.2017-3921.
- [52] Nguyen Van, E., Troillard, P., Jézégou, J., Alazard, D., Pastor, P., and Döll, C., "Reduction of Vertical Tail Using Differential Thrust : Influence on Flight Control and Certification," in: *Adv. Aircr. Effic. a Glob. Air Transp. Syst.*, Toulouse (France), 2018.
- [53] Nguyen Van, E., Alazard, D., Pastor, P., and Döll, C., "Towards an aircraft with reduced lateral static stability using electric differential thrust," in: *2018 Aviat. Technol. Integr. Oper. Conf.*, 2018. doi:10.2514/6.2018-3209.
- [54] Nguyen Van, E., Alazard, D., Döll, C., and Pastor, P., "Co-design of aircraft vertical tail and control laws using distributed electric propulsion," *IFAC-PapersOnLine*, Vol. 52, No. 12, 2019. doi:10.1016/j.ifacol.2019.11.295.
- [55] Freeman, J.L., and Klunk, G.T., "Dynamic Flight Simulation of Spanwise Distributed Electric Propulsion for Directional Control Authority," *2018 AIAA/IEEE Electric Aircraft Technologies Symposium, EATS 2018*, 2018. doi:10.2514/6.2018-4997.
- [56] Budziszewski, N., and Friedrichs, J., "Modelling of a boundary layer ingesting propulsor," *Energies*, Vol. 11, No. 4, 2018. doi:10.3390/en11040708.
- [57] Valencia, E., Alulema, V., Rodriguez, D., Laskaridis, P., and Roumeliotis, I., "Novel fan configuration for distributed propulsion systems with boundary layer ingestion on an hybrid wing body airframe," *Thermal Science and Engineering Progress*, Vol. 18, 2020. doi:10.1016/j.tsep.2020.100515.
- [58] Hartuç, T., "Boundary Layer Ingestion Theoretical and Experimental Research.."
- [59] Ashcraft, S.W., Padron, A.S., Pascioni, K.A., Stout Jr., G.W., and Huff, D.L., "Review of

- Propulsion Technologies for N+3 Subsonic Vehicle Concepts," October 2011, 2011.
- [60] Synodinos, A., Self, R., and Torija, A., "Preliminary Noise Assessment of Aircraft with Distributed Electric Propulsion," in: *2018 AIAA/CEAS Aeroacoustics Conf.*, American Institute of Aeronautics and Astronautics, 2018. doi:10.2514/6.2018-2817.
- [61] Rizzi, S.A., Palumbo, D.L., Rathsam, J., Christian, A.W., and Rafaelof, M., "Annoyance to Noise Produced by a Distributed Electric Propulsion High-Lift System," in: *23rd AIAA/CEAS Aeroacoustics Conf.*, American Institute of Aeronautics and Astronautics, June 2017. doi:10.2514/6.2017-4050.
- [62] ACARE, "2008 Addendum to the Strategic Research Agenda," 2008.
- [63] Fink, M.R., "Approximate Prediction of Airframe Noise," *Journal of Aircraft*, Vol. 13, No. 11, 1976.
- [64] Huff, D.L., Henderson, B.S., and Envia, E., "Motor noise for electric powered aircraft," in: *22nd AIAA/CEAS Aeroacoustics Conf. 2016*, 2016. doi:10.2514/6.2016-2882.
- [65] Pascioni, K.A., Rizzi, S.A., and Schiller, N., "Noise Reduction Potential of Phase Control for Distributed Propulsion Vehicles," in: 2019. doi:10.2514/6.2019-1069.
- [66] Posey, J.W., Tinetti, A.F., and Dunn, M.H., "The low-noise potential of distributed propulsion on a catamaran aircraft," in: *Collect. Tech. Pap. - 12th AIAA/CEAS Aeroacoustics Conf.*, 2006. doi:10.2514/6.2006-2622.
- [67] Joslin, R.D., "Overview of Laminar Flow Control," *NASA Technical Paper*, 1998.
- [68] Pe, T., and Thielecke, F., "Methodik zur Leistungsabschätzung von HLFC-Absaugsystemen im Flugzeugvorentwurf," in: *Dtsch. Luft- Und Raumfahrtkongress, Hambg. 31. August - 2. Sept. 2010*, 2010.
- [69] Beck, N., Landa, T., Seitz, A., Boermans, L., Liu, Y., and Radespiel, R., "Drag reduction by laminar flow control," *Energies*, 2018. doi:10.3390/en11010252.
- [70] Abbas, A., De Vicente, J., and Valero, E., "Aerodynamic technologies to improve aircraft performance," *Aerospace Science and Technology*, Vol. 28, No. 1, 2013. doi:10.1016/j.ast.2012.10.008.
- [71] Collier, F.S., "An overview of recent subsonic laminar flow control flight experiments," in: *AIAA 23rd Fluid Dyn. Plasmadynamics, Lasers Conf. 1993*, 1993. doi:10.2514/6.1993-2987.
- [72] Fujino, M., Yoshizaki, Y., and Kawamura, Y., "Natural-laminar-flow airfoil development for a lightweight business jet," *Journal of Aircraft*, 2003. doi:10.2514/2.3145.
- [73] Fujino, M., "Design and development of the HondaJet," *Journal of Aircraft*, 2005. doi:10.2514/1.12268.
- [74] Pe, T., and Thielecke, F., "Synthesis and Topology Study of HLFC System Architectures in Preliminary Aircraft Design," in: *3rd CEAS Air Sp. Conf.*, 2011.
- [75] Bottemanne, M., and Atkin, C., "Tool for sizing suction pumps for hybrid laminar flow control concepts," *International Journal of Mechanical Engineering and Robotics Research*, 2018. doi:10.18178/ijmerr.7.1.1-8.
- [76] Schmitt, V., Archambaud, J.P., Hortstmann, K.H., and Quast, A., "Hybrid laminar fin investigations," in: *RTO AVT Symp. Act. Control Technol. Enhanc. Perform. Oper. Capab. Mil. Aircraft, L. Veh. Sea Veh. Braunschweig (de), 08.-11.05.2000*, 2000.
- [77] Schrauf, G.H., and Horstmann, K.H., "Simplified hybrid laminar flow control," in: *ECCOMAS 2004 - Eur. Congr. Comput. Methods Appl. Sci. Eng.*, 2004.
- [78] Risse, K., Schueltke, F., Stumpf, E., and Schrauf, G., "Conceptual wing design methodology for aircraft with hybrid laminar flow control," in: *52nd Aerosp. Sci. Meet.*, 2014. doi:10.2514/6.2014-0023.
- [79] Risse, K., Anton, E., Lammering, T., Franz, K., and Hoernschemeyer, R., "An integrated environment for preliminary aircraft design and optimization," in: *Collect. Tech. Pap. - AIAA/ASME/ASCE/AHS/ASC Struct. Struct. Dyn. Mater. Conf.*, 2012. doi:10.2514/6.2012-1675.
- [80] Catalano, P., de Rosa, D., Mele, B., Tognaccini, R., and Moens, F., "Effects of riblets on the performances of a regional aircraft configuration in NLF conditions," in: *AIAA Aerosp. Sci. Meet. 2018*, 2018. doi:10.2514/6.2018-1260.
- [81] Lienhart, H., Breuer, M., and Köksoy, C., "Drag reduction by dimples? - A complementary experimental/numerical investigation," *International Journal of Heat and Fluid Flow*, 2008.

- doi:10.1016/j.ijheatfluidflow.2008.02.001.
- [82] Jimenez, J., "TURBULENT FLOWS OVER ROUGH WALLS," *Annual Review of Fluid Mechanics*, 2004. doi:10.1146/annurev.fluid.36.050802.122103.
- [83] García-Mayoral, R., and Jiménez, J., "Drag reduction by riblets," *Philosophical Transactions of the Royal Society A: Mathematical, Physical and Engineering Sciences*, 2011. doi:10.1098/rsta.2010.0359.
- [84] J.D. McLean, D.N. George-Falvy, P. S., "Flight-test of turbulent skin friction reduction by riblets," in: *Int. Conf. Turbul. Drag Reduct. by Passiv. Means*, 1987: pp. 1–17.
- [85] SZODRUCH, J., "Viscous drag reduction on transport aircraft," in: 1991. doi:10.2514/6.1991-685.
- [86] Torrigiani, F., Bussemaker, J., Ciampa, P.D., Fioriti, M., Tomasella, F., Aigner, B., Rajpal, D., Timmermans, H., Savelyev, A., and Charbonnier, D., "Design of the Strut Braced Wing Aircraft in the Agile Collaborative Mdo Framework," *31th Congress of the International Council of the Aeronautical Sciences, ICAS 2018*, No. 0, 2018.
- [87] Zhao, W., Kapania, R.K., Schetz, J.A., and Coggin, J.M., "Nonlinear Aeroelastic Analysis of SUGAR Truss-braced Wing (TBW) Wind-tunnel Model (WTM) Under In-plane Loads," in: *56th AIAA/ASCE/AHS/ASC Struct. Struct. Dyn. Mater. Conf.*, American Institute of Aeronautics and Astronautics, Reston, Virginia, No. January, 2015. doi:10.2514/6.2015-1173.
- [88] Bradley, M.K., and Dronney, C.K., "Subsonic Ultra Green Aircraft Research : Phase I Final Report," 2011.
- [89] Rajpal, D., Breuker, R. De, Timmermans, H., Lammen, W.F., and Torrigiani, F., "Including Aeroelastic Tailoring In The Conceptual Design Process Of A Composite Strut Based Wing," *31th Congress of the International Council of the Aeronautical Sciences, ICAS 2018*, 2018.
- [90] Ciobaca, vlad, and Wild, J., "An Overview of Recent DLR Contributions on Active Flow-Separation Control Studies for High-Lift Configurations," *Aerospace Lab*, 2013.
- [91] "MIL-HDBK 17-3F - Composite Materials Handbook," in: *Dep. Def. Handb.*, USA Department of Defense, USA, 2002.
- [92] "JSSG-2006, Aircraft Structures," in: *Dep. Def. Jt. Serv. Specif. Guid.*, USA Department of Defense, 1988.
- [93] "Aviation Safety: Status of FAA's Actions to Oversee the Safety of Composite Airplanes," in: United States Government Accountability Office, USA, 2011.
- [94] Abrate, S., *Impact on Composite Structures*, 1998. doi:10.1017/cbo9780511574504.
- [95] Kim, E.H., Rim, M.S., Lee, I., and Hwang, T.K., "Composite damage model based on continuum damage mechanics and low velocity impact analysis of composite plates," *Composite Structures*, 2013. doi:10.1016/j.compstruct.2012.07.002.
- [96] Maio, L., Monaco, E., Ricci, F., and Lecce, L., "Simulation of low velocity impact on composite laminates with progressive failure analysis," *Composite Structures*, 2013. doi:10.1016/j.compstruct.2013.02.027.
- [97] Wang, H., and vu-Khanh, T., "Fracture Mechanics and Mechanisms of Impact-Induced Delamination in Laminated Composites," *Journal of Composite Materials*, 1995. doi:10.1177/002199839502900202.
- [98] Lee, J., and Soutis, C., "Experimental investigation on the behaviour of CFRP laminated composites under impact and compression after impact (CAI)," in: *Springer Proc. Phys.*, 2008. doi:10.1007/978-3-540-85190-5_29.
- [99] wu, H.Y.T., and Springer, G.S., "Measurements of Matrix Cracking and Delamination Caused by Impact on Composite Plates," *Journal of Composite Materials*, 1988. doi:10.1177/002199838802200602.
- [100] Guynn, E.G., and O'Brien, T.K., "INFLUENCE OF LAY-UP AND THICKNESS ON COMPOSITE IMPACT DAMAGE AND COMPRESSION STRENGTH.," in: *Collect. Tech. Pap. - AIAA/ASME/ASCE/AHS/ASC Struct. Struct. Dyn. Mater. Conf.*, 1985.
- [101] Takeda, S., Minakuchi, S., Okabe, Y., and Takeda, N., "Delamination monitoring of laminated composites subjected to low-velocity impact using small-diameter FBG sensors," *Composites Part A: Applied Science and Manufacturing*, 2005. doi:10.1016/j.compositesa.2004.12.005.

- [102] "AC No: 20-107B. Composite Aircraft Structure," in: U.S. Department of Transportation - Federal Aviation Administration, USA, 2009.
- [103] "AC No: 25.571-1D - Damage Tolerance and Fatigue Evaluation of Structure," in: U.S. Department of Transportation - Federal Aviation Administration, USA, 2011.
- [104] "MIL-HDBK No: 1823A. Non destructive evaluation system reliability assessment," in: U.S. Department of Defence, USA, 2009.
- [105] Mitchell, M.R., Link, R.E., Liew, C.K., Veidt, M., Rajic, N., Tsoi, K., Rowlands, D., and Morton, H., "Inspections of Helicopter Composite Airframe Structures using Conventional and Emerging Nondestructive Testing Methods," *Journal of Testing and Evaluation*, 2011. doi:10.1520/jte103842.
- [106] Peng, W., Zhang, Y., Qiu, B., and Xue, H., "A Brief Review of the Application and Problems in Ultrasonic Fatigue Testing," *AASRI Procedia*, 2012. doi:10.1016/j.aasri.2012.09.024.
- [107] Kroeger, T., "Thermographic inspection of composites," *Reinforced Plastics*, 2014. doi:10.1016/S0034-3617(14)70183-3.
- [108] Vavilov, V.P., Budadin, O.N., and Kulkov, A.A., "Infrared thermographic evaluation of large composite grid parts subjected to axial loading," *Polymer Testing*, 2015. doi:10.1016/j.polymertesting.2014.10.010.
- [109] Tan, K.T., Watanabe, N., and Iwahori, Y., "X-ray radiography and micro-computed tomography examination of damage characteristics in stitched composites subjected to impact loading," *Composites Part B: Engineering*, 2011. doi:10.1016/j.compositesb.2011.01.011.
- [110] Bossi, R.H., and Giurgiutiu, V., "Nondestructive testing of damage in aerospace composites," in: *Polym. Compos. Aerosp. Ind.*, 2015. doi:10.1016/B978-0-85709-523-7.00015-3.
- [111] Sarasini, F., and Santulli, C., "Non-destructive testing (NDT) of natural fibre composites: Acoustic emission technique," in: *Nat. Fibre Compos. Mater. Process. Appl.*, 2013. doi:10.1533/9780857099228.3.273.
- [112] Su, Z., Zhou, C., Hong, M., Cheng, L., Wang, Q., and Qing, X., "Acousto-ultrasonics-based fatigue damage characterization: Linear versus nonlinear signal features," *Mechanical Systems and Signal Processing*, 2014. doi:10.1016/j.ymssp.2013.10.017.
- [113] Hung, Y.Y., Yang, L.X., and Huang, Y.H., "5 Non-destructive evaluation (NDE) of composites: digital shearography BT - Non-Destructive Evaluation (NDE) of Polymer Matrix Composites," in: *Non-Destructive Eval. Polym. Matrix Compos.*, 2013.
- [114] Yang, S.H., Kim, K.B., Oh, H.G., and Kang, J.S., "Non-contact detection of impact damage in CFRP composites using millimeter-wave reflection and considering carbon fiber direction," *NDT and E International*, 2013. doi:10.1016/j.ndteint.2013.03.006.
- [115] El-Sayed, A.F., *Bird strike in aviation : statistics, analysis and management*, n.d.
- [116] F. Ricci, E. Monaco, L. Maio, N. Boffa, and V. Memmolo, "The role of SHM in the design and maintenance of modern and aging structures," in: *Proc. Int. Symp. Dyn. Response Fail. Compos. Mater.*, Island of Ischia, 2016.
- [117] "SAE ARP6275 - Determination of Cost Benefits from Implementing an Integrated Vehicle Health Management System," in: SAE International, n.d.
- [118] Renee M. Kent and Dennis A. Murphy, "Health Monitoring System Technology Assessments - Cost Benefits Analysis," 2000.
- [119] Rytter, A., "Vibrational Based Inspection of Civil Engineering Structures," 1993. doi:10.1016/j.jsv.2016.06.047.
- [120] Růžek, R., Lohonka, R., and Jironč, J., "Ultrasonic C-scan and shearography NDI techniques evaluation of impact defects identification," *NDT and E International*, 2006. doi:10.1016/j.ndteint.2005.07.012.
- [121] Worden, K., Allen, D.W., Sohn, H., and Farrar, C.R., "<title>Damage detection in mechanical structures using extreme value statistics</title>," in: *Smart Struct. Mater. 2002 Model. Signal Process. Control*, 2002. doi:10.1117/12.475226.
- [122] Sohn, H., Farrar, C.R., Hunter, N.F., and Worden, K., "Structural health monitoring using statistical pattern recognition techniques," *Journal of Dynamic Systems, Measurement and Control, Transactions of the ASME*, 2001. doi:10.1115/1.1410933.
- [123] Cottone, G., Gollwitzer, S., Heckenberger, U., and Straub, D., "Reliability-oriented

- optimization of replacement strategies for monitored composite panels for aircraft structures," in: *Struct. Heal. Monit. 2013 A Roadmap to Intell. Struct. - Proc. 9th Int. Work. Struct. Heal. Monit. IWSHM 2013*, 2013.
- [124] Gianneo, A., Carboni, M., and Giglio, M., "Feasibility study of a multi-parameter probability of detection formulation for a Lamb waves-based structural health monitoring approach to light alloy aeronautical plates," *Structural Health Monitoring*, 2017. doi:10.1177/1475921716670841.
- [125] Eleftheroglou, N., Zarouchas, D., and Benedictus, R., "An adaptive probabilistic data-driven methodology for prognosis of the fatigue life of composite structures," *Composite Structures*, 2020. doi:10.1016/j.compstruct.2020.112386.
- [126] Thöns, S., "On the Value of Monitoring Information for the Structural Integrity and Risk Management," *Computer-Aided Civil and Infrastructure Engineering*, 2018. doi:10.1111/mice.12332.
- [127] Currey, N.S., "Aircraft Landing Gear Design: Principles and Practices," *Aircraft Landing Gear Design: Principles and Practices*, 1988. doi:10.2514/4.861468.
- [128] VN Divakaran, RM Subrahmanya, G.R., "Integrated Vehicle Health Management of a Transport Aircraft Landing gear system," 2018.
- [129] Stinton, D., "Aircraft Design – a Conceptual Approach – Fourth edition; and RDSStudent: Software for Aircraft Design, Sizing and Performance D.P. Raymer American Institute of Aeronautics and Astronautics, 1801 Alexander Bell Drive, Suite 500, Reston, VA 20191-4344, USA," *The Aeronautical Journal*, 2007. doi:10.1017/s0001924000086887.
- [130] Roskam, J., *Airplane Design Part III Layout Design of Cockpit, Fuselage, Wing and Empennage: Cutaways and Inboard Profiles*, 1989. doi:kid537 [pii]r10.1046/j.1523-1755.2001.059002682.x.
- [131] Torenbeek, E., *Synthesis of Subsonic Airplane Design*, 1982. doi:10.1007/978-94-017-3202-4.
- [132] Kundu, A.K., and Kundu, A.K., "International Standard Atmosphere," in: *Aircr. Des.*, 2012. doi:10.1017/cbo9780511844652.021.
- [133] Howe, D., *Aircraft Conceptual Design Synthesis*, 2000. doi:10.1002/9781118903094.
- [134] Ajaj, R.M., Friswell, M.I., Smith, D., and Isikveren, A.T., "A conceptual wing-box weight estimation model for transport aircraft," *Aeronautical Journal*, 2013. doi:10.1017/S0001924000008174.
- [135] Van der Velden, A., Kelm, R., Kokan, D., and Mertens, J., "Application of MDO to large subsonic transport aircraft," in: *38th Aerosp. Sci. Meet. Exhib.*, 2000. doi:10.2514/6.2000-844.
- [136] Dababneh, O., and Kayran, A., "Design, analysis and optimization of thin walled semi-monocoque wing structures using different structural idealization in the preliminary design phase," *International Journal of Structural Integrity*, 2014. doi:10.1108/IJSI-12-2013-0050.
- [137] Dorbath, F., Nagel, B., and Gollnick, V., "A Knowledge Based Approach for Automated Modelling of Extended Wing Structures in Preliminary Aircraft Design," *Deutscher Luft- und Raumfahrtkongress*, 2011.
- [138] Elham, A., and Van Tooren, M.J.L., "Tool for preliminary structural sizing, weight estimation, and aeroelastic optimization of lifting surfaces," *Proceedings of the Institution of Mechanical Engineers, Part G: Journal of Aerospace Engineering*, 2016. doi:10.1177/0954410015591045.
- [139] Mardanpour, P., and Hodges, D.H., "On the Importance of Nonlinear Aeroelasticity and Energy Efficiency in Design of Flying Wing Aircraft," *Advances in Aerospace Engineering*, 2015. doi:10.1155/2015/613962.
- [140] Mardanpour, P., Hodges, D.H., and Rezvani, R., "Nonlinear aeroelasticity of high-aspect-ratio wings excited by time-dependent thrust," *Nonlinear Dynamics*, 2014. doi:10.1007/s11071-013-1079-1.
- [141] Mardanpour, P., Hodges, D.H., Neuhart, R., and Graybeal, N., "Engine placement effect on nonlinear trim and stability of flying wing aircraft," in: *J. Aircr.*, 2013. doi:10.2514/1.C031955.
- [142] Mardanpour, P., Richards, P.W., Nabipour, O., and Hodges, D.H., "Effect of multiple engine placement on aeroelastic trim and stability of flying wing aircraft," *Journal of Fluids and*

- Structures*, 2014. doi:10.1016/j.jfluidstructs.2013.09.018.
- [143] Hoover, C.B., Shen, J., Kreshock, A.R., Stanford, B.K., Piatak, D.J., and Heeg, J., "Whirl flutter stability and its influence on the design of the distributed electric propeller aircraft X-57," in: *17th AIAA Aviat. Technol. Integr. Oper. Conf. 2017*, 2017. doi:10.2514/6.2017-3785.
- [144] Hoover, C.B., Shen, J., and Kreshock, A.R., "Propeller whirl flutter stability and its influence on X-57 aircraft design," in: *J. Aircr.*, 2018. doi:10.2514/1.C034950.
- [145] Joslin, R.D., "AIRCRAFT LAMINAR FLOW CONTROL," *Annual Review of Fluid Mechanics*, 1998. doi:10.1146/annurev.fluid.30.1.1.
- [146] Kulfan, R. M., and Vachal, J.D., "Wing Planform Geometry Effects on Large Subsonic Military Transport Airplanes," *AFFDL-TR-78-16*, Vol. U.S. Air F,n.d.
- [147] PARK, P., "The effect on block fuel consumption of a strutted versus cantileverwing for a short-haul transport including strut aeroelastic considerations," in: 1978. doi:10.2514/6.1978-1454.
- [148] Turriziani, R.V., Lovell, W.A., Martin, G.L., Price, J.E., Swanson, E.E., and Washburn, G.F., "Preliminary Design Characteristics of a Subsonic Business Jet Concept Employing an Aspect Ratio 25 Strut-Braced Wing," *October*, 1980.
- [149] Gern, F.H., Naghshineh-Pour, A.H., Sulaeman, E., Kapania, R.K., and Haftka, R.T., "Structural wing sizing for multidisciplinary design optimization of a strut-braced wing," *Journal of Aircraft*, 2001. doi:10.2514/2.2747.
- [150] Barbarino, S., Bilgen, O., Ajaj, R.M., Friswell, M.I., and Inman, D.J., "A review of morphing aircraft," *Journal of Intelligent Material Systems and Structures*, 2011. doi:10.1177/1045389X11414084.
- [151] Pecora, R., Concilio, A., Dimino, I., Amoroso, F., and Ciminello, M., "Structural design of an adaptive wing trailing edge for enhanced cruise performance," in: *24th AIAA/AHS Adapt. Struct. Conf.*, 2016. doi:10.2514/6.2016-1317.
- [152] Amendola, G., Dimino, I., Concilio, A., Pecora, R., Amoroso, F., and Arena, M., "Morphing Aileron," in: *Morphing Wing Technol. Large Commer. Aircr. Civ. Helicopters*, 2018. doi:10.1016/B978-0-08-100964-2.00018-6.
- [153] Moens, F., "Augmented aircraft performance with the use of morphing technology for a turboprop regional aircraftwing," *Biomimetics*, 2019. doi:10.3390/biomimetics4030064.
- [154] Boffa, N.D., Monaco, E., Ricci, F., Lecce, L., Barile, M., and Memmolo, V., "Hybrid structural health monitoring on a composite plate manufactured with automatic fibers placement including embedded fiber Bragg gratings and bonded piezoelectric patches," in: 2019. doi:10.1117/12.2516537.
- [155] Ebert, L.B., "Science of fullerenes and carbon nanotubes," *Carbon*, 1997. doi:10.1016/s0008-6223(97)89618-2.
- [156] Qian, H., Greenhalgh, E.S., Shaffer, M.S.P., and Bismarck, A., "Carbon nanotube-based hierarchical composites: A review," *Journal of Materials Chemistry*, 2010. doi:10.1039/c000041h.
- [157] Hawkins, S.C., Poole, J.M., and Huynh, C.P., "Catalyst distribution and carbon nanotube morphology in multilayer forests by mixed CVD processes," *Journal of Physical Chemistry C*, 2009. doi:10.1021/jp810072j.
- [158] Bhanushali, H., and Bradford, P.D., "Woven Glass Fiber Composites with Aligned Carbon Nanotube Sheet Interlayers," *Journal of Nanomaterials*, 2016. doi:10.1155/2016/9705257.
- [159] Nistal, A., Falzon, B.G., Hawkins, S.C., Chitwan, R., García-Diego, C., and Rubio, F., "Enhancing the fracture toughness of hierarchical composites through amino-functionalised carbon nanotube webs," *Composites Part B: Engineering*, 2019. doi:10.1016/j.compositesb.2019.02.001.
- [160] Kumar, S., Falzon, B.G., Kun, J., Wilson, E., Graninger, G., and Hawkins, S.C., "High performance multiscale glass fibre epoxy composites integrated with cellulose nanocrystals for advanced structural applications," *Composites Part A: Applied Science and Manufacturing*, 2020. doi:10.1016/j.compositesa.2020.105801.
- [161] Zhang, Y., Ma, J., Singh, A.K., Cao, L., Seo, J., Rahn, C.D., Bakis, C.E., and Hickner, M.A., "Multifunctional structural lithium-ion battery for electric vehicles," *Journal of Intelligent Material Systems and Structures*, 2017. doi:10.1177/1045389X16679021.

- [162] Roberts, S.C., and Aglietti, G.S., "Satellite multi-functional power structure: Feasibility and mass savings," *Proceedings of the Institution of Mechanical Engineers, Part G: Journal of Aerospace Engineering*, 2008. doi:10.1243/09544100JAERO255.
- [163] Roberts, S.C., and Aglietti, G.S., "Structural performance of a multifunctional spacecraft structure based on plastic lithium-ion batteries," *Acta Astronautica*, 2010. doi:10.1016/j.actaastro.2010.03.004.
- [164] Thomas, J.P., Qidwai, S.M., Pogue, W.R., and Pham, G.T., "Multifunctional structure-battery composites for marine systems," *Journal of Composite Materials*, 2013. doi:10.1177/0021998312460262.
- [165] Pereira, T., Zhanhu Guo, Nieh, S., Arias, J., and Hahn, H.T., "Energy Storage Structural Composites: A Review," *Journal of Composite Materials*, 2009. doi:10.1177/0021998308097682.
- [166] Ekstedt, S., Wysocki, M., and Asp, L.E., "Structural batteries made from fibre reinforced composites," in: *Plast. Rubber Compos.*, 2010. doi:10.1179/174328910X12647080902259.
- [167] Ding, J., Tian, T., Meng, Q., Guo, Z., Li, W., Zhang, P., Ciacchi, F.T., Huang, J., and Yang, W., "Smart multifunctional fluids for lithium ion batteries: Enhanced rate performance and intrinsic mechanical protection," *Scientific Reports*, 2013. doi:10.1038/srep02485.
- [168] "Federal Aviation Regulations," in: *FAR/AIM*, Department of U.S. Transportation, November 2016: p. 1113.
- [169] EASA, "Certification Specifications for Normal-Category Aeroplanes," Amendment 5, 2017. doi:10.1002/9780470664797.